Chem Soc Rev

Functionalized Graphene and Other Two-Dimensional Materials for Photovoltaic Devices: Device Design and Processing

Journal:	*Chemical Society Reviews*
Manuscript ID:	CS-REV-12-2014-000455.R4
Article Type:	Review Article
Date Submitted by the Author:	13-Apr-2015
Complete List of Authors:	Liu, Zhike; The Hong Kong Polytechnic University, Department of Applied Physics Lau, Shu Ping; The Hong Kong Polytechnic University, Department of Applied Physics YAN, Feng; The Hong Kong Polytechnic University, Department of Applied Physics

Submitted to

Functionalized Graphene and Other Two-Dimensional Materials for Photovoltaic Devices: Device Design and Processing

Zhike Liu, Shu-Ping Lau and Feng Yan*

Department of Applied Physics and Materials Research Centre
The Hong Kong Polytechnic University, Hong Kong (China)
E-mail: apafyan@polyu.edu.hk

Keywords: (Graphene; 2D material; photovoltaic device; organic solar cell; Schottky junction solar cell; dye-sensitized solar cell; perovskite solar cell)

Abstract

Graphene is the thinnest two-dimensional (2D) carbon material with many advantages including high carrier mobilities and conductivity, high optical transparency, excellent mechanical flexible and chemical stability, which make graphene an ideal material for various optoelectronic devices. The major applications of graphene in photovoltaic devices are for transparent electrodes and charge transport layers. Several other 2D materials also showed advantages in charge transport and light absorption over traditional semiconductor materials used in photovoltaic devices. Great achievements in the applications of 2D materials in photovoltaic devices have been reported, yet numerous challenges still remain open. For practical applications, the device performance should be further improved by optimizing the 2D material synthesis, film transfer, surface functionalization and chemical/physical doping processes. In this review, we will focus on the recent advances of the applications of graphene and other 2D materials in various photovoltaic devices, including organic solar cells, Schottky junction solar cells, dye-sensitized solar cells, quantum dot-sensitized solar cells and other inorganic solar cells, and perovskite solar cells, in terms of the functionalization techniques of materials, the device design and the device performance. In the end, conclusions and an outlook for the future development of this field will be addressed.

CONTENTS

List of Abbreviations

2D	two-dimensional
3D	three-dimensional
APCVD	atmospheric pressure CVD
BCP	bathocuproine
CNT	carbon nanotube
CuPc	copper phthalocyanine
CV	cyclic voltammetry
CVD	chemical vapor deposition
DMF	N,N-dimethylformamide
DMSO	dimethyl sulfoxide
DSSC	dye-sensitized solar cell
EIS	electrochemical impedance spectroscopy
EQE	external quantum efficiency
ETL	electron transport layers
FF	fill factor
FTO	fluorine-doped tin oxide
GF	framework
GNP	graphene nanoplatelet
GO	graphene oxide
GQD	graphene quantum dot
HOMO	highest occupied molecular orbital
HTL	hole transport layer
ICBA	indene-C_{60} bisadduct
IPA	isopropyl alcohol
IPCE	incident photon-to-electron conversion efficiencies
ITO	indium tin oxide
J_{sc}	short-circuit current
LBL	layer-by-layer
LUMO	lowest unoccupied molecular orbital
MLG	multilayer graphene
MPCVD	mist pyrolysis CVD
N719	di-tetrabutylammoniumcis-bis(isothiocyanato)bis(2,2'-bipyridyl-4,4'-dicarboxylato)ruthenium(II)
NMP	*n*-methyl-2-pyrrolidone
NP	nanoparticle
NW	nanowire
OLED	organic light emitting diode
OPV	organic photovoltaic device
P(VDF-TrFE)	poly(vinylidene fluoride-co-tri-fluoroethylene)

P3HT	poly(3-hexylthiophene)
P3OT	Poly(3-octylthiophene)
PBASE	pyrene butanoic acid succidymidyl ester
PBDTT-DPP	poly{2,6′-4,8-di(5-ethylhexylthienyl)benzo[1,2-*b*;3,4-b]dithiophene-alt-5-dibutyloctyl-3,6-bis(5-bromothiophen-2-yl)pyrrolo[3,4-*c*]pyrrole-1,4-dione}
PBDTTT-CF	poly[1-(6-{4,8-bis[(2-ethylhexyl)oxy]-6-methylbenzo[1,2-*b*:4,5-*b*′]dithiophen-2-yl}-3-fluoro-4-methylthieno[3,4-*b*]thiophen-2-yl)-1-octanone]
PBTTTT-C	poly[(4,8-bis-(2-ethylhexyloxy)-benzo[I,2-b;4,5-b')dithiophene)-2,6-diyl-alt-(4-(2-ethylhexanoyl)-thieno[3,4-b)thiopene)-2,6-diyl)
$PC_{71}BM$	[6,6]-phenyl-C_{71}butyric acid methyl ester
PCA	1-pyrenecarboxylic acid
PCBM	[6,6]-phenyl-C_{61} butyric acid methyl ester
PCDTBT	poly[N-9’-heptadecanyl-2,7-carbazole-alt-5,5-(4,7-di-2-thienyl-2’,1’,3’-benzothiadiazole]
PCE	power conversion efficiency
PDDA	poly(diallydimethylammonium chloride)
PDI	3,4,9,10-perylenetetracarboxylic diimide bisbenzenesulfonic acid
PDMS	polydimethylsiloxane
PEDOT:PSS	poly-(3,4-ethylenedioxythiophene): poly(styrenesulfonate)
PEG	polyethylene glycol
PEI	polyethylenimine
PEN	polyethylene naphthalate
PEO	poly(ethylene oxide)
PET	poly(ethylene terephthalate)
PI	polyimide
PLD	pulsed laser deposition
PMMA	poly(methylmethacrylate)
PTB7	poly[[4,8-bis[(2-ethylhexyl)oxy]benzo[1,2-b:4,5-b’]dithiophene-2,6-diyl][3-fluoro-2-[(2-ethylheyl)carbonyl]-thieno[3,4-b]thiophenediyl]]
PTCDA	perylene-3,4,9,10-tetracarboxylic dianhydride
p-$TosNHNH_2$	p-toluenesulfonyl hydrazide
PVA	polyvinyl alcohol
PyS	pyrene-1-sulfonic acid sodium salt
QD	quantum dot
QDSSC	quantum dot-sensitized sensitized solar cells
RG 1200	poly(thiophene-3-[2-(2-methoxyethoxy)ethoxy]-2,5-diyl)
rGO	reduced graphene oxide
R_s	sheet resistance
SAM	self-assembled monolayer
SDBS	sodium dodecylbenzene sulfonate
SHE	standard hydrogen electrode

spiro-OMeTAD	(2,2’,7,7’-tetrakis-(N,N-di-p-methoxyphenylamine)-9,9’-spirobifluorene)
SWCNT	single walled carbon nanotube
TCNQ	tetracyanoquinodimethane
TCO	transparent conductive oxide
TFSA	bis(trifluoromethanesulfonyl) amide
TMD	transition-metal dichalcogenide
TPAS	perylene-3,4,9,10-tetracarboxylic acid tetrapotassium salt
TQ1	poly[2,3-bis-(3-octyloxyphenyl)quinoxaline-5,8-diyl-*alt*-thiophene-2,5-diyl]
V_{oc}	open circuit voltage
WPF-6-oxy-F	poly[(9,9-bis((6′-(*N*,*N*,*N*-trimethylammonium)hexyl)-2,7-fluorene)-*alt*-(9,9-bis(2-(2-(2-methoxyethoxy)ethoxy)ethyl)-9-fluorene)) dibromide
Y123	3-{6-{4-[bis(2’,4’-dihexyloxybiphenyl-4-yl)amino-]phenyl}-4,4-dihexyl-cyclopenta-[2,1-b:3,4-b’]dithiphene-2-yl}-2-cyanoacrylic acid
ZnPc	zinc phtalocyanine

1. Introduction

The energy consumption in the world has reached 16 terawatts in 2006 and is predicted to rise to ~30 terawatts by 2050.[1] However, the traditional energy sources like fossil fuels would increase CO_2 emission and cause severe environmental problems. Solar energy has been recognized as an important green energy source. Various solar technologies including solar heating, solar photovoltaic and solar thermal electricity have been employed to harness solar energy in the world. Solar photovoltaic technology has attracted much attention in recent years because it is a feasible way to solve some urgent problems that the world now faces, like environmental pollution and energy crisis. Silicon *p*-*n* junction solar cells, for their advantages in high efficiency and stability, are the dominant photovoltaic products in the market and have been popularly used in our normal life. The best single crystalline silicon solar cells have shown power conversion efficiencies (PCE) up to 25% and the commercial solar cell modules have achieved efficiencies of about 19%.[2] However, silicon wafers are high cost, fragile, and have a complex manufacturing process, which limit their competition against other energy sources.[3] Therefore, several new generation thin film solar cells, including organic solar cells (OPVs), Schottky junction solar cells, dye-sensitized solar cells (DSSCs), quantum dot (QD) -sensitized solar cells and perovskite solar cells, have attracted much research interests in the past decade and astonishing progress has been made in these fields.

As shown in **Fig. 1**, 2D materials especially graphene, a single atomic layer composed of sp^2-hybridized carbon, are rapidly rising star materials, which have very broad applications in recent years. Graphene was successfully isolated from graphite using a technique called mechanical exfoliation in 2004.[4] Since then, the study of graphene has been making a huge impact on many areas of science and technology due to its outstanding electronic, optical and mechanical properties,[5] followed by a series of investigations on other 2D materials,[6,7] such as the 2D crystals of MX_2 type (M = Mo, W, Nb, Re, Ti, Ta, *etc.*; X = S, Se, Te) transition-metal dichalcogenides (TMDs),[8-11] phosphorene,[12,13] transition oxides (e.g., MoO_3, La_2CuO_4),[14] silicene,[15] germanene[16] and perovskite materials (e.g., $[NH_3(CH_2)_{12}NH_3]PbX_4$).[17] To obtain full pictures of these applications, interested readers may refer to a number of reviews of 2D materials in different fields, including fundamental properties,[8,18-21] photonic applications,[22-25] electronic applications,[26] energy devices,[27,28] biomaterials and sensors.[29-31]

Due to its high conductivity and transparency, graphene has been successfully used in almost all types of photovoltaic devices as transparent electrodes or interlayers.[32,33] Other 2D

materials, such as MoS_2, WS_2 and black phosphorus, have demonstrated distinct electrical, optical, mechanical, thermal, and chemical properties from their bulk three-dimensional (3D) counterparts and are promising for photovoltaic devices as interlayers or active layers as evidenced in recent research.[34,35] Therefore, we provide a comprehensive review here on the applications of 2D materials in solar cells, mainly focusing on the critical issues of device design and processing techniques in using these materials.

2. Preparation and Properties of Graphene and other 2D Materials

2.1. Exfoliation Methods

In 2004, graphene was firstly prepared, transferred and characterized by Novoselov et al. and its field effect and quantum hall effect were observed.[4] Since then, graphene and other 2D materials, such as MoS_2, WS_2, WSe_2 and $MoSe_2$, are quickly became hot topics for physics, chemistry, material science and biology *etc*. The methods for synthesizing 2D materials can be categorized into mechanical exfoliation, chemically assisted and solution based exfoliation, and chemical vapor deposition (CVD). The 2D materials prepared by these techniques have different size, quality and chemical properties, which in turn determine their applications.

2.1.1. Mechanical exfoliation

In graphite, the adjacent graphene layers are bound by weak van der Waals forces (2 eV/nm^2), so pristine graphene can be exfoliated from graphite by using adhesive tapes. In 2004, Novoselov *et al*. obtained graphene by mechanical exfoliation of highly oriented pyrolytic graphite.[4] This method involves repeatedly sticking and peeling apart graphite flakes into thinner layers with scotch tape until single or few-layer graphene flakes are obtained on the tape, and transferring it onto a Si wafer with a thermal oxide layer. The average size of such graphene is about several micrometers. The graphene showed ballistic transport in field-effect transistors with carrier mobilities ranging from 3000 to 10,000 $cm^2V^{-1}s^{-1}$ at room temperature,[36] and the electronic characteristics of graphene can be tuned by applying a gate voltage.

This technique has also been applied to produce other 2D TMDs, such as MoS_2, WS_2, WSe_2 and $MoSe_2$. TMDs are layered compounds with three-coordinate dichalcogenides and trigonal prismatic transition-metal centers. Each layer, being 6-7 Å thick, consists of a hexagonally packed transition-metal atom layer sandwiched between two layers of dichalcogenides atoms.[21] The neighboring layers are bound by weak van der Waals force,

which facilitates the exfoliation of bulk TMDs into atomically thin 2D films. Therefore, the mechanical method has been widely used to prepare 2D TMDs for various applications.[37-39]

To date, mechanical exfoliation is the most effective way to prepare highly crystalline and lowest defective 2D materials, which makes the exfoliated 2D materials as the first choice for fundamental studies. However, mechanical exfoliation process is far from scalable and suffered from low throughput. The transfer process can also leave glue residues on 2D films. More importantly, the thickness, size and location of the peeled 2D films are largely uncontrollable and thus the exfoliation method can't be scaled up to the level of industrial production for the applications in large-size electronic devices.

2.1.2. Chemical Exfoliation

Chemical exfoliation methods were developed to exfoliate single or few-layer graphene oxide (GO) from oxidized graphite for mass-production. GO is an important graphene derivative,[40-42] which in general is synthesized by Brodie,[43] Staudenmaier,[44] Hummers method,[45] or some other variations of these methods.[46] All these methods utilized strong acids (H_2SO_4, HNO_3 or $HClO_4$) and oxidants ($KClO_3$, $NaNO_3$ or $KMnO_4$) to produce GO from graphite. GO has epoxide, carbonyl and hydroxyl groups attached to the surfaces of graphene layer, which render GO strongly hydrophilic and dispersible in many solvents, particularly in water. The resulting GO aqueous colloidal suspension can be deposited on various substrates to prepare conductive films by means of several convenient methods such as spin-coating,[47] drop-casting,[48] Langmuir-Blodgett assembly,[33] printing[41,49] or spraying.[50] GO can also be reduced by several reducing agents (hydrazine,[40] hydroquinone,[51] ascorbic acid[52]) via thermal treatment. Compared with mechanical exfoliation, chemical exfoliation provides the possibility of preparing GO or reduced graphene oxide (rGO) in relatively large quantities for scientific research as well as commercial applications. In 2008, Cote *et al*. prepared graphene nanoplates via chemical exfoliation of graphite oxide, which can be readily exfoliated as individual GO sheets by ultrasonication in water. The monolayer GO films were dispersed homogeneously on SiO_2 substrates without aggregation, and then GO sheets were reduced using hydrazine hydrate solution to obtain the graphene sheets.[41]

Although many works on chemically exfoliated TMDs have been conducted since the 1960s, a focus on the isolation of high-quality and large-quantity 2D TMDs materials was re-initiated after the discovery of graphene.[4] In a typical chemically exfoliated procedure, bulk TMDs were submerged in a solution of a lithium-containing compound such as n-butyl

lithium for more than one day to allow lithium ions to intercalate, and then the lithiated TMDs were exposed to water and separated by H_2 that evolved during the reaction of water and lithium. For example, Eda *et al.* applied n-butyl lithium dissolved in hexane as the intercalation agent to exfoliate bulk MoS_2. The lithiated MoS_2 was retrieved by filtration and washed with hexane. Then the extracted product was exfoliated by sonication in water, and a yield of almost 100% atomically thin MoS_2 was obtained.[53] Unlike chemically exfoliated graphene, 2D TMDs prepared by the lithium intercalated method remain chemically unmodified so that their fundamental electronic properties are largely preserved.

2.1.3. Liquid Phase Exfoliation

Reducing GO obtained by chemical exfoliation to graphene is relatively easy. However, rGO often shows much lower conductivity than pristine graphene because of uncompleted reduction and the presence of large defects that disrupt the graphene sp^2 network. Therefore, a new liquid phase exfoliation method was developed to obtain stable colloidal suspension of graphene sheets.[54,55] The liquid phase exfoliation process is to disperse graphite into organic solvent. The solvent molecules can interpenetrate within the graphite layers, and oxide-free graphene can then be exfoliated from graphite during sonication process. The quality of these graphene is undoubtedly higher than that of those exfoliated from graphite oxide due to the absence of oxygen in the former. For example, Hernandez *et al*. produced single or few-layer graphene through dispersion and exfoliation of pure graphite in N-methyl-pyrrolidone with the yield of 12 wt%.[55] Lotya *et al*. used the similar method to produce single or few-layer graphene by using graphite power dispersed in sodium dodecylbenzene sulfonate (SDBS).[56] Blake *et al*. reported that sonicating graphite in N,N-dimethylformamide (DMF) returned a high yield of monolayer graphene up to 50%.[57] In 2010, Behabtu *et al*. directly exfoliated single-layer graphene from graphite in chlorosulphonic acid.[58] The graphene obtained through this technique is of high quality and over 70% is single layer with few defects. The conducting films based on the graphene showed sheet resistance (R_s) of 1000 Ω/□ and transmittance of 80%.

Well-dispersed TMD nanoflakes can form high-quality films by solution coating and are useful in high-performance devices, such as transistors and solar cells. They can be easily produced in a solvent (DMF or *N*-methyl-2-pyrrolidone (NMP)) by ultrasonication.[59,60] Firstly, TMD powders are expanded by reacting with solvents in hydrothermal condition. The solvents have low energy to intercalate into TMD layers and can expand the TMD sheets by more than 100 times in their volume. Then the expanded TMDs were ultrasonicated to

produce atomically thin flakes that are water dispersible. However, a drawback of this method is the low yield of single layers.

2.1.4. Electrochemical Exfoliation

In an electrochemical exfoliation process, graphite rods were used as both anode and cathode in an electrochemical cell. A static potential of 10-20 V is added between the two electrodes. The anode graphene rod will be exfoliated into graphene sheets in the ionic liquid solution. The graphene sheets can be individually and homogeneously suspended in DMF, Dimethyl sulfoxide (DMSO) or NMP solvent without the need of further deoxidization.[59] For example, Su *et al.* demonstated a novel one-step approach of exfoliating high-quality graphene film by this electrochemical method.[60] The size of the exfoliated grahene films ranges from several up to 30 μm. A transparent conducting film was prepared by drop coating the exfoliated graphene on a glass substrate, which exhibits excellent conductivty and transparency (sheet resistance R_s = 210 Ω/□ at T ~ 96%).

The electrochemical technique can also be applied to intercalate TMDs with lithium, which is faster and more controllable compared with chemical exfoliation process. In this kind of electrochemical cell, the lithium foil and bulk TMDs were used as anode and cathode, respectively. A galvanostatic discharge was applied on two electrodes to intercalate lithium into bulk TMDs. The intercalated product was then washed and ultrasonicated to exfoliate 2D TMDs.[61]

The aforementioned exfoliation methods can produce gram or even kilogram quantities of 2D materials yet face drawbacks such as low production yield of single layer, small size of flakes, residual compounds on products and/or expensive intercalations. Therefore, alternative exfoliation methods besides the above are expected to be developed in the future.

2.2. CVD Methods

Although the mechanical exfoliation method can lead to high-quality graphene and chemical exfoliation methods can provide large quantities of graphene, the average size of graphene prepared by these methods is too small to be suitable for applications in large electronic devices. CVD is a promising and inexpensive large-area producing method for growing high-quality, large-scale and continuous graphene on transition metal substrates (Ni,[62] Cu,[63] Pt,[64] Ru,[65] or Ir[66]). The conductivity of CVD grown graphene is approximately

one order of magnitude higher than that of graphene films produced by chemical or liquid phase exfoliation methods, which makes CVD graphene more attractive for applications in high-performance optoelectronic devices. Similarly, other 2D materials can be prepared with CVD methods on solid substrates, like SiO_2.

2.2.1. Graphene Synthesis on Ni

Because Ni has high carbon solubility, carbon atoms can be dissolved in Ni at high temperature and then precipitate onto Ni surface to form single or multilayer graphene upon cooling. The first work on synthesizing large scale graphene on Ni by CVD method was reported in 2006.[67] It was estimated to have approximately 35-layer graphene, and this study opened a new processing route for graphene preparation. Later, Yu *et al*. prepared three to four-layer graphene through CVD process on Ni foils.[68] It was found that the formation of graphene on Ni occurred only under moderate cooling rates and the graphene synthesis were demolished at higher or lower cooling rates. This study provides better understanding about the growth mechanism of graphene on Ni in CVD process. In 2008, Kim *et al*, could grow high-quality graphene on patterned Ni films and transfer them on arbitrary substrates by using polydimethylsiloxane (PDMS).[62] The obtained graphene showed a transmittance of about 77% with R_s as low as 280 Ω/□. However, under the cooling process of CVD, the segregation rate of carbon from metal carbide is heterogeneous at Ni grains and grain boundaries, and the layers and homology of graphene are difficulty to be controlled. Therefore, single or few-layer graphene does not homogeneously cover the entire substrate but just in few to tens of micrometers region. In 2010, in order to improve the uniformity of graphene, Zhang *et al*. reported the formation of graphene on single-crystalline Ni (111) surface by CVD method.[69] Compared to graphene grown on polycrystalline Ni, the as-grown graphene on single-crystalline Ni (111) shows a smoother surface and more uniform thickness, micro-Raman surface mapping reveals that monolayer and bilayer graphene is 91.4%, which is much higher than the percentage on polycrystalline Ni (72.8%).

2.2.2. Graphene Synthesis on Cu

Up to now, Cu foils are the mostly used substrates for the growth of high-quality monolayer graphene films. In 2009, Li *et al*. grew large-area graphene films on Cu foils by CVD method.[63,70] The graphene films exhibited predominantly single-layer (95%) with small fractions of bilayer and few-layer graphene areas.[63] The resulted graphene transistors showed electron mobilities as high as 4050 $cm^2V^{-1}s^{-1}$. The single-layer graphene has R_s of 2.1 kΩ/□

with a transmittance of about 97% whereas the R_s of four-layer graphene is decreased to 350 kΩ/□ with a transmittance of about 90%.[70]

The growth process of graphene on Cu is different from that on Ni for the different solubility of carbon in the two metals. Cu has an ultralow solubility of carbon, and the growth mechanism of graphene on Cu is based on a catalytic process. After one or two-layer graphene is deposited, the surface of Cu will lose the catalytic properties to decompose the hydrocarbon and precipitate extra carbon on its surface, so mainly single or bi-layer graphene can be grown on polycrystalline Cu substrates.

2.2.3. Graphene Synthesis on Pt

In 2012, Gao *et al*. demonstrated the growth of high-quality and large-size graphene on Pt foil by CVD, and a bubbling method was employed to transfer graphene films from Pt to arbitrary substrates.[71] The Pt foils can be reused as catalyst with almost no limit, and the graphene obtained on a repeatedly used Pt substrate has almost the same quality as that obtained originally. More importantly, the electrochemically separated graphene showed high crystal quality with the lowest wrinkle height and the highest carrier mobilities (7100 $cm^2V^{-1}S^{-1}$) compared with the samples prepared by other transfer methods.

2.2.4. Other Bottom-up Methods

Graphene can be directly synthesized on insulating substrates,[72] which however is difficult to be transferred to other substrates. So it is suitable for wafer-based applications and has limited applications on solar cells. For example, epitaxial growth of graphene on SiC surfaces is another bottom-up approach to obtain high-quality graphene.[73,74] After the sublimation of Si on SiC surfaces at high temperature (>1000 °C), the excess carbon left behind can graphitize and form nearly perfect graphene structure on both silicon-rich face (0001) and carbon-rich face of the hexagonal phase SiC.

2.2.5. Transfer of CVD Graphene

CVD graphene grown on metal substrates must be transferred onto substrates for various applications. The transfer process of graphene films from transition metal (Ni, Cu, Pt) to target substrates will inevitably lead to cracking and introduce residual, which will influence the electrical properties of graphene. Therefore, the transfer process plays an important role in keeping the pristine properties of graphene. Two methods are often used to transfer graphene, one is wet-transfer, and another one is dry-transfer. The wet-transfer is typically done by

depositing a thin layer of PDMS or poly(methylmethacrylate) (PMMA) on top of graphene, and then etching the metal in acidic aqueous solution of $FeCl_3$ or $(NH_4)SO_8$. After that, the polymer-coated graphene can be readily obtained and is strong enough to allow handing on desired substrates.[70] Once the transfer process is completed, the polymer on graphene surface is removed by a corresponding solvent (e.g. acetone for the case of PMMA). The dry-transfer is to use a thermal release tape as the transfer polymer. Firstly, graphene deposited on a metal foil is attached on thermal tape by applying soft pressure, and then the metal foil is etched away. After that, the graphene on the tape is transferred on a target substrate, which is then heated (~ 100^{o}C) to release the thermal tape. Eventually, graphene is transferred from the tape to the target substrate. In 2010, S. Bae *et al*. have demonstrated the transfer of single layer graphene over 30-inch by this method.[75]

Apart from these main transfer routes of wet-transfer and dry-transfer, there have been attempts to transfer graphene through other techniques. One is the clean-lifting transfer method by using electrostatic force to transfer graphene on various substrates recently reported by Wang et al.[76] This method does not involve any organic residual on graphene surface and thus has great potential for future industrial production of graphene-based optoelectronic devices. Another one is the bubbling transfer method that is suitable for Pt foils. A Pt foil with the grown graphene is spin-coated with PMMA and used as a cathode in an electrochemical cell. Graphene is separated from Pt foil upon H_2 evolution by applying a constant current across the cell. This bubbling transfer technology is nondestructive not only to graphene but also to the Pt substrate, which allows for the repeated growth of graphene on Pt.[71]

The highest field-effect mobility and the lowest R_s for transferred single-layer CVD grown graphene have been reported to be 7100 $cm^2V^{-1}s^{-1}$ and 125 Ω/□ at room temperature, respectively.[18, 75,77] But in most cases, the mobilities and R_s of CVD graphene range from 300 to 5000 $cm^2V^{-1}s^{-1}$ and 600 to 3000 Ω/□, respectively.[78,79]

2.2.6. Synthesis of Other 2D materials

High-quality 2D TMDs with large areas can also be prepared by CVD methods. Unlike graphene grown on transition metal catalysts, TMDs can be directly deposited on SiO_2 or sapphire substrates using transition metal (e.g. Mo or W) and sulfur powder as the precursors.[80,81] For example, in the preparation of MoS_2, Mo thin films are firstly deposited on SiO_2 substrates by evaporation. Then the Mo/SiO_2 substrates are put into a CVD furnace

containing sulfur vapor. Vapor-solid reaction takes place at a temperature of ~750°C in an Ar environment, leading to MoS_2 film growth driven by the increase in enthalpy. After the growth, the samples will be annealed at high temperature (~1000°C) to improve the crystallinity and uniformity.

The second strategy reported for the deposition of 2D MoS_2 by CVD method is based on a thermolysis of ammonium thiomolybdates [$(NH_4)_2MoS_4$] process.[82] Firstly, $(NH_4)_2MoS_4$ dip-coated substrates (SiO_2 or sapphire) are placed into a CVD furnace to convert $(NH_4)_2MoS_4$ to MoS_2 in a gas mixture (Ar/H_2: 4/1) at a temperature of ~500°C. Then the sample is subjected to a second annealing at 1000°C in a gas mixture of Ar and sulfur as a protection gas to improve the crystallinity of MoS_2.

The third method is to use the MoO_3 and S powders as precursors to deposit 2D MoS_2 by a gas-phase reaction.[83] The MoO_3 and S powders were separately placed in CVD furnace with a SiO_2 substrate on their top. The SiO_2 substrate could be treated with aromatic molecules such as rGO, perylene-3,4,9,10-tetracarboxylic acid tetrapotassium salt (TPAS) and perylene-3,4,9,10-tetracarboxylic dianhydride (PTCDA) to promote the layer growth of MoS_2. In the growth process, MoO_3 was firstly reduced by the sulfur vapor to form volatile suboxide MoO_{3-x} at a temperature of ~650°C in an N_2 environment, and then the MoO_{3-x} diffused to the substrate and further reacted with sulfur vapor to grow MoS_2 film. These MoS_2 films produced by the above three methods can be peeled off from the SiO_2 or sapphire substrates and transferred onto arbitrary substrates with the help of PMMA and NaOH.[84]

2.3. Properties

Mobility Graphene is known to be a zero band gap semiconductor (**Fig. 1**), and shows an ambipolar conduction in its field effect transistor (FET). In 2008, charge carrier mobilities of ~ 200,000 $cm^2V^{-1}s^{-1}$ have been observed in mechanically exfoliated graphene FET,[85-87] which exceed those of semiconducting carbon nanotubes and InSb, and are the known highest mobilities for semiconductors. The high carrier mobilities make graphene potentially useful in highly conductive electrodes and high frequency electronic devices. TMDs (MoS_2, WSe_2, $MoSe_2$, WS_2) monolayers, another type of 2D materials, have direct band gaps (**Fig. 1**). In 2003, the recorded mobility of 980 $cm^2V^{-1}s^{-1}$ was obtained in a multilayer MoS_2-based FET. The MoS_2 was obtained by mechanically exfoliated method and showed an n-type semiconductor property.[39] In 2004, WSe_2 was prepared by vapor phase transport

technique (VPTT) and characterized via its FET, showing a p-type transport property with the mobility of up to 500 $cm^2V^{-1}s^{-1}$ at room temperature.[88] Although the mobilities of MoS_2 and WSe_2 are much lower than that of graphene, they are still comparable to the mobility of silicon and exceed the mobilities of amorphous silicon and organic semiconductors by 2-3 orders of magnitude. Recently, a mobility of ~250 $cm^2V^{-1}s^{-1}$ was obtained in $MoSe_2$-based FET, which was fabricated by exfoliating VPTT-$MoSe_2$ onto SiO_2 substrate and showed an ambipolar behavior.[89] Compared with that of other TMDs materials, fewer work has been reported for 2D WS_2, a mobility of ~50 $cm^2V^{-1}s^{-1}$ was recently obtained in a WS_2-based FET, which was fabricated by the same process as $MoSe_2$-based FETs.[90] 2D phosphorene (monolayer or few-layer) is a direct band gap semiconductor (1.2-1.5 eV) (**Fig. 1**), showing a p-type behavior and high carrier mobilities of up to 1000 $cm^2V^{-1}s^{-1}$ in its FETs at room temperature.[91]

Absorbance The theoretical transmittance of single-layer graphene can be calculated by the equation[25,92]:

$$T = \left(1 + \frac{\pi\alpha}{2}\right)^{-2} \approx 1 - \pi\alpha \approx 97.7\% \qquad (1)$$

where α is the fine structure constant, $\alpha = e^2/\hbar c = 1/137$. So the absorbance of single-layer graphene can be obtained by $A = 1-T = \pi\alpha = 2.3\%$. Experimentally, as shown in **Fig. 2a** and **2b**, the absorbance of mechanically exfoliated and CVD grown single-layer graphene is ~ 2.3%,[63,93] which is in excellent agreement with the theoretical result given by the above equation. Further measurements showed that single-layer graphene only reflects <0.1% of incident light over the visible spectrum.[93,94]

The absorbance of 2D TMDs (MoS_2, WSe_2, $MoSe_2$, WS_2) can be calculated by a simplified equation:

$$A = 1 - \exp(-aL) \qquad (2)$$

where A, a, L are the absorbance, absorption coefficient and thickness of the 2D film, respectively.[95] For MoS_2, a~1-1.5×$10^6$$cm^{-1}$, has an absorbance of 5-10% in a thickness of 0.65 nm, which is one order of magnitude higher than that of GaAs and Si with the same thickness. So, 2D TMDs have a great potential application for solar energy absorption and conversion.

Conductivity property The sheet resistance R_s of graphene can be calculated by the equation[96]:

$$R_S = 1/e\mu N_i N \quad (3)$$

Where μ is the carrier mobility of graphene, N_i is the carrier density in graphene, N is the number of graphene layers. It is found that the carrier density of graphene can reach $N_i = 10^{12}$ cm^{-2} after chemical doping while the carrier mobility of $\mu = 10^5$ $cm^2V^{-1}s^{-1}$ can be maintained. According to the above equation, the R_s of single layer graphene is ~62.4 Ω/□. If continuously increasing the number of graphene layers, as shown in **Fig. 2c**, we can get a graphene film with a better conductivity compared with indium tin oxide (ITO) at the same transmittance. As shown in the **Fig. 2d**, HNO_3 doped four-layer graphene with R_s of 30 Ω/□ and transmittance of 90% was obtained,[75] which makes graphene an ideal candidate for transparent electrodes. The electrical conductivities of 2D TMDs (MoS_2, WSe_2, $MoSe_2$, WS_2) are very low for their semiconducting characters (band gap: 1.5-2.0eV).[97] However, these semiconductors have high light absorbance and carrier mobilities, and could be applied as active layers or charge transport layers in solar cells.

Mechanical flexibility The 2D Young's modulus and intrinsic breaking strength of monolayer graphene have been measured to be ~340 N/m and ~42 N/m, respectively.[98] Assuming an effective monolayer graphene thickness of 0.355 nm, the corresponding 3D Young's modulus and intrinsic strength are ~1.0 TPa and ~130 Gpa, respectively, which indicated that graphene is the strongest material ever measured with atomic layer thickness. Therefore, graphene is suitable for flexible electronic devices. For monolayer MoS_2, the 2D Young's modulus and intrinsic breaking strength are ~180 N/m and ~15 N/m, respectively.[99,100] Assuming a monolayer MoS_2 thickness of 0.65 nm, the corresponding 3D Young's modulus and intrinsic strength are ~270 GPa and ~23 Gpa, respectively.

Specific surface area In theory, the surface area of single-layer graphene is 2630 m^2g^{-1}.[101,102] Recently, a surface area as high as 2150 m^2g^{-1} was obtained in chemically exfoliated graphene sheets.[103] Therefore, graphene is a promising electrode material for super-capacitors, solar cells and sensors due to the possible ability of storing high densities of ions/charge on its surface. Other 2D materials can also have high specific surface areas. For example, MoS_2 prepared through the reaction of $(NH_4)_2MoS_4$ and N_2H_4 in aqueous solution exhibits a specific surface area of 210 m^2g^{-1}.[104]

2.4. Characterization Methods

Material characterization is critical to the study of 2D materials. Today, there are a vast number of scientific methods that can be utilized to characterize graphene and other 2D materials in the following properties:

Microstructure. The surface morphology and film thicknesses can be characterized by transmission electron microscopy (TEM), scanning electron microscopy (SEM) and atomic force microscopy (AFM). Scanning Kelvin probe microscopy (SKPM) can be used to characterize the surface potential or work function distribution of 2D materials.

Optical Properties. The optical properties including transmittance and absorption of 2D materials can be measured by using UV-Vis spectrophotometer. X-ray photoelectron spectrometry (XPS) can be used to confirm the chemical components and electronic states of the elements in the graphene and other 2D materials. Some groups (nitro groups, oxygen-containing groups, *etc.*) and bonds (C-F, C-N, *etc.*) on graphene can be analyzed by Fourier transformed infrared spectroscopy (FTIR). Ultraviolet photoelectron spectroscopy (UPS) can be used to characterize the work functions of 2D materials. Raman spectroscopy is a convenient technique for deciding the number of layers or doping levels of 2D materials. In graphene Raman spectra, p (n)-type doping effect can cause the blue (red) shifts of 2D and G bands of graphene due to the influence of Fermi level on the photon frequencies of graphene.[105]

Electrical Properties. The sheet resistance R_s of 2D materials can be characterized by four-point probe apparatus. Field effect transistors (FETs) can be used to measure the carrier mobilities and the doping type (p-type or n-type) of 2D materials. In graphene FETs, the carrier mobilities of graphene can be calculated from the slope of linear regimes of the transfer curves (channel current I_{DS} vs. gate voltage V_G). The p (n)-type doping effect can be confirm when the Dirac point of graphene FET moves to a more positive (more negative) gate voltage.[106] Cyclic voltammograms (CV) and electrochemical impedance spectroscopy (EIS) can be used to analyze the electrocatalytic properties of graphene and other 2D materials.

3. Graphene Transparent Electrodes

The most important application of graphene in photovotaic devices is for transparent electrodes due to the high conductivity and transparency of graphene. In this application, some other physical properties, such as the Fermi level, carrier mobilities and the surface

properties, of graphene electrodes are also critical to the device performance, which will be addressed in details in this section.

3.1. Transparent electrodes

Transparent electrode is an essential component of modern electronic devices, such as displays, touch-panels, organic light emitting diodes (OLEDs) and photovoltaic devices. Traditionally, transparent conductive oxides (TCOs), such as ITO and fluorine-doped tin oxide (FTO),[107] play a dominant role in transparent electrodes. For example, ITO has been popularly used in OPVs as anode/cathode with transparencies of 80-90% and R_s of 10-30 Ω/□.[108] However, TCO electrodes have a number of disadvantages including high cost, fragility, fabrication in vacuum, instability toward acid or base, and poor transparency in near infrared region.[77,109,110]

The next generation optoelectronic devices require transparent electrodes to be cheap, lightweight, flexible and compatible with large-scale manufacturing methods. So many of the alternative transparent electrodes have been developed in order to replace TCO, such as metal grids,[111,112] metallic nanowires,[113,114] conductive polymers like poly(3,4-ethylenedioxythiophene): poly(styrenesulfonate) (PEDOT:PSS),[115-117] carbon nanotubes (CNTs)[118-120] and graphene films.[62,121,122] Metal grids are often prepared by photolithography with lift-off and metal evaporation processes,[121] which is challenging in preparing large-area transparent electrodes. Metal (Ag[123,124] Cu,[125] and Au[126]) nanowire transparent electrodes can be prepared by solution process and show the sheet resistance R_s less than 30 Ω/□ at transparency of ~ 90% , being comparable to that of ITO.[127] However, there are two critical issues that currently prohibit metal nanowire films for large-scale application in optoelectronic devices: (1) metal nanowire films have high surface roughness that may lead to short circuit in some devices, such as OPVs; (2) the adhesion of the films with substrates is not solid and the film can be easily removed just by adhesion or friction. Doped PEDOT:PSS with high conductivity has been used as transparent electrodes in many optoelectronic devices, like OPVs[128] and OLEDs.[129] But the stability of PEDOT:PSS upon exposure to high temperature, humidity, or UV light is a major problem for practical applications. So the environmental stability of PEDOT:PSS film must be improved before gaining widespread applications. CNTs are relatively cheap and can be deposited into large-area conductive films with various thicknesses. The transparent electrodes based on CNTs films have been used in OLEDs,[130,131] OPVs,[132] touch screens,[133] and biosensors.[134]

Although the conductivity for individual CNT is high, there is a high contact resistance at CNT-CNT junction area, which limits the conductive pathway within the whole films.

It has been demonstrated that graphene has some advantages over conventional materials for transparent electrodes owing to its outstanding electronic, optical and mechanical properties.[47,109] The comparison between them is summarized in Table I. Graphene transparent electrodes have been successfully used in touch screens,[75] liquid crystal displays,[57] memories,[135,136] photodetectors,[137,138] biosensors,[139,140] field effect transistors,[141] light-emitting diodes [96,142] and photovoltaic devices, *etc.*[101,143]

However, the carrier mobilities of graphene are dependent on its quality that is largely limited by the fabrication process. For example, the mobility of large-area graphene synthesized by CVD method is 300-5000 $cm^2V^{-1}s^{-1}$ at room temperature,[62,63,72,144] which is much lower than the theoretical value, and the sheet resistance R_s of undoped graphene is normally several kΩ/□. Therefore, the key challenge for using graphene to replace ITO in transparent electrodes is the high sheet resistance. According to equation (2), R_s of graphene could be reduced by increasing its carrier concentration, mobility, or number of layers (stacking multilayer of graphene). The carrier mobility of graphene is determined by the synthesis method and can be increased by optimizing the fabrication process. The density of charge carriers in graphene can be adjusted by shifting the Fermi level of graphene away from the Dirac point, where the carrier density is very low. There are many methods that can be used to modulate the charge carrier density in graphene, such as acidic doping,[75,145-147] electrostatic gating,[148] metal contact,[149,150] organic or polymer doping.[151-153] The modulation process can be simply classified by the type of induced carriers into n-type and p-type doping. If graphene is provided with electrons, n-type doping can be induced. Similarly, if electrons are extracted from graphene, p-type doping can be achieved.

3.2. P-type Doping in Graphene Electrodes

Because all carbon atoms of a graphene layer were exposed to the surrounding, the electrical properties of graphene are sensitive to the surface materials with which graphene are in contact.[154] Under ambient conditions, p-type transport behavior is often observed in graphene, which is usually caused by moisture, oxygen or other chemical residues introduced during the fabrication and transfer process. For example, any transfer method utilizing solution etching can easily dope graphene due to the strongly oxidizing nature of the etching, which corresponds to the decrease of the Fermi level below the Dirac point and shows a p-type doping effect. To date, in order to control p-type doping in graphene, several

approaches have been employed to modulate hole densities in graphene by means of metallic contact,[150] acid modification,[147,155] or molecule coating.[156] For example, by immersing graphene films in $AuCl_3$ or $HAuCl_4$ solution, Au nanoparticles (NPs) can be formed on the surface of graphene, which can increase the surface potential and the conductivity of graphene.[157] According to Raman spectra, the Au NPs lead to a heavy p-type doping in graphene films. It was observed that R_s of single layer graphene was decreased from 448 to 150 Ω/□, and the transmittance was only decreased for 2% after Au doping. By immersing graphene films in HNO_3 solution, HNO_3 molecules can be absorbed on the surface of graphene, which also shows a heavy p-type doping effect.[147] It is notable that high-quality 4-layer CVD graphene doped with HNO_3 show R_s of ~ 30 Ω/□ and transmittance of ~ 90% in **Fig. 2d**, which are comparable to those of ITO (R_s = 20 Ω/□, T ~ 80%).[75]

Organic materials can be used to dope graphene films as well. Lee *et al*. employed fluoropolymer both as supporting layer for graphene transfer and p-type doping layer.[158] CVD grown graphene transferred with fluropolymer exhibits an average R_s of 320 Ω/□ that is lower than R_s of graphene transferred with PMMA (650 Ω/□) due to the doping effect of fluropolymer in the former. Hsu *et al*. developed a layer by layer tetracyanoquinodimethane (TCNQ) doping process on CVD-graphene.[153] The optimized four-layer graphene with sandwiched three-layer TCNQ shows R_s of 117 Ω/□ and a transmittance of 88%. Besides normal polymers, ferroelectric polymers such as P(VDF-TrFE) were also applied as agents for doping graphene.[159,160] Large-area CVD graphene can be heavily doped by ferroelectric dipoles provided by P(VDF-TrFE) and showed a R_s of 120 Ω/□ and a transmittance of 95%. The doping effect of graphene can be tuned by changing the polarization of P(VDF-TrFE) layer.

3.3. N-type Doping in Graphene Electrodes

Due to the different requirements of electronic devices, it is necessary to obtain n-type doped graphene for logic circuits or as cathodes in photovoltaic devices. However, it is more difficult to realize n-type doping in graphene than p-type doping. For example, the substitution of carbon with nitrogen or boron atoms in graphene lattice under vacuum condition can result in n-type doped graphene, which however may increase the defect density and deteriorate the carrier mobilities of graphene.[161-163] For example, Guo *et al.* annealed ion irradiated graphene in ammonia for n-type doping.[163] Ion irradiation will introduce defect sites in graphene. After annealing in ammonia, some defects are filled by nitrogen atoms and

graphene shows n-type doping behavior. However, as shown in **Fig. 3a**, the conductivity of graphene is decreased seriously after the doping process.[161,164]

Alkali carbonate salts can also be used to realize n-type doping in graphene.[165] For example, Huang *et al*. manipulated the work function of a graphene/CNT composite film by using alkali carbonate salts (Li_2CO_3, Na_2CO_3, K_2CO_3, Rb_2CO_3, Cs_2CO_3).[166] These salts can form lots of interfacial dipoles on the surface of the composite films and the directions of the dipoles point from composite films to alkali salts, which thereby can decrease the work function of the composite films. It was found that the work function of the composite film was decreased from 5.1 to 3.4 eV after being doped by Cs_2CO_3, and these doped composite films can be used as cathodes in OPVs. However, the doping effect of alkali carbonate salts on graphene will be gradually decreased after the composite films are exposed to air.

Low work function metals can be deposited on graphene for n-type doping as well. For example, Szafranek *et al*. thermally evaporated a thin aluminum layer (1 nm) on graphene for n-type doping,[167] it was found that aluminum causes a quite strong n-type doping in graphene. The gate voltage corresponding to the Dirac point of graphene in a graphene transistor was shifted from 0 V to -42 V and the R_s of graphene was decreased from 8.7 kΩ/□ to lest than 2 kΩ/□ after depositing aluminum on the surface, as shown in **Fig. 3b**. N-type inorganic semiconductors have also been deposited on graphene for n-type doping. Ho *et al*. covered graphene with TiO_x thin films of different thicknesses for controllable n-type doping.[168] The TiO_x thin layers exhibited strong n-type doping in graphene, leading to the increase of conductivity for about 4 times and the increase of electron mobility for 2 times, as shown in **Fig. 3c**. The n-type doping effect is relatively stable, and exhibits little degradation even after 5 days of exposure in the ambient condition.

Some doping techniques involve the introduction of a dipole moment using self-assembled monolayer (SAM) polymers or molecules, such as polyethylene glycol (PEG),[169] polyvinyl alcohol (PVA)[57] and polyethylenimine (PEI),[170] poly[(9,9-bis((6′-(*N*,*N*,*N*-trimethylammonium)hexyl)-2,7-fluorene)-*alt*-(9,9-bis(2-(2-(2-methoxyethoxy)ethoxy)ethyl)-9-fluorene)) dibromide (WPF-6-oxy-F),[171] and poly(ethylene oxide) (PEO),[171] which have larger electron positivity compared to carbon atoms. These kinds of polyol and multiamino compounds can physically adsorb onto the surface of graphene and create the strong interface dipoles to shift the work function and modify the conductivity of graphene.[154] This type of noncovalent attachment of polymer on graphene is effective and simple, which is a significant way to tailor the electronic properties of graphene with little

damage on carbon lattice. For example, Blake *et al*. found that the R_s of graphene can be decreased from 6 to 0.4 kΩ/□ after PVA doping,[57] as shown in **Fig. 3d**, while the optical transmittance of graphene was not influenced.

3.4. Hybrid Graphene Electrodes

Graphene can be combined with other highly conductive materials for hybrid electrodes. For example, highly conductive metals like Au or Ag can be used to make conductive grid or net, and graphene can be transferred on the top of them to fill the uncovered area for hybrid graphene electrodes.[172] CVD-graphene/Au grid hybrid electrodes show R_s as low as 3 Ω/□ and transmittance of ~ 80%,[121] which even outperformed all reported transparent electrodes. The hybrid electrodes can be fabricated on not only rigid substrates (glass) but also flexible ones, such as poly(ethylene terephthalate) (PET), with excellent bending stability.[121] Similar cases were observed in graphene and Ag nanowire (NW) or Cu NW hybrid electrodes.[110,173-175] Moreover, highly conductive transparent electrodes can be realized by combining graphene with carbon nanotubes (CNTs) and conductive polymers.[176] For example, the composite films of rGO and CNTs have been used as transparent electrodes, which exhibited higher conductivity compared to either graphene or CNTs while maintained high transmittance. King *et al*. developed a water-based method to prepare graphene/CNTs composite films.[177] After the addition of 3 wt% graphene into CNTs solution, the direct current conductivity (σ_{DC}) to optical conductivity (σ_{OP}) ratio of the graphene/CNTs composite film was increased for 40% from 12.5 to 18, compared to that of a CNT-only film. PEDOT:PSS is the most widely explored conductive polymer,[178,179] which has much lower conductivity compared with ITO. It was found that adding graphene flakes into PEDOT:PSS can effectively improve its conductivity.[122,123,180,181] Chang *et al*. composited surfactant-modified graphene and PEDOT:PSS with different ratio and obtained transparent electrodes with the sheet resistance and transmittance of 80 Ω/□ and 79%, respectively.[180]

4. OPVs

OPVs typically with a bulk-heterojunction structure of the mixture of n-type and p-type organic semiconductors have been intensively investigated in the past decade and the reported efficiencies have exceeded 10%.[182-184] The performance of OPVs, including the open circuit voltage (V_{oc}), fill factor (*FF*), short circuit current (J_{sc}) and long-term stability, is closely related to the material properties of the electrodes, interlayers and semiconductors. As shown in Table II, it is notable that graphene has been successfully used in OPVs as many essential

parts, including transparent electrodes (anode and cathode), electron transport layers (ETLs), hole transport layers (HTLs), n-type acceptors and packaging layers, which will be addressed in more details as follows.

4.1. CVD-Graphene Anodes in OPVs

The compatibility of a graphene anode in an OPV lies on its conductivity, work function and surface properties. Pristine CVD graphene has the conductivity much lower than that of ITO and its work function (~ 4.5 eV) cannot match the highest occupied molecular orbital (HOMO) of many donor organic semiconductors (~5.0 eV), which introduces a large hole-injection barrier between graphene and the donor materials. Therefore, it is necessary to have p-type doping in graphene in its applications as anodes. Moreover, it is not easy to directly coat organic thin films on graphene due to its hydrophobic surface and thus the device design and fabrication process should be optimized.

In 2009, Wang *et al*. noncovalently modified few-layer CVD graphene with pyrene butanoic acid succidymidyl ester (PBASE) via π-π interaction in order to improve the work function of graphene.[185] The aromatic ring of PBASE has strong electron affinity, which was able to withdraw electrons from graphene to provide p-type doping. The work function of graphene films was adjusted from 4.2 to 4.7 eV after the modification, which is close to the HOMO level of PEDOT for efficient hole collection. Moreover, the hydrophilic property of graphene was also improved. The modified graphene was used as anode of OPVs with a structure of graphene/PEDOT:PSS/P3HT:PCBM/LiF/Al **(Fig 4a)**, the PCE of OPVs based on modified graphene was increased to 1.71%, which is much higher than that of a device based on unmodified graphene (η = 0.21%). In 2010, Park *et al*. found that $AuCl_3$ doping on few-layer CVD-graphene can improve the conductivity, change the work function and alter the surface wetting properties of graphene for uniform PEDOT:PSS coating.[186] The PCE of an OPV with a structure of graphene/PEDOT:PSS/copper phthalocyanine(CuPc)/C_{60}/ bathocuproine(BCP)/Ag **(Fig 4b)** was significantly improved from 0.57 to 1.63% after $AuCl_3$ doping.

To have higher conductivity, multilayer graphene can be used in transparent anodes, which however decreases the transparency of the electrodes. In 2011, Wang *et al*. prepared multilayer graphene films by layer-by-layer transfer method.[187] During transfer process, the individual graphene layers were doped by HCl to improve their conductivity. HCl-doped four-layer graphene films exhibited R_s of 80 Ω/□ with a transmittance of 90%. Then a thin layer of molybdenum oxide (MoO_3 ~ 2 nm) was evaporated on graphene to improve its work

function and hydrophilic property. The work function of graphene was improved from 4.36 to 5.47 eV after MoO_3 coating and PEDOT:PSS can be uniformly deposited on graphene, which are favorable for hole transport from PEDOT:PSS to graphene. The doped multilayer graphene was used as anodes of OPVs with a structure of graphene/MoO_3/PEDOT:PSS /P3HT:PCBM/LiF/Al, and a PCE of 2.5% was obtained, as shown in **Fig. 4c** and **4d**. In 2012, Hsu *et al*. reported a layer-by-layer organic molecular doping process in multilayer graphene anodes in OPVs.[153] Tetracyanoquinodimethane (TCNQ) molecules were thermally evaporated onto the surface of each layer, and embedded between two adjacent graphene layers. The anodes with two TCNQ layers sandwiched by three graphene layers exhibited R_s of ~140 Ω/□ and transmittance of ~90%. The OPVs based on the hybrid electrodes showed the maximum PCE of 2.58%.

In 2012, Park *et al*. introduced a vapor printing method to evaporate PEDOT film on graphene surface and used it in OPVs.[188] Compared with the poor wettability of spin-coated PEDOT:PSS on graphene, the vapor printing method can produce a complete, uniform and smooth PEDOT layer on graphene. Recently, they found that poly(3,4-ethylenedioxythiophene) -block-poly(ethylene glycol) (PEDOT:PEG) shows a better wettability on graphene compared with PEDOT:PSS.[189] So they inserted a thin PEDOT:PEG layer between the pristine graphene and PEDOT:PSS as composite buffer layer in organic solar cells. They also found that isopropyl alcohol (IPA) can be added into the PEDOT:PSS solution to tailor the wettability of PEDOT:PSS on graphene.[190] By mixing PEDOT:PSS with IPA (volume ratio is 3:1), the contact angles of PEDOT:PSS on graphene were decreased to 19.6^o, and thus PEDOT:PSS could form uniform and complete coverage on graphene surface. More recently, they employed another type of polythiophene derivative RG 1200 as hole transport layer, which has the comparable electrical and optical properties to PEDOT:PSS and good wetting capability on graphene film (contact angle: ~4.9^o).[191] RG 1200 can produce a uniform coating on graphene electrode without any additional treatment, and the resulted OPVs show similar performance to the control devices with ITO electrodes.

Thanks to its excellent mechanical strength and elasticity, graphene is a good candidate for bendable, foldable and even stretchable electrodes. In 2010, Gomez De Arco *et al*. have synthesized high-quality CVD graphene and transferred it on flexible PET substrates to fabricate flexible OPVs,[192] which showed PCEs of about 1.18%. More importantly, the flexible devices could maintain their performance under a harsh bending condition up to 138^o, while the ITO-based devices were cracked and completely failed just at the bending degree of

60 °. It was also found that the conductivity of the flexible graphene electrode was very stable even after hundreds of bending cycles. Similarly, Lee *et al*. transferred multilayer graphene on PET, doped the graphene with HNO_3 and $SOCl_2$, and obtained flexible OPVs with PCEs of about 2.5%.[193]

In 2013, our group reported the fabrication of flexible OPVs on polyimide (PI) substrates with highly doped multilayer graphene as anode and P3HT:PCBM as active layer.[194] As shown in **Fig. 5a**, the devices have the structure of graphene/PEDOT:PSS /P3HT:PCBM/ZnO/Ag/PI. One- to four-layers of CVD graphene were used in the devices. The R_s of two-layer graphene was decreased from 320 to 92 Ω/□ after the doping of PEDOT:PSS and Au NPs on the surface. The optimized OPVs showed PCEs up to 3.2% with the two-layer graphene as anode (**Fig. 5b**). Being fabricated on a thin PI substrate (thickness: 50 μm), the device showed an excellent bending stability and its PCE was decreased for only 8% relatively after 1000 times bending cycles with the curved radius of about 3 mm, as shown in **Fig. 5c**. More importantly, multilayer graphene has a package effect on the flexible OPVs, which can substantially improve the device stability in air (**Fig. 5d**). It is notable that the flexible OPVs with graphene top electrodes may not need additional packaging, which will simplify the device fabrication, enhance the flexibility and decrease the cost of the devices.

In 2013, Liu *et al*. demonstarted a fiber-shaped OPV wrapped by an Au NP-doped graphene anode.[195] The flexible fiber-shaped device can keep its PCE of about 2.5% under bending conditions. The graphene layer not only serves as a flexible transparent electrode for the fiber-shaped device, but also provides good encapsulation on the polymer layers, resulting in excellent flexibility and device stability in ambient atmosphere. In 2014, Lee *et al*. reported a "doping-transfer" method to transfer and dope graphene by PEDOT:PSS films,[196] which solves the problem of polymer residue introduced during graphene transfer. The OPVs with the PCEs of 5.5% (glass substrate) and 4.8% (flexible substrate) were fabricated by using the PEDOT:PSS-doped graphene as anode and showed excellent stability even after 2000 bending cycles on flexible substrates. Meanwhile, Kim *et al*. transferred multilayer graphene on ferroelectric polymer (P(VDF-TrFE)) for flexible OPVs,[197] in which the ferroelectric polymer has an electrostatic doping effect on graphene. The OPVs exhibited PCEs of about 2% and good mechanical flexibility.

OPVs based on polythieno[3,4-b]-thiophene/benzodithiophene:[6,6]-phenyl C_{71}-butyric acid methyl ester (PTB7: $PC_{71}BM$) can have PCEs higher than 9.2%.[183] In 2014, Park *et al.* used PEDOT:PSS-doped graphene as anode in flexible PTB7:PCBM solar cells and showed

the record PCE of 6.1%.[198] More importantly, the flexible device was extremely stable and there was no significant change in the device performance after 100 compressive flexing cycles at ~5 mm radius.

Semitransparent OPVs have been realized by using both graphene and ITO transparent electrodes.[199-201] The device can be illuminated from both sides and has some potential applications like power windows for buildings and automobiles. Lee *et al*. laminated multilayer graphene as a top electrode in a semitransparent inverted OPV,[199] as shown in **Fig. 6a**, which has the device structure of ITO/ZnO/P3HT:PCBM/GO/multilayer graphene. The semitransparent OPVs showed PCEs of 2.5% and 2% illuminated from ITO and graphene side, respectively, as shown in **Fig. 6b**.

In 2012, our group reported the use of single-layer graphene as top electrodes in semitransparent OPVs based on P3HT:PCBM,[200] as shown in **Fig. 6c**. The R_s of single-layer graphene was decreased to less than 100 Ω/□ with a transmittance of ~ 90% after the doping with Au NPs and PEDOT:PSS. The semitransparent OPVs were fabricated with single-layer graphene and ITO as the top and bottom electrodes, respectively. All of the devices exhibited higher PCEs when illuminated from graphene side due to the higher transmittance of the graphene electrodes in comparison with ITO in visible region. The PCEs up to 3% were observed in the devices illuminated from graphene electrodes, as shown in **Fig. 6d**. The influence of the active areas of the devices on the performance was also studied. When the active areas increased from 6 to 50 mm^2, the PCEs of OPVs decreased from 3% to 2.3% because of the increased series resistances. All of the semitransparent devices were very stable and showed little changes in PCEs (<5%) after 6-months storage.

4.2. rGO Anodes in OPVs

Solution processable rGO has also been widely employed in preparing transparent electrodes of OPVs because of the advantages of low cost and convenient fabrication.[202] rGO conductive films can be deposited by spin-coating, dip-coating or Langmuir-Blodgett assembly methods. There are many effective approaches for improving the dispersion and conductivity of rGO, such as chemical doping and the preparation of hybrid rGO films with other conductive materials,[176,203] which have been used in optimizing the performance of OPVs with rGO electrodes.

In 2008, Wu *et al*. prepared rGO conductive films by hydrazine reduction and thermal annealing process, and used the rGO films as anodes of OPVs with a structure of

rGO/CuPc/C_{60}/BCP/Ag.[204] The R_s and transmittance of the rGO films were measured to be 100~500 kΩ/□ and 85~95%, respectively. However, the PCEs of the OPVs were just about 0.4%, much lower than that of normal OPVs with ITO electrodes. To improve the conductivity of rGO, Su *et al*. modified a donor-acceptor complex on rGO surface using Pyrene-1-sulfonic acid sodium salt (PyS) as an electronic donor and 3,4,9,10-perylenetetracarboxylic diimide bisbenzenesulfonic acid (PDI) as an electronic acceptor.[203] For the negative charges in both molecules, the stability of aqueous dispersion of rGO was greatly enhanced. At the same time, the conductivity of the modified rGO was improved for about 100% compared with that of pristine rGO. Then OPVs with a structure of rGO/PEDOT:PSS/P3HT:PCBM/ZnO/Al were prepared on quartz substrates and PCEs up to 1.12% were achieved. Recently, Kymakis *et al*. prepared OPVs with the similar device structure and displayed the maximum PCE of ~1.1%.[205]

In 2013, Zhang *et al*. fabricated rGO mash electrodes (GMEs) by photolithography and O_2 plasma etching process using rGO solution.[206] The GMEs with different thicknesses were prepared on glass substrates for the tradeoff between the transparency and conductivity. OPVs employing GME (R_s ~ 608 Ω/□, T ~55%) as anodes and P3HT:PCBM as active layers exhibited the maximum PCE of 2.04%, as shown in **Fig. 7a** and **7b**. Recently, Yusoff *et al*. fabricated a high-performance semitransparent tandem solar cell using solution processed rGO mesh and laminated Ag NW as the transparent anode and cathode, respectively, as shown in **Fig. 7c**.[207] The transparent rGO mesh electrode, with the R_s of 521 Ω/□ and the transparency of 70%, was prepared by using standard photolithography and O_2 plasma methods. The PCEs of 8.02% and 6.47% are obtained when devices were illuminated from graphene anode and Ag NW cathode, respectively (**Fig. 7d**), which are comparable to that of tandem devices with ITO electrodes.

Flexible OPVs have been realized by using rGO transparent electrodes. In 2010, Yin *et al*. deposited rGO films on PET substrates by spin coating method and used them as transparent electrodes in flexible OPVs with a structure of rGO/PEDOT:PSS/P3HT:PCBM/TiO_2/Al.[208] The rGO film had a transmittance of 55% and R_s of 1.6 kΩ/□, and the PCEs of the devices were only 0.78%, which is much lower than that of a standard OPV with an ITO electrode due to the high R_s of the rGO films. It is notable that the device exhibited excellent mechanical flexibility and its performance was well maintained after one thousand cycles of bending.

4.3. CVD-Graphene Cathodes in OPVs

A graphene cathode in an OPV needs not only a high conductivity but also an appropriate work function that should be close to the lowest unoccupied molecular orbital (LUMO) of the n-type organic semiconductor in the device to form an Ohmic contact for the collection of electrons. However, due to physically absorbed oxygen and water during graphene fabrication and transfer process, pristine graphene often shows p-type doping with a work function (>4.5 eV) higher than the LUMO levels of normally used organic acceptors, such as PCBM (LUMO: ~ 4.2 eV). Thus, n-type doping in graphene to decrease its work function is necessary in graphene cathodes, which is addressed in more details in section 3.4.

Huang *et al*. adjusted the work functions of rGO/CNT composite electrodes by doping alkali carbonates.[166] The efficiencies of the OPVs with an inverted structure of rGO/CNT/P3HT:PCBM/V_2O_5/Al increased with the decrease of the work function of rGO/CNT cathodes and an optimized PCE of 1.27% was obtained. Jo *et al*. firstly demonstrated the application of polymer (WPF-6-oxy-F) doped graphene as cathode in OPVs with an inverted structure of graphene(WPF-6-oxy-F)/P3HT:PCBM/PEDOT:PSS/Al.[171] They found that WPF-6-oxy-F can form dipoles on the surface of graphene and decrease the work function of graphene from 4.58 to 4.25 eV, which is close to the LUMO (~ 4.2 eV) of PCBM. Thus, the built-in potential of OPVs and charge collection of graphene are all increased. The devices showed the maximum PCE of 1.23%.

In addition to the high conductivity and appropriate work function of graphene, the interface control of graphene is very important especially in its applications as bottom cathode electrode. In 2013, Park *et al*. found that spin-coating a poly(3,4-ethylenedioxythiophene) -block-poly(ethylene glycol) (PEDOT:PEG) film on graphene can change the wettability of graphene surface, then high-quality ZnO or TiO_x film can be deposited on the graphene as hole blocking layers by solution process. An inverted solar cell with P3HT:PCBM as active layer and PEDOT:PEG modified graphene as cathode was prepared and showed an efficiency of 2.27%.[189] Meanwhile, they employed PEDOT:PEG-modified three-layer graphene as a substrate for the growth of ZnO nanowires, and combined the ZnO nanowires with P3HT for hybrid solar cells **(Fig 8a)**, which showed the PCE of 0.4%.[209] In 2013, Zhang *et al*. prepared an inverted device with a structure of graphene/Al/TiO_2/P3HT:PCBM/MoO_3/Ag **(Fig 8b)** and showed a PCE of 1.59%.[210] To further improve the device performance, a layer of Au nanogrids was transferred below graphene to improve its conductivity and the optimized device with a PCE of 2.58% was obtained.

Graphene was also used in flexible OPVs as cathodes. In 2012, Shin *et al*. deposited high-quality ZnO films on CVD-graphene/polyethylene naphthalate (PEN) substrates by the mist pyrolysis CVD (MPCVD) method at a low growth temperature of 160^{o}C.[45] A flexible OPV with a PCE of 1.55% was obtained based on the ZnO/graphene electrode and P3HT:PCBM active layer. More recently, Park *et al.* discovered that zinc acetate in methanol can be unformly spin-coated on graphene for hole blocking layer without the aid of stablilizer and surfactant.[198] Then a highly efficient flexible OPV based on ZnO/graphene cathode and PTB7:$PC_{71}BM$ was fabricated on a PEN substrate, which exhibited the highest PCE of 7.1% and excellent flexibility, as shown in **Fig. 8c** and **8d**.

4.4. Graphene Interlayers in OPVs

4.4.1. Hole Transport Layers (HTLs)

In OPVs with bulk-heterojunction structures, HTLs are used to block electrons but transport holes to minimize carrier recombination.[211] An ideal HTL must be a p-type material with a wide band gap, and can play the following roles[77]: (1) To adjust the energetic barrier height between the active layer and electrode; (2) To transport holes while block electrons; (3) To enable optimum morphology of active layer; (4) To prohibit the reaction between the active layer and electrode; (5) To act as an optical spacer. Conventionally, PEDOT:PSS has been used as HTL in OPVs, which is solution processable and can minimize the detrimental effect of ITO and align the energy barrier between the active layer and ITO. OPVs with P3HT:PCBM as active layers and PEDOT:PSS as HTLs can yield PCEs close to 5%.[212] However, PEDOT:PSS is a highly acidic composite material (pH ~1) that can erode ITO electrodes and result in poor stability of OPVs. To address this issue, some inorganic materials, such as V_2O_5,[213] MoO_3[214] and NiO[215] have been used to replace PEDOT:PSS as the HTLs in OPVs, and the PCEs as high as 5% have been achieved. However, these inorganic oxides are usually deposited by cost-intensive vacuum techniques (e.g. pulsed laser deposition (PLD), thermal evaporation), which are incompatible with low-cost, solution processable and roll-to-roll processed OPVs.

Solution processable GO or rGO was found to be able to replace inorganic oxides or PEDOT:PSS as HTLs in OPVs (Table II). GO is normally deposited by neutral aqueous solution, which can avoid erosion of ITO that occurs when PEDOT:PSS is coated. Moreover, GO HTLs (2-5 nm thick) used in OPVs are much thinner and more transparent than PEDOT:PSS counterparts (40-50 nm). GO has been successfully used as HTLs in OPVs based on P3HT:PCBM and the resulted devices have shown comparable PCEs to those of the

devices with PEDOT:PSS HTLs. In 2010, Li *et al*. spin-coated ultrathin GO films on ITO for OPVs (**Fig. 9a**).[211] The 2 nm-thick GO film led to little change in the transparency of the ITO electrode. The device with a structure of ITO/GO/P3HT:PCBM/Al had an efficiency of 3.5%. More importantly, the OPV showed better stability in air than the device with a PEDOT:PSS HTL. Yun *et al*. prepared rGO by using a novel p-toluenesulfonyl hydrazide (*p*-TosNHNH$_2$) as reductant and used it as HTLs in OPVs with PCEs of ~3.6%.[216] In 2014, Liu *et al*. synthesized GO nanoribbons from single-wall CNTs and applied it as HTLs in P3HT:PCBM solar cells, showing an improved PCE of 4.14% in comparison with the aforementioned devices.[217]

GO or rGO was also used in high-efficiency OPVs with narrow bandgap polymers as HTLs.[218-220] Murray *et al*. reported the employment of solution processable GO as HTL in high-efficient OPVs based on the narrow band polymer PTB7 and PC$_{71}$BM, as shown in **Fig. 9b**.[221] The OPVs exhibited PCEs as high as 7.5% and a long lifetime in air. Recently, Yeo et al introduced a versatile rGO with sulfonic acid groups modified on its edge and basal plane.[220] The rGO was applied as HTLs in various OPVs regardless of their HOMO values, resulting in PCEs of 3.64%, 4.80%, 7.18% and 7.18% for P3HT, poly[2,3-bis-(3-octyloxyphenyl)quinoxaline-5,8-diyl-*alt*-thiophene-2,5-diyl] (TQ1), PTB7 and **(**PBDTTT-CF) based devices, respectively.

However, when the thicknesses of GO HTLs are bigger than 3 nm, the performance of the OPVs mentioned above will be rapidly decreased due to the high resistances of the GO layers. Spin-coating such a thin GO film (1-3 nm) that can fully cover the ITO surface is technically difficult. To address this issue, Kim *et al*. created a composition of GO and SWCNTs by direct mixing them in water by sonication before deposition.[222] The optimum thickness of the GO/SWCNT HTL was increased (3-4 nm) due to the increase of the conductivity and the device based on the new HTL and P3HT:PCBM active layer showed a PCE of 4.1%. In 2012, Liu *et al*. developed a sulfated GO with –OSO$_3$H groups attached to its carbon basal plane.[223] Compare with that of GO, the conductivity of GO–OSO$_3$H was much improved, leading to greatly improved *FF*s and PCEs (4.37%) in the resulted P3HT:PCBM solar cells. The performance of the device was nearly independent on the thickness of the GO–OSO$_3$H HTL over the range of 2 to 6 nm.

The composite films of GO and PEDOT:PSS were found to be excellent HTLs in OPVs.[224-226] In 2010, Yin *et al*. employed GO/PEDOT:PSS composite instead of PEDOT:PSS in normal structure OPVs.[225] The maximum PCE of the device was observed to be 3.8% at the

optimized thickness of 40 nm for the GO/PEDOT:PSS HTL, which is easier to be deposited than ultrathin GO film. Recently, Yu *et al*. homogenously dispersed GO in PEDOT:PSS solution/film by adjusting the pH of GO solution, and the GO/PEDOT:PSS composited film was used as HTL in PTB7:$PC_{71}BM$ solar cells.[226] A PCE of 8.21% was achieved, which was improved by 12% in comparison to a control device with a PEDOT:PSS HTL. In addition, many other composite films based on GO and inorganic oxides (VO_x, MoO_3) were successfully used as HTL in OPVs.[227,228] For example, Intemann *et al*. sequentially spin-coated GO and MoO_3 films as a hybrid HTL for solar cells and showed a PCE of 7.3%.[228]

GO can be spin-coated not only on ITO but also on organic active layers. Gao *et al*. spin-coated a layer of GO on top of the active layer P3HT:PCBM as HTL for inverted OPVs (**Fig. 9c**).[229] Optimized performance (η = 3.61%) was observed in the device with a thin GO (2-3 nm) HTL. It was found that the performance of the inverted OPV was not as sensitive to the thickness of GO as that of a normal OPV.[230] Later, Gao *et al*. found that GO contained high density of proton due to the presence of carboxylic acid, phenolic and enolic groups, which led to protonic doping in P3HT at GO/polymer interface.[231] After doping, the electrical conductivity of P3HT was increased by six orders of magnitude, leading to the improvement of the device performance. Recently, Mohd Yusoff *et al*. fabricated inverted OPVs with GO HTLs and PCDTBT:$PC_{70}BM$ active layers and demonstrated PCEs of 6.2% and good air stability.[232] In 2013, Chao *et al.* sequentially spin-coated two layers of GO and vanadium oxide (VO_x) as a hybrid HTL for an inverted OPV.[227] The OPV was based on PTh_4FBT:$PC_{71}BM$ active layer and showed a PCE of 6.7%.

It is noteworthy that the work function of GO HTL can influence the performance of OPVs. Yang *et al*. reported that the work function of GO was increased from 5.0 to 5.2 eV after O_2 plasma treatment. So they employed O_2 plasma treated GO as HTL in OPVs, which can more effectively block electrons and extract holes and result in an apparent increase of PCE.[233] More recently, it was reported that the work function of GO can be continuously tuned to more than 5.2 eV by photochemical chlorination or other methods,[234-236] and lead to the improvement of OPV performance. The PCEs of OPVs based on poly[(4,8-bis-(2-ethylhexyloxy)-benzo[I,2-b;4,5-b')dithiophene)-2,6-diyl-alt-(4-(2-ethylhexanoyl)-thieno[3,4-b)thiopene)-2,6-diyl) (PBTTTT-C):$PC_{71}BM$ active layers and photochlorinated GO HTLs were found to be up to 7.6%.

4.4.2. Electron Transport Layer (ETLs)

N-type doped GO can be used as ETLs in OPVs, which is a promising alternative to Ca and LiF ETLs that need to be prepared by thermal evaporation. As mentioned in section 3.4, Cs_2CO_3 can provide n-type doping in graphene, lower its work function and increase its electron density. So Cs_2CO_3 functionalized GO has been used as ETLs in OPVs.[237,238] For example, Liu *et al*. fabricated an OPV by using GO as HTL and Cs_2CO_3 functionalized GO as ETL.[237] It is found that the periphery-COOH groups in GO can be replaced by -COOCs groups through Cs_2CO_3 functionalization. After Cs_2CO_3 treatment, the work function of GO was decreased to 4.0 eV, which matches well with the LUMO level of PCBM for efficient electron extraction. Both normal and inverted OPVs were prepared and showed PCEs of 3.67% and 2.97%, respectively.

In 2013, Qu *et al*. attached PCBM on rGO via a noncovalent functionalization approach.[239] Pyrene was employed to anchor PCBM to rGO via π-π interaction, and the attached PCBM can prohibit the restacking of rGO sheets. The rGO-pyrene-PCBM was successfully applied as ETLs for P3HT:PCBM-based OPVs and the PCEs up to 3.89% were observed in the devices.

Although alkali salts such as Cs_2CO_3 can provide effective n-type doping in graphene, this kind of doping through intercalation of graphene and alkali metal often suffers from rapid degradation upon exposure to air,[168] which will limit its practical applications in OPVs. Therefore, GO or rGO was composited with other stable oxides (e.g. TiO_2, ZnO or TiO_x) for ETLs.[240-242] In 2014, Beliatis *et al*. prepared a novel hybrid ETL by chemically modifying TiO_2 or ZnO with rGO.[240] The OPVs based on PCDTBT: $PC_{71}BM$ active layer with the hybrid ZnO-rGO and TiO_2-rGO ETLs showed PCEs of 6.72% and 6.57%, respectively. Meantime, they prepared OPVs with PTB7:PCBM active layers and displayed PCEs in the range of 7.4-7.5% when using hybrid ZnO-rGO or TiO_2-rGO as ETLs.[241]

4.5. Graphene-Based Interlayers for Tandem OPVs

Tandem OPVs with stacked two or more single-junction cells can provide higher efficiency due to their accumulated V_{oc} of single cells and better light absorption in broader wavelength regions in comparison with a single-junction cell.[184] Graphene and GO films have been successfully used in tandem OPVs as interlayers that are able to collect both electrons and holes from stacked two cells.

In 2011, Tong *et al*. firstly employed multilayer CVD-graphene/MoO_3 as an interlayer in a tandem OPV, which can extract electrons and holes from the bottom and top cells.[243] Two bulk heterojunction layers P3HT:PCBM and ZnPc:C_{60} with complementary absorption were stacked together for bottom and top cells, respectively. The tandem OPVs showed high V_{oc} of about 1 V and PCE of about 2.3%.

GO/PEDOT:PSS composite can be used not only as HTLs introduced in section 4.4.1 but also as interlayers for tandem OPVs. In 2011, Tung *et al*. added small amount of GO (0.1-2 wt%) into PEDOT:PSS solution to get a sticky gel[181] which can dramatically increase the viscosity and electrical conductivity of PEDOT:PSS. Based on the sticky GO/PEDOT:PSS gel, as shown in **Fig 9d**, the tandem OPVs with two P3HT:PCBM bulk heterojunctions were fabricated by direct adhesive lamination process. The V_{oc} and PCE of the tandem OPV are 0.94 V and 4.1%, respectively. Afterwards, they composited GO with CNTs as interconnect layer for tandem OPVs using the same method.[244] Both regular and inverted tandem solar cells are all prepared with PCEs of 4.1% and 3.5%, respectively. So these kind of sticky interconnects based on GO can greatly simplify the fabrication process of organic tandem OPVs and facilitate the stacking of active layers with complementary absorption while minimize their intermixing during deposition, which could also be applied in other tandem organic electronic devices.

Recently, Chen *et al*. reported a tandem OPV with Al modified GO-Cs (cesium functionalized GO) as ETL and MoO_3 modified GO as HTL.[245] The work function of GO-Cs can be reduced to 4.0 eV after Al modification, matching well with the LUMO level of PCBM, while the work function of MoO_3 modified GO (20 nm) can be increased to 5.3 eV, matching well with HOMO level of PCDTBT. Therefore, GO-Cs/Al/GO/MoO_3 can act as an efficient interconnecting layer in tandem OPVs to achieve a significantly increased V_{oc}, reaching almost 100% of the sum of V_{oc} of the subcells.

4.6. Graphene Acceptors in OPVs

To date, the most efficient OPVs are based on the bulk heterojunction structure employing fullerene derivatives such as PCBM as electron acceptors. Recently, graphene derivatives have emerged as new electron acceptors to replace PCBM in bulk heterojunction OPVs owing to their high electron mobility and large surface area for donor/acceptor interfaces. Moreover, the composite of graphene and Poly(3-octylthiophene) (P3OT) shows remarkably reduced photoluminescence and consequently efficient charge transfer, indicating that the composite can be used in OPVs.

In 2008, Liu *et al*. firstly fabricated OPVs by using phenyl isocyanate functionalized GO as an acceptor and P3OT as a donor.[246] The best PCE of 1.4% was obtained in the devices with the optimized content of GO in the active layer. Afterwards, functionalized GO was blended with P3HT in OPVs and a PCE over 1% was obtained.[247] In 2010, Li *et al*. prepared GQDs with the sizes of 3-5 nm by an electrochemical method and used them in OPVs with the device structure of ITO/PEDOT:PSS/P3HT:GQDs/Al.[248] The LUMO level of GQDs was measured to be in the range of 4.2-4.4 eV and the HOMO level for P3HT was ~ 5.2 eV, thus the V_{oc} of the OPV was expected to be around 0.8 V, which was higher than that of an OPV based on P3HT:PCBM (V_{oc}~0.6 V). In their experiments, they observed an optimized PCE of 1.28% and a V_{oc} of 0.77 V that is close to the expected value as mentioned above.

Yu *et al*. chemically grafted CH_2OH-terminated P3HT on the carboxylic group of GO via esterification reaction and the resultant P3HT-GO sheets were soluble in many organic solvents.[249] Photoluminescence spectra showed that P3HT-GO can facilitate exciton dissociation and charge transfer, which is an advantage of using it in OPVs. Bilayer devices based on the P3HT-GO/C_{60} heterostructure were fabricated and showed 200% PCE enhancement than devices based on P3HT/C_{60}. GO can enhance electron delocalization and light absorption, and lead to large P3HT/C_{60} interface area, which are the main reasons for the PCE enhancement. Later, they grafted C_{60} on rGO sheets by lithiation reaction as electron acceptor in P3HT-based OPVs. Compared to a P3HT/C_{60} film, the absorption band of the P3HT/C_{60}-rGO film was red shifted by 18 nm, and the light absorbance in the wavelength region of 500-650 nm was increased significantly. In comparison with OPVs based on P3HT/C_{60}, J_{sc} and PCEs of P3HT/C_{60}-rGO devices were increased for about 2 times and 2.5 times, respectively, and the maximum PCE of 1.22% was obtained.[250] More recently, Mahmoudi *et al*. grafted rGO with 1-pyrenecarboxylic acid (PCA), and yielded highly soluble rGO with a high conductivity of ~ 1.52×10^5 S m^{-1}.[251] Upon incorporating rGO-PCA in active and electron transport layers of OPVs (**Fig. 10a**), the optimized PCE of the P3HT/rGO-PCA devices was 2.85%, being comparable to that of the OPVs based on P3HT:PCBM, as shown in **Fig. 10b**.

Graphene has been used as additives in OPVs with promising performance. In 2013, Jun *et al*. demonstrated an improvement of the PCE in P3HT:PCBM solar cells by incorporating charge-selective graphene flakes into the active layers.[252] The graphene flakes doped by nitrogen can provide transport pathways to specific charge carriers when mixed into the active layer of OPVs. The PCEs of the resultant devices were found to be increased significantly

from 3.2% to 4.5% after the addition. Meanwhile, Kim *et al*. added partially reduced GQDs in PTB7:$PC_{71}BM$ OPVs (**Fig. 10c**).[253] Compared with devices without GQDs, the devices showed a considerable enhancement of the light absorptivity and J_{sc}. On the other hand, due to the metallic properties of the GQDs, charge carrier extraction in the PTB7:$PC_{71}BM$ devices was also enhanced, which increased the *FF* of the devices. The PCEs of devices were thus increased from 6.7% to 7.6% for the addition of GQDs in the active layers (**Fig. 10d**).

4.7. Other 2D materials in OPVs

2D materials such as MoS_2 have tunable bandgaps (1.2 ~ 1.8eV for MoS_2) with the layer number. On the other hand, their carrier mobilities (200 ~517 $cm^2V^{-1}S^{-1}$ for MoS_2) are much higher than organic semiconductors.[39,254] Therefore, many 2D materials are considered to be good candidates for photovoltaic applications. For example, n-type 2D materials have been used to replace PCBM to combine P3HT for bulk heterojunction solar cells.[255,256] Shanmugam *et al.* prepared MoS_2 nanoflakes by ultrasonicating MoS_2 small crystals in acetonitrile and combined them with TiO_2 and P3HT as active layers in OPVs.[255] The device with a structure of ITO/TiO_2/MoS_2:P3HT/Au exhibited J_{sc} and PCE of 4.7 mA/cm^2 and 1.3%, respectively. More recently, they prepared TiO_2/WS_2/P3HT solar cells by the same method and showed improved J_{sc} and PCE of 7.1mA/cm^2 and 2.6%, respectively.[256]

Some TMDs, including MoS_2,[35,257,258] WS_2,[259] $NbSe_2$[260] and TaS_2,[261] have been used as interlayers (HTLs or ETLs) in OPVs. Ibrahem *et al.* prepared 2D MoS_2 and WS_2 nanosheets and used as ETLs in OPVs.[262] The solar cells with MoS_2 and WS_2 ETLs exhibited PCEs of 3.35% and 2.98%, respectively, and good stability in air. Meanwhile, Yun *et al.* modulated the work function of MoS_2 and successfully used p- and n-type doped MoS_2 films as HTL and ETL in OPVs, respectively.[263] More recently, Gu *et al.* prepared MoS_2 nanosheets by chemical exfoliation and used as HTLs in OPVs based on PTB7:PCBM, as shown in **Fig. 11**.[35] The MoS_2 nanosheets have surface dipoles that are favor for charge extraction and can suppress charge recombination. The resulted devices showed an average PCE of 8.11%, a little bit higher than that of a standard OPV with a PEDOT:PSS HTLs.

$NbSe_2$ nanosheets prepared by chemical exfoliation are chemically inert and have few trap states. The work function of $NbSe_2$ is also tunable in the range of 4.4-5.9 eV depending on the layer number.[260] $NbSe_2$ was found to be an ideal candidate material for HTLs in OPVs and its surface dipoles were favorable for charge extraction in OPVs.[260] The maximum PCE of 8.1% was achieved in OPVs with PTB7:PCBM as active layer and $NbSe_2$ as HTL.

TaS_2 has the similar structure to MoS_2 and WS_2, consisting of a hexagonally packed Ta atomic layer sandwiched between two layers of S atoms. It was reported that TaS_2 has a low electrical resistivity of 10^{-3} Ω cm, which is much lower than that of MoS_2 (18 Ω cm) and WS_2 (0.1 Ω cm).[261] TaS_2 was found to be promising in the applications as charge transport layers in OPVs. Recently, Le *et al.* prepared TaS_2 nanosheets by a sonication-based exfoliation method.[261] The TaS_2 was treated by UV-ozone, resulting in an increase of the work function from 4.4 to 4.96 eV. The pristine and UV-ozone treated TaS_2 films were used as ETL and HTL in P3HT:PCBM OPVs and exhibited PCEs of 2.73% and 3.06%, respectively.

4.8. Graphene Barrier Films for OPVs

Besides efficiency, the stability and lifetime of OPVs are also important for their practical applications. However, the performance of unpackaged OPVs normally degrades rapidly under ambient conditions due to the instability of conjugated polymers. So the encapsulation of the devices is critical to maintain their performance. Since graphene is very stable and almost impermeable to all gases and moisture, it is a promising encapsulation material for OPVs or other optoelectronic devices that are sensitive to their ambient environment.[16,264,265] As mentioned in section 4.1, our group found that multilayer CVD graphene is impermeable to air and can be applied as air barrier to package the OPVs.[131] More recently, H. Yamaguchi *et al*. reported a lifetime increase of 1300 h for OPVs with the structure of ITO/MoO_3/P3HT:PCBM/Al encapsulated by a uniform and continuous rGO film (10 nm), which was attributed to the close interlayer packing and the absence of pinholes within the impermeable rGO sheets.[266] The normalized PCE of the rGO-encapsulated OPV was 20% higher than that of device without the encapsulation over the period of 50 h. Similarly, Kim *et al*. directly spin-coated a rGO film on an OPV based on PCDTBT:PCBM as a environment barrier.[267] The lifetime of the device was increased by 50% over that of the control device without rGO.

5. Schottky Junction and Other Junction Solar Cells

5.1 Graphene in Schottky Junction Solar cells

A Schottky junction solar cell is an alternative structure for solar cell for its simple design, low cost and easy fabrication process. Compared to metal or ITO electrodes conventionally used in Schottky junction solar cells, CVD graphene electrodes have the advantages of low cost, easy fabrication, high transparency and mechanical flexibility.[268] Therefore, in the past several years, larger-scale highly transparent graphene has been transferred on n-type silicon (n-Si) as transparent electrodes to build Schottky junction solar

cells (Table III). In 2010, Li *et al*. firstly reported such as a Schottky junction solar cell with PCEs up to 1.5% (**Fig. 12a**).[269] The CVD-graphene served as not only transparent electrodes but also anti-reflection coating layers (reduced 70% reflection) in the devices. However, the efficiencies of the devices were much lower than that of a typical Schottky junction solar cell. Afterwards, in order to further improve the device performance, Fan *et al*. replaced planer Si substrate with silicon nanowires (SiNW).[270] The graphene/SiNW junction had enhanced light trapping and faster carrier transport compared to the device with planar Si and showed PCEs up to 2.86%. Similar efficiencies (~2.9%) of the devices based on graphene/silicon-pillar-array were reported by Feng *et al*. as well.[271]

The performance of graphene/Si Schottky junction solar cells can be dramatically improved by doping the graphene layer, which will not only reduce series resistance of the device but also enhance its built-in potential. So far, various materials have been employed for doping graphene, such as Boron,[272] HNO_3,[269,271,273-277] $SOCl_2$,[278] $AuCl_3$[279] and 1-pyrenecarboxylic acid (PCA),[251] Bis(trifluoromethanesulfonyl) amide (TFSA).[280,281] In 2013, Lin *et al.* doped graphene by HNO_3, and transferred on pillar silicon for graphene/Si Schottky solar cells (**Fig. 12b**). The pillar silicon can reduce 20% light reflectance. Compared with device with undoped graphene, the series resistance of device doped by HNO_3 was decreased from 120 to 20 Ω cm^2. The Schottky junction solar cell based on the HNO_3 doped graphene and silicon pillar exhibits an efficiency of up to 7.7%.[273] Li *et al*. directly synthesized multilayer graphene (MLG) by atmospheric pressure CVD (APCVD) method. The MLG film showed a R_s of ~ 500 Ω/□ and transparency of ~ 84% and the PCE of the corresponding solar cell was 4.98%.[282] Then the device was exposed to the vapor of nitric acid for doping, which decreased the R_s of MLG film from ~ 500 to ~ 200 Ω/□ and nearly doubled PCEs of devices from 4.98% to 9.63%. They also compared the effects of $SOCl_2$-doping and HNO_3-doping on graphene and showed the PCEs of 8.94% and 9.27%, respectively.[283] Recently, Miao *et al*. doped graphene in graphene/Si Schottky junction solar cells by TFAS (**Fig. 12c**),[281] which can increase the carrier density of graphene and decrease the series resistance of the devices. In addition, V_{oc} of the devices were improved due to the increases of the built-in potentials at the junctions. As a result, TFSA doping gave rise to 3-5 times increases in PCEs of the devices (from 1.9% to 8.6%), as shown in **Fig. 12d**.

Recently, Xie *et al*. demonstrated the effect of surface modification of Si on the performance of graphene/Si Schottky junction devices.[284] They found that methylation on Si could suppress the surface recombination and tune the energy alignment near Si surface,[285]

which led to a remarkable improvement of device efficiency. Carrier recombination was further reduced by inserting a 10 nm P3HT layer between graphene and Si to prevent the transfer of electrons from n-Si to graphene anode so as to minimize the current leakage, as shown in **Fig. 13a**. These methods, along with acid doping process, gave rise to a PCE as high as 10.56% (**Fig. 13b**). Afterwards, they replaced planer Si with Si nanoarrays (SiNAs) in the devices.[286,287] The SiNAs provided a lower reflectance and a larger Schottky junction area and enhanced the light absorption and J_{sc} of the devices.

Meanwhile, Shi *et al*. reported a novel graphene/Si Schottky junction device involving an antireflection TiO_2 layer on HNO_3-doped graphene surface by a simple spin-coating process,[288] as shown in **Fig. 13c**. After spin-coating the TiO_2 layer, more than 30% reflected light was reduced. Consequently, the J_{sc} of the TiO_2/graphene/Si Schottky junction device was increased for 30% from 23.9 to 32.5 mA/cm^2 and the PCE was increased from 8.9% to 14.5% (**Fig. 13d**), which is the highest reported value for graphene/Si Schottky junction solar cells to date. However, they noticed that the doping in graphene by volatile acid (HNO_3) was unstable and the device performance degraded after the loss of acid, which was a major problem in practical applications.

More recently, Yang *et al*. demonstrated a new structure of graphene/Si Schottky junction solar cells by introducing a GO interlayer to engineer the graphene/Si interface.[289] They found that the GO interlayer could effectively increase V_{oc} and meanwhile suppress the interface recombination of the solar cells. An optimized PCE of 6.18% was achieved for the graphene/GO/Si solar cells with undoped monolayer graphene as top electrodes. In the meantime, Jiao *et al*. demonstrated a Schottky junction solar cell with the structure of TiO_2/graphene/GO/Si.[290] The GO film was used as an interface tailor and hole-extraction material, which led to a dramatic improvement of the device PCE by >100%. The device with HNO_3-doped graphene electrode, GO interlayer and TiO_2 antireflection coating showed the highest PCEs of 12.3%.

Graphene was also combined with inorganic nanomaterials for Schottky junction solar cells. For example, Ye *et al*. patterned graphene by ultraviolet lithography and lift-off process, then the patterned graphene was combined with CdS NWs[291] or CdSe nanobelts (NBs)[292]. The CdS NWs/graphene and CdSe NBs/graphene Schottky junction solar cells with the sizes of ~100 μm^2 showed the PCEs of 1.65% and 1.25%, respectively, which may find some applications in nano-photoelectronic systems to provide electricity.

In summary, these results demonstrated that CVD-graphene is a promising material for transparent electrodes in Schottky junction solar cells. However, effective and stable doping techniques for the graphene electrodes should be further developed to improve the device performance for practical applications.

5.2 Other 2D Materials in Schottky Junction Solar Cells

It has been reported that 2D TMDs (MoS_2 and WS_2) can absorb up to 5-10% of incident sunlight at the thickness of less than 1 nm, which is one order of magnitude higher than the light absorption of GaAs and silicon.[95,293] Therefore, MoS_2 and WS_2 have been successfully used in Schottky junction solar cells as photoactive layers. For example, Shanmugam *et al.* demonstrated Schottky junction solar cells by depositing CVD grown MoS_2 or WS_2 films on ITO substrates as photoactive layers.[294] The devices showed PCEs of ~1.8% and effective photon absorption in the wavelength range of 350-900 nm. Ultrathin Schottky junction solar cells can also be prepared based on graphene and TMDs. For example, MoS_2/graphene monolayer-based solar cells have been reported as the thinnest solar cells with ultrahigh power densities per kilogram.[95] These devices have ~1 nm thick active layers and can attain PCEs of ~ 1%. Despite the relatively low efficiency compared to GaAs and Si solar cells with thicker active layers (> 1μm), the power densities per kilogram of these ultrathin devices are up to 2.5 MW/kg, which is approximately 1-3 orders of magnitude higher than that of the best existing thin-film photovoltaic cells. Obviously, for such ultrathin solar cells, much higher efficiency could be observed in the devices with multilayer stacked films. With the same structure of graphene/Si Schottky junction devices, more recently, Tsai et al. reported photovoltaic devices with CVD MoS_2 monolayer on p-type silicon (p-Si) substrates (**Fig. 14a**, **14b**), giving rise to a short circuit current of 23.36 mA/cm^2 (**Fig. 14c**) and an efficiency of 5.23%.[295] The MoS_2 monolayer could absorb light and show significant contribution in the EQE spectrum of the device below 680 nm (**Fig. 14d**).

Cobalt sulfide (CoS), another transition-metal chalcogenide with a high conductivity, has been successfully used in many kinds of energy devices.[296,297] Fang *et al.* demonstrated that 2D CoS nanosheets can dramatically enhance the PCEs of Si/PEDOT:PSS Schottky junction solar cells from 9.5% to 11.2%.[298] CoS nanosheets can lead to increased conductivity and higher work function level of PEDOT:PSS films, which will enhance the hole transport and increase the built-in potential in the Si/PEDOT:PSS devices, respectively. Meanwhile, it was found that charge recombination in the devices was suppressed in the presence of CoS nanosheets. It is notable that the study on this area is just started. With the development of 2D

materials in synthesis and functionalization techniques, much higher performance of the solar cells based on 2D materials is expected in the near future.

5.3 2D Materials in *p-n* Junction or Heterojunction Photovoltaic Devices

p-n junctions are essential building blocks for traditional silicon solar cells and organic solar cells. In the former devices, *p*- and *n*-type silicon regions are formed by phosphorous and boron doping, respectively. In the latter devices, p- and n-type regions are formed by using p-type polymers and n-type small molecules. Most recently, *p-n* junctions based on 2D materials such as graphene and TMDs have been prepared for optoelectronic applications due to their great potential for flexible and semitransparent devices. Graphene *p-n* junctions can be fabricated by proving p- and n-type doping on its different parts. However, these junctions cannot exhibit diode-like rectification behavior and high photovoltaic performance due to the zero bandgap of graphene.[299,300] So it is more suitable to choose other semiconducting 2D materials, such as black phosphorus, which has a tunable direct bandgap from 1.51 eV for monolayer to 0.3 eV for bulk. Recently, Buscema *et al.* transferred hexagonal boron nitride (h-BN) and few-layer black phosphorus on a pair of gates as dielectric and *p-n* junction layers, respectively.[301] The gates were used to control the charge carrier types (p- and n-type) in different regions of black phosphorus. Other two electrodes were deposited on the black phosphorus layer as source and drain electrodes for measurements. The black phosphorus *p-n* junction device showed an ideality factor of 1.96 and a current modulation of more than 10^4. A significant photocurrent and open circuit voltage were also observed due to the photovoltaic effect of the *p-n* junction, leading to the maximum EQE of 0.1% at 640 nm and energy harvesting up to the near-infrared region.

Although the bulk TMDs are indirect semiconductors, their monolayers normally exhibit direct bandgaps that fulfill the requirement for *p-n* junction photovoltaic devices. It has been demonstrated that combining monolayer TMDs with a lateral *p-n* junction architecture by electrostatic doping could also lead to electrically tunable photovoltaic effects (**Fig. 15a**). For example, Baugher *et al.* demonstrated an electrically tunable lateral *p-n* junction based on mechanically exfoliated monolayer WSe_2.[302] As shown in **Fig. 15b**, the junction shows a strongly rectified current with an ideality factor of 1.9 and a rectification ratio of 10^5, which is also direction selectable through independently reversing the voltages of two gates (± 10V). A bias voltage is applied between source and drain to measure the photoresponse of the WSe_2 *p-n* junction. At high bias, the junction produces a large photocurrent with a responsivity of 210 mA/W. At low bias, the junction generates electric

power via the photovoltaic effect, with a peak EQE of 0.2% at 522 nm (**Fig. 15c**, **15d**). Meanwhile, a WSe_2 *p-n* junction with the similar device structure was prepared by Pospischil *et al.*, by applying higher opposite gate voltages (± 40 V), the *p-n* junction device shows an ideality factor of 2.6 and a PCE of ~ 0.5%, which is comparable to that reported for bulk WSe_2 *p-n* junctions (η ~ 0.1-0.5%).[303]

Deng *et al.* demonstrated a gate-tunable *p-n* heterojunction based on a *p*-type black phosphorus and *n*-type monolayer MoS_2.[304] The heterojunction shows a maximum rectification ratio of ~10^5 under back gate voltage of -30 V, the maximum responsivity of 418 mA/W and an EQE of 0.3% at wavelength of 633 nm. These *p-n* junction or heterojunction photovoltaic devices mentioned above can be operated by electrostatically controlling the doping in 2D semiconductors. However, an extra electric power needs to be applied when they are used as photovoltaic devices, which is unpractical for real applications.

2D TMD heterojunctions have recently emerged as a new class of structures for novel optoelectronic and photovoltaic applications, because the photoexcited excitons in TMD heterojunctions can transfer very fast, which will facilitate efficient electron-hole separation for light detection and harvesting.[305] Cheng *et al.* vertically stacked *p*-type monolayer WSe_2 and *n*-type few-layer MoS_2 for a *p-n* heterojunction, as shown in **Fig. 16a**.[306] The monolayer WSe_2 was prepared by a CVD method on a Si/SiO_2 substrate, then a MoS_2 flake was exfoliated onto the WSe_2 film by mechanical exfoliation. The scanning photocurrent measurement shows that the *p-n* heterojunction was formed over the entire overlapping region of WSe_2 and MoS_2 with a maximum EQE of 12% (**Fig. 16b**). Meanwhile, Lee *et al.* fabricated the graphene sandwiched *p*-WSe_2 /*n*-MoS_2 heterojunctions with different layer numbers.[34] The measured EQEs at 532 nm were 2.4%, 12% and 34% for monolayer, bilayer and multilayer WSe_2/MoS_2 heterojunctions, respectively. The spectral photoresponse indicated that both WSe_2 and MoS_2 layers generate excitons and have contributions to the photocurrent. Similarly, Wi *et al.* reported a *p-n* heterojunction type MoS_2 photovoltaic device with a structure of ITO/pristine MoS_2/plasma-doped MoS_2/Au, as shown in **Fig. 16c**.[307] The pristine and plasma treated multilayer MoS_2 flakes (10-140 nm) were prepared by exfoliating bulk MoS_2 ingot. The photovoltaic device based on the whole MoS_2 active layer exhibited a PCE of 2.8% and J_{sc} of 20.9 mA/cm^2 (**Fig. 16d**).

So far, the 2D based *p-n* junction or heterojunction photovoltaic devices with small sizes were often prepared by mechanical exfoliation of monolayer or multilayer from their bulk counterparts, and show low photovoltaic efficiencies. Therefore, the growth of

large-scale and high quality 2D materials is urgently required for the realization of 2D-based photovoltaic devices with a larger size and higher efficiency.

6. DSSCs

DSSC, a type of thin-film solar cell, is normally based on a semiconductor (e.g. TiO_2) modified with photosensitive dye and an electrolyte.[308] DSSCs have received much attention because of their low cost, convenient manufacturing process, and comparable efficiency to polycrystalline silicon solar cells. However, the high cost of platinum-based counter electrodes (Pt-CEs) and FTO-based transparent electrodes normally used in DSSCs are obstacles to the commercialization of this technology.[309] Thus, it is necessary to explore new electrode materials to replace FTO and noble metals. Recently, much progress has been made in the applications of graphene in photoanodes and CEs in DSSCs.[310] The graphene-based electrodes have shown many advantages, including high transparency, large specific surface area, high conductivity, and remarkable flexibility, over conventional electrodes used in DSSCs. The performance of DSSCs based on graphene electrodes reported recently is summarized in Table III.

6.1. Graphene Photoanodes

The application of graphene as photoanodes in DSSCs has been studied since 2008. Wang *et al*. firstly revealed the possibility of employing rGO as photoanodes in DSSCs (**Fig. 17a**).[107] The rGO electrode was prepared by dip coating aqueous rGO on a quartz substrate, which exhibited a transparency of ~60% in the wavelength range from 500 to 3000 nm and a conductivity of 550 S/cm. However, the DSSC showed a PCE of only 0.26% due to the low conductivity of the rGO electrode. Therefore, the rGO film cannot replace FTO as a photoanode for high-performance DSSC. On the other hand, due to its high electron mobility, high transparency and large specific surface area, graphene can be incorporated into TiO_2 matrix to enhance electron transport and reduce charge recombination in DSSCs, leading to improved device performance.[311-313] For example, Yang *et al*. composited rGO with TiO_2 nanoparticles as the photoanodes for DSSCs,[314] as shown in **Fig. 17b**. The J_{sc} and PCE (η = 6.97%) of the devices were increased by 45% and 39% compared with that of the device with pure TiO_2 (η = 5.01%). In 2014, Liu *et al*. uniformly composited graphene with TiO_2 nanoparticles as photoanodes for DSSCs.[315] After thermal treatment at 400 ^oC for several hours, the interface between graphene and TiO_2 was well formed. The device showed a PCE of 8.25%, which was increased by 65% in comparison with that of a device with TiO_2 only.

6.2. Graphene Counter Electrodes (CEs)

In DSSCs, CEs play an important role of injecting electrons into electrolytes and restoring the redox couple (from I_3^- to I^-). An ideal CE should simultaneously possess both high conductivity and considerable electrochemical activity.[316] Conventional CEs used in DSSCs are made of Pt, which possesses superior catalytic activity and high conductivity. However, Pt-CEs are unsuitable for mass production of DSSCs due to the scarce source and high cost. Carbonaceous materials, such as carbon black,[317] carbon nanofibers,[318,319] carbon nanotubes,[320,321] and mesoporous carbon,[322] were under intensive investigations in recent years for their low cost and high electrical conductivity and catalytic activity. Compared with the conventional carbonaceous materials, graphene and its derivatives show much better optical transparency and mechanical flexibility and have thus attracted much research interests in replacing Pt as CE.

rGO has been successfully used as CE in DSSC (Table III). In 2008, Xu *et al*. spin-coated 1-pyrenebutyrate functionalized rGO on FTO as CE in DSSC.[323] However, the devices showed PCEs of only 2.2%, which was much lower than that of a control device with Pt-CE due to the high R_s of the functionalized rGO. In order to improve the performance of DSSCs, Hong *et al*. have composited rGO with PEDOT:PSS as CE for DSSC, which showed higher PCEs up to 4.5%.[324]

Graphene CEs with 3D structures that possess large specific surface areas have been successfully used in DSSCs. In 2011, Zhang *et al*. screen-printed rGO dispersion onto FTO as CEs for DSSCs, as shown in **Fig. 17c**. The annealed rGO film presented an unusual 3D network structure.[325] It was found that the special 3D structure was beneficial for charge transfer at the electrode-electrolyte interface due to the enlarged effective reaction area. DSSCs with the 3D rGO CEs showed PCEs of 6.81%, being comparable to that of a control device with Pt-CE (η = 7.59%), as shown in **Fig. 17d**. In 2012, Lee *et al*. reported the use of CVD grown 3D graphene as CE in DSSC and showed a PCE of 5.2%.[326] Recently, Wang *et al*. synthesized graphene sheets with a 3D honeycomb-like structure by a simple reaction between Li_2O and CO.[327] These graphene sheets exhibited excellent catalytic activity as CEs of DSSCs and PCEs as high as 7.8% were achieved. In 2014, Wei *et al*. synthesized a 3D cauliflower fungus like graphene (CFG) by reaction between Li liquid and CO_2 gas.[328] The CFG showed high conductivity and catalytic activity, and excellent performance as CE for DSSC, leading to a PCE as high as 8.1%, which is much higher than that of the first DSSC

with a regular graphene CE reported by Xu et al.[323] and even better than that of the DSSCs with Pt-CEs.

In order to improve the conductivity of graphene-based CEs of DSSCs, graphene has been combined with some other conductive materials such as CNTs,[329,330] Pt NPs,[331,332] Ni NPs[333,334] and Ag NPs[335] for hybrid CEs. For example, Yang *et al*. composite rGO with CNTs and used as hybrid CEs of DSSCs, in which CNTs can bridge graphene flakes to increase the conductivity of the electrodes.[336] The DSSCs with rGO/CNT hybrid CEs showed PCEs up to 8.23%. In 2014, Yeh *et al*. synthesized Pt NPs (2-5 nm) on graphene by using a polyol reduction method.[331] The graphene/Pt NPs hybrid films with different amounts (10-60%) of Pt NPs were perpared and used as CEs of DSSCs. The electrochemical impedance spectroscopy (EIS) and cyclic voltammetry (CV) analysis revealed that the Pt NPs on graphene actually decreased the charge-transfer resistance at the CE/electrolyte interface and increased the electrocatalytic activity of graphene. The DSSCs with the graphene/Pt NPs (20%) CE showed the highest PCE of 8.79%. Meanwhile, Bi *et al*. synthesized a novel quasi core-shell structure of cobalt sulfide (CoS)/N-doped graphene (NG),[337] which showed high catalytic activity and conductivity owing to the close interactions between the core (CoS) and the shell (NG). The DSSCs based on the core-shell CoS/NG CEs showed PCE of 10.7%, which is the highest reported efficiency for DSSCs based on Pt-free CEs so far.

Another method for improving the performance of DSSCs based on graphene CEs is to enhance the electrochemical catalytic activity of graphene. So far, various approaches have been developed. One method is to introduce oxygen-containing functional groups in graphene (**Fig. 18a)**.[338-340] For example, Roy-Mayhew *et al*. found that the catalytic activity of graphene increased with the increasing density of oxygen-containing groups.[339] However, the conductivity of graphene was decreased dramatically when oxygen content is too high. Later, Das *et al*. covalently attached C-OH, C(O)OH and NO^{3-} moieties on graphene by using HNO_3.[340] The covalently attached groups can cause the enrichment of the electrocatalytic active sites and facilitate charge transfer from graphene CE to redox couples.

The second approach is to dope or codope heteroatoms (N,[341,342] B,[343,344] S,[345] F[346]) into graphene basal plane, which may lead to less damage in the conductivity of graphene. Xue *et al*. prepared 3D N-doped graphene foams (N-GFs) and used them as metal-free CE in DSSCs.[347] N atoms were introduced by annealing the freeze-dried graphene oxide foams (GOF) in ammonia, as shown in **Fig. 18b**, which can enhance the catalytic activity of graphene and meanwhile maintain its conductivity. The DSSCs with N-GFs CEs showed

PCEs as high as 7.07 %, being comparable to that of a DSSC with a Pt-CE (η = 7.44%) and much higher than that of a device with an undoped graphene electrode (η = 4.84%). Similar results were reported by other research groups.[348, 349]

The third method is to decorate graphene by nitrogen-containing polyelectrolyte. In 2013, Xu *et al*. reported a layer-by-layer (LBL) assembling technique to fabricate poly(diallydimethylammonium chloride) (PDDA) decorated GO thin films,[350] as shown in **Fig. 18c**. The electrostatic interaction between the quaternary N of PDDA and COO^- like groups of GO would render GO-based CEs high catalytic activities toward the reduction of I_3^-. DSSCs with CEs of PDDA decorated GO exhibited PCEs up to 9.54 % (**Fig. 18d**), which is even higher than that of a control device with a Pt electrode (η = 9.14%). The considerable enhancement in PCE of the DSSCs was mainly attributed to the high electrochemical catalytic activities of GO arisen from the electron-withdrawing ability of PDDA.

The above DSSCs are mostly based on redox electrolytes with I_3^-/I^-, which have low redox potential of ca. 0.35 V vs standard hydrogen electrode (SHE), and have some disadvantages such as low V_{oc}, visible light absorption and corrosive effects with some metals.[351,352] Although I_3^-/I^- is the dominant redox couple in typical DSSCs, the PCEs of DSSCs based on I_3^-/I^- are often less than 10%.[353] Another redox system $Co(bpy)_3^{3+/2+}$ with a redox potential of ca. 0.56V vs SHE has been explored for DSSCs, which showed PCEs up to 12.3%.[354,355] Graphene-based CEs have been confirmed to have superior catalytic activities towards $Co(bpy)_3^{3+/2+}$ redox couples.[356-358] In 2011, Kavan *et al*. employed solution processable graphene CEs in such DSSCs and found that the graphene electrodes had better electrocatalytic activity to $Co(bpy)_3^{3+/2+}$ redox in comparison with a Pt electrode, which could be attributable to the lower charge transfer resistance (R_{CT}) at the graphene/electrolyte interface (graphene-CE: 3.3 Ωcm^2, Pt-CE: 5.5Ωcm^2).[357] The resulted DSSC showed a higher PCE (η = 9.4%) than that of a device with a standard Pt-CEs (η = 8.2%). Similar results were recently reported by Ju *et al*., who used nitrogen-doped graphene nanoplatelets film as CEs in DSSCs and obtained the PCEs higher than 10%.[359,360] Meanwhile, they prepared edge-carboxylated graphene nanoplatelets (ECGNPs) by the simple and eco-friendly ball-milling of graphite.[361] They found that ECGNP (R_{CT}: 0.87 Ωcm^2) has higher catalytic activity to $Co(bpy)_3^{3+/2+}$ redox couple than other materials such as Pt (R_{CT}: 2.19 Ωcm^2), rGO (R_{CT}: 1.21 Ωcm^2) and PEDOT:PSS (R_{CT}: 2.63 Ωcm^2). Furthermore, the ECGNP CE exhibited better electrochemical stability under prolonged cycling potential than that of the Pt, rGO and PEDOT:PSS counterparts.

In addition, semitransparent DSSCs that could be illuminated from both front and rear sides have been prepared by using graphene CEs. For example, Dao *et al*. synthesized Pt NPs (1-2.5 nm) on CVD grown graphene by using dry plasma reduction method near room temperature under atmospheric pressure, which has a transmittance of ~ 80%.[362] The DSSC with the Pt NPs/graphene electrode showed the PCEs of 6.55% and 5.17% illuminated from front and rear sides, respectively. Similarly, Shih *et al*. prepared a hybrid film by synthesizing Pt NPs (4-10 nm) on graphene nanoplatelets and used as CEs in DSSC, which showed PCEs of 8.0% and 7.0% from front and rear sides, respectively.[363]

Being similar to OPVs, graphene has been successfully used in flexible DSSCs. The composites of graphene with polymers[364] or carbon nanotubes[365], and graphene fibers[366] or ribbons[367] have been reported as flexible CEs in DSSCs. Lee *et al*. have prepared a flexible CE by spin-coating PEDOT:PSS on graphene/PET substrate, which showed not only superior electrochemical activity but also excellent conductivity,[364] as shown in **Fig. 18e**. Moreover, the flexible DSSCs showed excellent performance even under bending conditions. In 2011, Li *et al*. prepared an all-carbon electrode by growing vertically aligned carbon nanotubes on a free-standing graphene paper, which resulted in a PCE of 6.05% in the device.[365] More recently, Yang *et al*. have developed a novel wire-shaped DSSC with a graphene fiber electrodeposited with Pt NPs as a CE and a titanium wire impregnated with titania nanotubes as a working electrode (**Fig. 18f**).[366] The graphene fiber exhibited high flexibility, mechanical strength (10^2-10^3 MPa) and electrical conductivity (10^2-10^3 Scm^{-1}), which resulted in the recorded PCE of 8.45% for fiber-shaped DSSCs.

6.3 Other 2D Materials as CEs

Promisingly, some other 2D materials, such as MoS_2[368,369], $MoSe_2$,[370] FeS_2,[371] CoS, CoSe[372] and NiSe,[372] have been used in efficient CEs with remarkable stability. For example, Al-Mamun *et al.* grew MoS_2 films on FTO substrates by a facile one-pot hydrothermal method.[368] The resulted MoS_2 films exhibited high electrocatalytic activity and were directly used as CEs for DSSCs, which showed the higher PCE of 7.41% compared to DSSCs with Pt-CEs (η = 7.13%). To further improve the electrocatalytic activity of MoS_2, it can be composited with carbon materials, such as graphene,[373,374] CNT[375] and porous carbon.[376] Recently, Yue *et al.* prepared a porous MoS_2-carbon hybrid film by using an *in situ* hydrothermal route.[376] The MoS_2-carbon CE possesses low charge transfer resistance at the electrolyte-electrode interface, high electrocatalytic activity and fast reaction for the reduction of I_3^-, which is attributed to the high specific surface area and the unique structure of the

MoS_2-carbon composited film. The PCEs of the DSSCs were up to 7.69%. In 2014, Lee *et al.* prepared few layer $MoSe_2$ by surface selenization of Mo-coated soda-lime glass.[370] The $MoSe_2$/Mo substrate was used to replace commonly used Pt/FTO substrate for DSSCs. The results showed that few-layer $MoSe_2$ displayed high catalytic efficiency for the reduction of I_3^-, leading to a PCE of 9.0%.

Gong *et al. in situ* grew 2D metal selenides ($Co_{0.85}Se$ and $Ni_{0.85}Se$) on FTO by a low-temperature hydrothermal method and directly used them as CEs in DSSCs,[372] as shown in **Fig 19**. The graphene-like $Co_{0.85}Se$ exhibited higher electrocatalytic activity than Pt for the reduction of I_3^-, and the resulted DSSC achieved a PCE of 9.4% versus 8.64% for a control device with a typical Pt-CE.

7. Quantum Dot-Sensitized Solar Cells and Others Inorganic Solar Cells

Similarly, graphene is promising in the applications as transparent electrodes or charge transport materials in some inorganic solar cells, such as the QD sensitized solar cells (QDSSCs). In 2010, Guo *et al*. hybridized graphene with CdS QDs, prepared photovoltaic devices with a novel multilayer graphene/CdS QD structure on ITO and showed incident photon-to-electron conversion efficiencies (IPCEs) of the devices up to 16%.[377]

Functionalized graphene can be used as both photoanodes and CEs in QDSSCs.[102,378,379] For example, Zhu *et al*. incorporated graphene frameworks (GFs) into TiO_2 photoanodes as electron transport medium to improve the performance of CdS/CdSe QDSCCs.[380] It is found that the GFs/TiO_2 electrode has a shorter electron transport time, longer electron lifetime and diffusion path length than those of conventional 2D graphene sheets/TiO_2. A PCE of 4.2% was obtained in the QDSSC with the GFs/TiO_2 photoanode, which was higher than those of the QDSSCs with a TiO_2 photoanode (η = 3.17%) or a 2D graphene sheets/TiO_2 photoanode (η = 3.58%). Meanwhile, Ye *et al*. wrapped Cu_2S by rGO via a one-step solvothermal process.[381] The rGO/Cu_2S hybrid film was used as CEs in CdS/CdSe QDSSCs, which showed better electrocatalytic activity, greater stability, lower charge-transfer resistance and higher exchange current density in comparison with Pt or Cu_2S electrodes. The QDSSCs based on rGO/Cu_2S CEs showed η =3.85% higher than those of devices with Pt (2.14%) or Cu_2S (η = 3.39%) electrodes.

Graphene has been used as transparent electrodes in solar cells based on PbS QDs.[382] For example, Park *et al*. used CVD-graphene as cathode for PbS-based hybrid solar cells.[209]

After coating a layer of PEDOT:PEG on graphene, ZnO nanowires were grown on graphene as an acceptor, and then PbS QDs were spin-coated on ZnO nanowires as a donor. The optimized PCE of the devices was 4.2%, which was comparable to the performance of the devices with ITO electrodes (η = 5.1%).

Meanwhile, graphene has been employed as transparent electrodes in conventional high-efficiency inorganic solar cells. In 2011, Bi *et al*. used multilayer CVD graphene as transparent electrodes in devices with the structure of graphene/ZnO/CdS/CdTe/(graphite paste), which showed an optimized PCE of 4.17%.[383] In order to improve the device performance, boron-doped graphene was employed as electrodes in CdS/CdTe solar cells by the same group.[384] The boron-doped graphene has better conductivity and higher work function, resulting in a PCE of 7.86%. Afterwards, they prepared 3D graphene networks on Ni foams by CVD method and employed the 3D graphene as electrodes in CdS/CdTe solar cells, which led to an improved PCE of 9.1% due to the high conductivity of the 3D graphene.[385] In 2012, they further improved the performance of CdS/CdTe solar cells by using Cu NWs-doped graphene as transparent electrodes and showed the maximum PCE of 12.1% and a good thermal stability.[386]

In 2014, Yin *et al*. firstly used a doped graphene to replace ZnO:Al (AZO) electrodes in Cu(In,Ga)Se_2 (CIGS) solar cells.[387] Compared with the CIGS solar cells with AZO electrodes, the devices with graphene electrodes showed decreased reflectance and enhanced quantum efficiency in the near infrared region. By optimizing the contact between graphene and the intrinsic ZnO (i-ZnO), a high PCE of 13.5% was achieved, which is comparable to that of a device with an AZO electrode (η = 14.9%). Moreover, the graphene film can protect the active layer from the damage by moisture, leading to a much better stability than that of a standard CIGS solar cell, being similar to the packaging effect of OPVs reported before.[194]

8. Perovskite Solar Cells

Perovskite solar cells based on hybrid organic-inorganic methylammonium lead halide perovskites have attracted much attention recently due to their large light absorption coefficient,[388] high charge carrier mobility,[389] long carrier diffusion length[390] and high efficiency. In the past 5 years, their efficiencies have skyrocketed from 3.8% to 19.3%,[390-392] making it possible to replace conventional photovoltaic devices based on crystalline silicon in commercial applications. In normal perovskite solar cells, $CH_3NH_3PbI_3$ or $CH_3NH_3PbI_{3-X}Cl_x$

is deposited on a submicrometer-thick mesoporous or planar TiO_2 film as a light absorber, TiO_2 and spiro-OMeTAD act as ETL and HTL, respectively. Similar to the cases in other types of photovoltaic devices, it is obvious that graphene can find important applications in perovskite solar cells. For example, a TiO_2 film requires high-temperature processing to increase it crystallinity and charge carrier mobility while adding graphene into it can not only increase its conductivity and mobility but also decrease its treatment temperature, which has been utilized in DSSCs as well.[393] On the other hand, the spiro-OMeTAD HTL is expensive and unstable in air, which is the bottleneck for realizing cost effective and stable perovskite devices. GO is stable in air, and can be prepared on a large scale, which has been effectively used as HTL in OPVs.[237] So it can also be applied as HTL to replace spiro-OMeTAD in perovskite solar cells.

In 2013, Wang *et al*. composited graphene nanoflakes with TiO_2 nanoparticles as the electron collection layer in perovskite solar cells, as shown in **Fig. 20a**.[394] The appropriate work function of graphene nanoflakes (4.4 eV) reduced the energy barrier between TiO_2 (4.2 eV) and FTO (4.5 eV) and led to better electron collection in TiO_2 (**Fig 20b**). On the other hand, the superior charge mobility of graphene nanoflakes provided the high electrical conductivity of the graphene/TiO_2 composites (**Fig. 20c**). Moreover, graphene nanoflakes enable the entire device to be fabricated at a temperature not higher than 150°C, and the solar cells based on graphene/TiO_2 composites showed the remarkable photovoltaic performance with a PCE up to 15.6% (**Fig. 20d**). Later, Zhu *et al*. inserted a thin GQDs layer between TiO_2 film and perovskite layer in the devices.[395] Upon the addition of GQDs, a strong quenching of perovskite photoluminescence was observed at about 760 nm, and the PCE of the device was improved from 8.81% to 10.15%, which were attributed to the shortened electron extraction time with the presence of GQDs (90-106 ps). More recently, Wu *et al*. spun GO films on ITO as HTL for inverted perovskite solar cells. The GO film can efficiently extract holes out of perovskite, facilitate the formation of homogenous large domains and improve surface coverage of perovskite. The perovskite film grown on GO showed high quality crystallization and preferential in plane orientation of (110) plane, which resulted in high mobilities in perovkite films to facilitate the exciton seperation and extraction. The inverted device with $CH_3NH_3PbI_{3-x}Cl_x$ as absorber and GO as HTL achieved a champion PCE of 12.4%.[396]

As reviewed in other sections, graphene can replace FTO or opaque metal as anode or cathode to realize flexible or semitransparent devices. However, until now, there is no report

on applying graphene as transparent electrodes in perovskite solar cells, which is expected in the near future.

9. Conclusions and Outlook

In summary, functionalized graphene and other 2D materials have been successfully used in photovoltaic devices, including OPVs, Schottky junction solar cells, DSSCs, perovskite solar cells, quantum dot-sensitized solar cells and other inorganic solar cells. The most important application of graphene in photovoltaic devices is for transparent electrodes that may replace conventional ITO or FTO transparent electrodes due to its high conductivity and transparency. On the other hand, GO and functionalized GO are promising interfacial materials for OPVs, Schottky junction solar cells and perovskite solar cells, which lead to pronounced improvement of device performance including efficiency, lifetime and stability. Moreover, other unique properties of graphene including excellent mechanical flexibility, large specific surface area, high electrocatalytic activity and gas impermeability make graphene promising in many specific applications, such as flexible electrodes, packaging layers and charge transport medium for solar cells. Other 2D materials have also shown outstanding properties in charge transfer, electrocatalytic activity and light absorption, and have been successfully used as interlayers, active layers and CEs in several types of solar cells.

Although dramatic progress has been made in this field, the photovoltaic applications of 2D materials are still at the early stage. Great challenges exist in commercializing photovoltaic devices with 2D materials because of the following critical issues yet to be solved. First of all, to achieve highly conductive, transparent and low cost graphene electrodes, synthesis methods should be optimized and further developed to improve the quality of graphene and decrease the cost, and the doping techniques being compatible with the fabrication process of solar cells should be explored to realize high charge carrier densities, good stability and tunable Fermi energy levels in graphene. CVD method is an important approach of preparing high-quality and large-area graphene for high performance optoelectronic devices and the preparation conditions especially the carbon sources and substrates should be further studied. The massively produced graphene derivatives (rGO or GO) from bulk graphite allows for the industrial-scale fabrication of electrodes or charge transport layers for photovoltaic devices. However, the conductivity of GO or rGO films is

significantly lower than that of high-quality graphene, thus novel doping techniques for GO-based composite materials should be investigated.

For OPVs, graphene has been successfully used as transparent electrodes (cathode and anode), interlayers (HTL and ETL) and additive for enhancing charge transfer. In addition, considering OPV is unstable in air, graphene and GO films can provide encapsulation on the device. The main challenge of using graphene in OPVs as transparent electrodes is the preparation of large-area devices with solution process. The realization of high efficiency large-area devices lies on the high conductivity and the solution processability of graphene electrodes. To have a high fill factor of the devices, the sheet resistance of the graphene electrodes is better to be less than 10 Ω/□. Large-area CVD graphene can be prepared and transferred by role to role process, which however have been rarely used in the fabrication of OPVs probably due to some technical difficulties. It is notable that the hydrophobic surface of graphene makes it difficult to uniformly coat organic solutions on the top. Thus, lots of surface modification techniques have been developed to make graphene being compatible with solution processible OPVs. Another issue should be noticed is the poor stability of the doped graphene by certain acid or ions, which should be avoided in its applications in OPVs.

For DSSCs, graphene has been successfully used as both photoanodes and CEs. Besides the high conductivity and transparency, the high electrocatalytic activity of graphene plays a key role in many devices. In terms of the device fabrication, it is much easier to incorporate graphene electrodes in DSSCs than in OPVs due to electrolytes used in the former. Therefore, various graphene-based composite electrodes to synergize with other functional materials have been the main trend in using graphene in DSSCs. For other photovoltaic devices, including Schottky junction solar cells, quantum dot-sensitized solar cells and perovskite solar cells, graphene has shown similar advantages in fast charge transfer and high transparency. High-efficiency perovskite solar cell is a hot topic in recent years. However, the applications of graphene transparent electrodes in perovskite solar cells have been rarely reported until now, which will be an important technique to be studied due to the great possibility of commercializing perovskite solar cells in the near future.

It is notable that the applications of other 2D materials in photovoltaic devices have been studied for only two years. Several materials, including MoS_2, WS_2, FeS_2, $MoSe_2$, WSe_2, CoS, CoSe, NiSe and so on, have been used in solar cells. Considering the big family of 2D materials current studied, many other 2D materials would be tested in the future. Some advantages have been found in the applications as interlayers (HTL and ETL) that can

enhance charge transfer from the active layer to the electrodes. In addition, given the same thickness, the light absorption of some 2D materials (e.g. MoS_2, WS_2) is higher than that of conventional bulk semiconductors and thus ultrathin solar cells can be realized based on them. However, there are many challenges in using the 2D materials for practical photovoltaic applications, including the fabrication of large-area devices and the way of improving the efficiency, which are expected to be solved by using more suitable materials and optimizing the device design and fabrication techniques, such as the preparation of multilayer 2D material photovoltaic devices.

Acknowledgements

This work is financially supported by the Research Grants Council (RGC) of Hong Kong, China (project number: T23-713/11) and the Hong Kong Polytechnic University (project number: G-YN09, G-YBB7 and 1-ZV8N).

Tables:

Table I Comparison of graphene with other materials for transparent electrodes.

Electrode material	T (%)	R_s (Ω/□)	Fabrication technique	Drawbacks
ITO [108]	85	25	sputtering	limited indium supply, brittle, unstable to acid
FTO [107]	80	15	sputtering	brittle, high roughness, expensive, low transparency in near-infrared
PEDOT:PSS [117]	80	100	chemical synthesis	low environmental stability
CNT [120]	90	150	arc discharge	low output, high resistance, high roughness
Au grid [121]	79	5	lithography/sputtering	complex process, small area
Ag NW [124]	90	110	thermal reaction	high roughness, poor adhesion
CVD-Graphene [75]	90	30	CVD	Low doping stability

T: Transmittance;

Table II Summary of OPVs with 2D materials as electrodes, HTLs or ETLs

Materials	Function	Modification	R_s (kΩ/□)	Device structure	PCE (%)	Ref.
CVD-G	Anode	TCNQ	0.278	G/PEDOT:PSS/P3HT:PCBM/Ca/Al	2.58	153
CVD-G	Anode	Acid/MoO_3	0.08	G/MoO_3/PEDOT:PSS/P3HT:PCBM/LiF/Al	2.50	187
CVD-G	Anode	Au/PEDOT:PSS	0.092	Ag/ZnO/P3HT:PCBM/PEDOT:PSS/G	3.17	194
CVD-G	Anode	$SOCl_2$	0.45	G/PEDOT:PSS/P3HT:PCBM/Ca/Al	2.60	193
CVD-G	Anode	P(VDF-TrFE)	0.07	P(VDF-TrFE)/G/PEDOT:PSS/P3HT:PCBM/Ca/Al	2.07	197
CVD-G	Anode	------	0.10	ITO/ZnO/P3HT:PCBM/GO/G	2.50	199
CVD-G	Anode	Au/PEDOT:PSS	0.096	ITO/ZnO/P3HT:PCBM/PEDOT:PSS/G	2.70	200
CVD-G	Anode	Au grid	0.022	ITO/TiO_2/P3HT:PCBM/PEDOT:PSS/G/Au	3.10	263
CVD-G	Anode	MoO_3	0.5-0.7	ITO/ZnO/P3HT:PCBM/MoO_3/G/MoO_3/ZnPc:C_{60}/LiF/Al	2.90	243
rGO	Anode	CNT	0.24	rGO-CNT/PEDOT:PSS/P3HT:PCBM/Ca/Al	0.85	176
rGO	Anode	------	1.6	rGO/PEDOT:PSS/P3HT:PCBM/Al	1.10	205
rGO	Anode	PyS/PDI	916 Scm^{-1}	rGO/PEDOT:PSS/P3HT:PCBM/ZnO/Al	1.12	203
rGO	Anode	------	0.61	rGO/PEDOT:PSS/P3HT:PCBM/LiF/Al	2.04	206
rGO	Anode	------	0.52	rGO/PEDOT:PSS/PSEHTT:IC_{60}BA/ZnO/ PEDOT:PSS/PBDTT-DPP:PC_{71}BM/TiO_2/Ag NW	8.02	207
CVD-G	Cathode	ZnO nanorod	0.278	G/ZnO/P3HT:PCBM/MoO_3/Ag	1.55	45
CVD-G	Cathode	PEDOT:PEG	0.30	G/PEDOT:PEG/ZnO/P3HT:PCBM/MoO_3/Au	2.27	189
CVD-G	Cathode	WPF-6-oxy-F	0.85-0.52	G/WPF-6-oxy-F/P3HT:PCBM/PEDOT:PSS/Al	1.23	171
CVD-G	Cathode	Al-TiO_2	1.2	Glass/Au grid/G/Al/TiO_2/P3HT:PCBM/MoO_3/Ag	2.58	210
CVD-G	Cathode	------	0.30	PEN/G/ZnO/PTB7:PCBM/MoO_3/Ag	7.1	198
GO	HTL	------		ITO/GO/PTB7:PC_{71}BM/LiF/Al	7.39	221
GO	HTL	CNT		ITO/GO/P3HT:PCBM/Ga/Al	4.1	222
GO	HTL	H_2SO_4:SO_3		ITO/GO-OSO_3H/P3HT:PCBM/Ga/Al	4.37	223
GO	HTL	------		ITO/ZnO/P3HT:PCBM/GO/Ag	3.94	231
GO	HTL	------		ITO/ZnO/PCDTBT:PC_{70}BM/GO/Ag	6.20	232
GO	HTL	PEDOT:PSS		ITO/PEDOT:PSS:GO/PTB7:PC_{71}BM/Al	8.21	226
GO	HTL	VO_x		ITO/ZnO/PTh_4FBT:PC_{71}BM/GO/VO_x/Ag	6.7	227
GO	HTL	MoO_3		ITO/ZnO/PIDTT-DFBT-TT:PC_{71}BM/GO/MoO_3/Ag	7.3	228
GO	HTL	Chlorination		ITO/Cl-GO/PCDTBT:PC_{71}BM/TiO_x/Al	6.56	234
GO	HTL	Chlorination		ITO/Cl-GO/PBDTTT-C:PC_{71}BM/Ga/Al	7.59	236
GO	HTL	Fluorine		ITO/Fr-GO/PBDTTT-C:PC_{71}BM/Ga/Al	6.71	235
GO	ETL	Cs_2CO_3		ITO/GO/P3HT:PCBM/GO-Cs/Al	3.67	237
rGO	ETL	PCBM		ITO/PEDOT:PSS/P3HT:PCBM/rGO-pyrene-PCBM/Al	3.89	239
rGO	ETL	ZnO		ITO/PEDOT:PSS/PCDTBT:PCBM/ZnO-rGO/Al	6.72	240
rGO	ETL	TiO_2		ITO/PEDOT:PSS/PTB7:PC_{71}BM/TiO_2-rGO/Al	7.46	241
GO	ETL	TiO_x		ITO/PEDOT:PSS/PCDTBT:PCBM/GO-TiO_x/Al	7.5	242
WS_2	HTL	UV/ozone		ITO/WS_2/PEDOT:PSS/P3HT:PCBM/Al	3.07	259
MoS_2	HTL	------		ITO/ZnO/PTB7:PC_{71}BM/WS_2/Ag	8.11	35
$NbSe_2$	HTL	------		ITO/ZnO/PTB7:PC_{71}BM/$NbSe_2$/Ag	8.1	260
WS_2/MoS_2	HTL	------		ITO/WS_2/P3HT:PCBM/V_2O_5/Al	2.98	262
				ITO/MoS_2/P3HT:PCBM/V_2O_5/Al	3.35	
MoS_2	HTL	$HAuCl_4$/$NaBH_4$		ITO/WS_2/PEDOT:PSS/P3HT:PCBM/Ca/Al	3.38	263
TaS_2	HTL	UV/ozone		ITO/TaS_2/P3HT:PCBM/LiF/Al	3.06	261
MoS_2	HTL	CTAC		ITO/MoS_2/PTB7:PC_{71}BM/PFN/Al	7.12	257
MoS_2	HTL	UV/ozone		ITO/MoS_2/PTB7:PC_{71}BM/PFN/Al	7.64	258

Table III Summary of 2D materials used in other photovoltaic devices

Device Type	Materials	Modification	Device structure	PCE (%)	Ref.
Schottky junction solar cell	CVD-G	HNO_3	G/Si	1.5	269
	CVD-G	HNO_3/PEDOT:PSS	PEDOT:PSS/G/Si	2.90	276
	CVD-G	HNO_3	G-Si NW	2.15	277
	CVD-G	HNO_3	G/SiPA(pillar-array)	7.7	273
	CVD-G	HNO_3	G/SiPA	4.5	271
	CVD-G	HNO_3	G/Si	9.63	282
	CVD-G	$SOCl_2$	G/Si	5.95	278
	CVD-G	Nitrate ions	G/Si	9.27	283
	CVD-G	TFSA	G/Si	7.5	280
	CVD-G	TFSA	G/Si	8.6	281
	CVD-G	HNO_3/P3HT	G/P3HT/CH_3-Si	10.56	284
	CVD-G	HNO_3/P3HT	G/P3HT/CH_3-SiNH (hole array)	10.3	287
	CVD-G	$AuCl_3$	G/SiNH (hole array)	10.40	286
	CVD-G	HNO_3/TiO_2	TiO_2/G/Si	14.5	288
	CVD-G	------	G/GO/Si	6.18	289
	CVD-G	HNO_3/TiO_2	G/GO/Si/TiO_2	12.3	290
	CoS	PEDOT:PSS	n-Si/PEDOT:PSS:CoS/Au	11.22	298
	MoS_2	------	p-Si/MoS_2/Al	5.23	295
	WSe_2/MoS_2	------	WSe_2/MoS_2	EQE (highest:12%)	306
	G/WS_2/MoS_2	------	Graphene/MoS_2 WS_2/MoS_2	0.1-1.0, 0.4-1.5	95
	MoS_2/WSe_2	------	MoS_2/WSe_2	EQE (highest:34%)	34
	MoS_2	Plasma	p-MoS_2/n-MoS_2	2.8	307
DSSCs	rGO	------	rGO/TiO_2/N3/spiro-OMeTAD/Au/FTO	0.84	107
	rGO	------	FTO/rGO-TiO_2/N3/(I_3^-/I^-)/Pt/FTO	6.97	314
	GNPs	PEDOT:PSS	ITO/TiO_2/N719/(I_3^-/I^-)/GNPs-PEODT:PSS	4.50	324
	rGO	------	FTO/TiO_2/N719/(I_3^-/I^-)/rGO/FTO	6.81	325
	CVD-G	------	FTO/TiO_2/N719/(I_3^-/I^-)/3D-G/FTO	5.2	326
	3D-G	------	FTO/TiO_2/N719/(I_3^-/I^-)/3D-G/FTO	7.8	327
	G	CoS	FTO/TiO_2/N719/(I_3^-/I^-)/NG:CoS/FTO	10.71	337
	rGO	N-doped	FTO/TiO_2/N719/(I_3^-/I^-)/N- rGO/FTO	7.07	347
	rGO	PDDA	FTO/TiO_2/C106TBA/electrolyte/rGO+PDDA/FTO	9.5	350
	GNPs	-------	FTO/TiO_2/Y123/Co(bpy)$3^{3+/2+}$/GNP/FTO	9.4	357
	GNPs	N-doped	FTO/TiO_2/O-alkylated-JK-225/Co(bpy)$3^{3+/2+}$/NGNP/FTO	9.05	359
	GNPs	N-doped	FTO/TiO_2/JK-306:SGT 301/Co(bpy)$3^{3+/2+}$/NGNPs/FTO	10.27	360
	GNPs	Carboxylated	FTO/TiO_2/JK-303:dye29/Co(bpy)$3^{3+/2+}$/ECGNPs/FTO	9.31	361
	CVD-G	PEDOT	FTO/TiO_2/N719/(I_3^-/I^-)/G-PEDOT	6.26	364
	GP	CNT	FTO/TiO_2/N719/(I_3^-/I^-)/GP-CNT	6.05	365
	G	Pt NPs	Ti/TiO_2/N719/(I_3^-/I^-)/G(Pt NPs)	8.45	366
	CVD-G	PbS QDs	G/PEDOT:PEG/ZnO/PbS:QDs/MoO_3/Au	4.2	209
	$Co_{0.85}Se$	------	FTO/TiO_2/N719/(I_3^-/I^-)/metal selenide/FTO	9.4	372
	MoS_2	rGO	FTO/TiO_2/N719/(I_3^-/I^-)/MoS_2-rGO/FTO	6.04	374
	MoS_2	MWCNT	FTO/TiO_2/N719/(I_3^-/I^-)/MoS_2-MWCNT/FTO	6.45	375
	MoS_2	Carbon	FTO/TiO_2/N719/(I_3^-/I^-)/MoS_2-C/FTO	7.69	376
	MoS_2	------	FTO/TiO_2/N719/(I_3^-/I^-)/MoS_2/FTO	5.8	369
	MoS_2	------	FTO/TiO_2/N719/(I_3^-/I^-)/MoS_2/FTO	7.41	368
	$MoSe_2$	------	FTO/TiO_2/N719/(I_3^-/I^-)/$MoSe_2$/Mo	9.00	370
QDSSCs	rGO	-------	ITO/rGO:CdS/Na_2S/Pt	16 (IPCE)	377
	rGO	-------	FTO/rGO:TiO_2/CdS:CdSe/Na_2S/ZnS	4.02	378
	rGO	Cu_2S	FTO/TiO_2/CdS:CdSe/Na_2S/rGO(Cu_2S)	3.85	381
	CVD-G	-------	G/Au/CdS	1.65	291
	CVD-G	-------	G/CdSe	1.25	292
	CVD-G	-------	G/ZnO/CdS/CdTe/Graphite	4.17	383
	CVD-G	-------	G/CdTe/CdS/FTO	9.1	385
	CVD-G	-------	FTO/CdS/CdTe/Cu NWs-G	12.1	386
	CVD-G	-------	Mo/Cu(In, Ga)Se_2/CdS/i-ZnO/G	13.5	387
Perovskite solar cells	Nanoflakes	-------	FTO/G:TiO_2/Al_2O_3:Perovskite/Spiro-OMeTAD/Au	15.6	394
	GQDs	-------	FTO/TiO_2/GQDs/Perovskite/Spiro-OMeTAD/Au	10.15	395
	GO	-------	ITO/GO/Perovskite/PCBM/ZnO/Al	11.11	396

DSSC: dye-sensitized solar cells, QDSSC: quantum dot-sensitized solar cells

Figures:

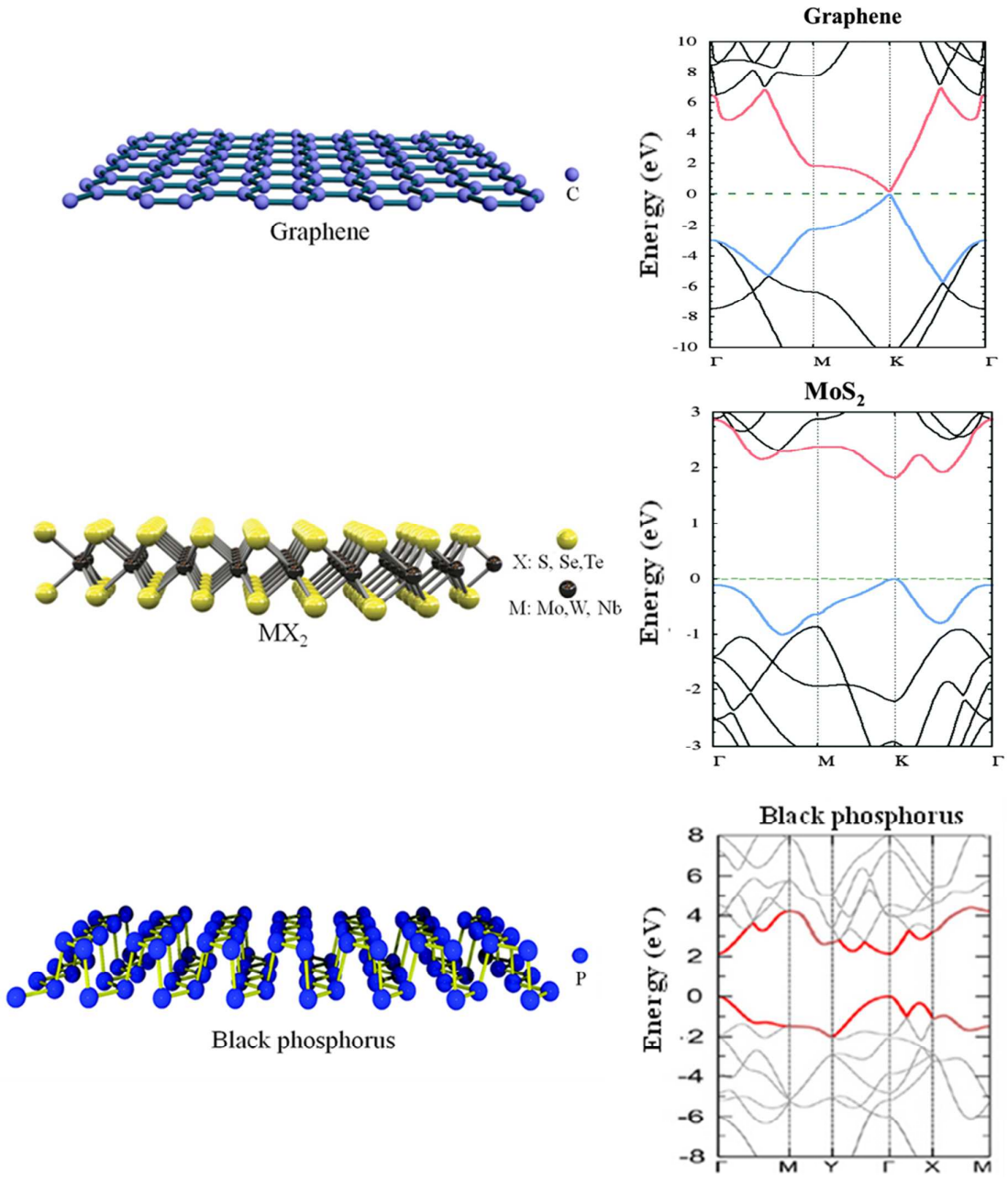

Fig. 1 Schematic structure of 2D materials, including graphene, MX_2 (M: Mo, W, Nb; X: S, Se, Te), black phosphorus[6,11,12] and the electronic band structure for monolayer graphene, MoS_2 and black phosphorus.[7,13]

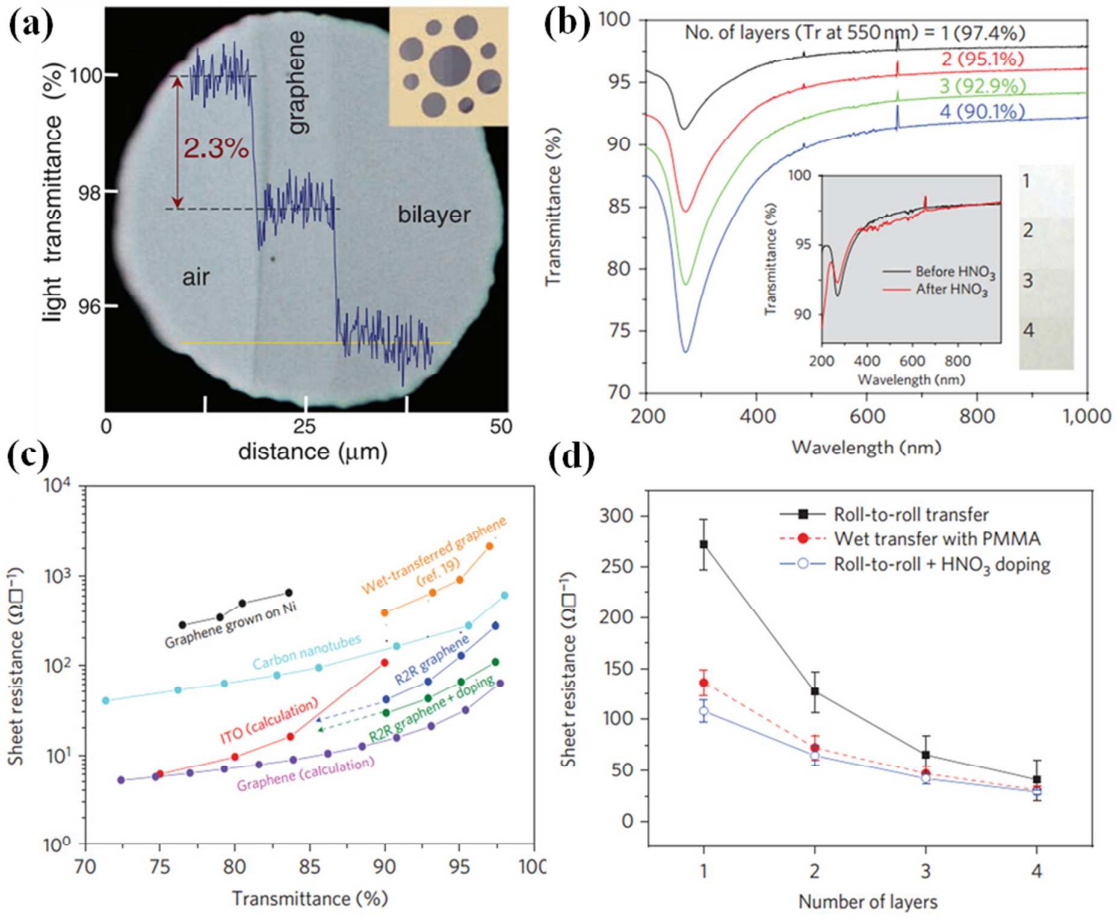

Fig. 2 (a) The transmittance of single or two layer graphene prepared by mechanically exfoliated method.[93] (b) The transmittance spectra of CVD-graphene with different layers.[75] (c) R_s as a function of transmittance for graphene prepared by different methods.[75] (d) R_s as a function of number of layers for CVD-graphene before and after HNO_3 doping.[75]

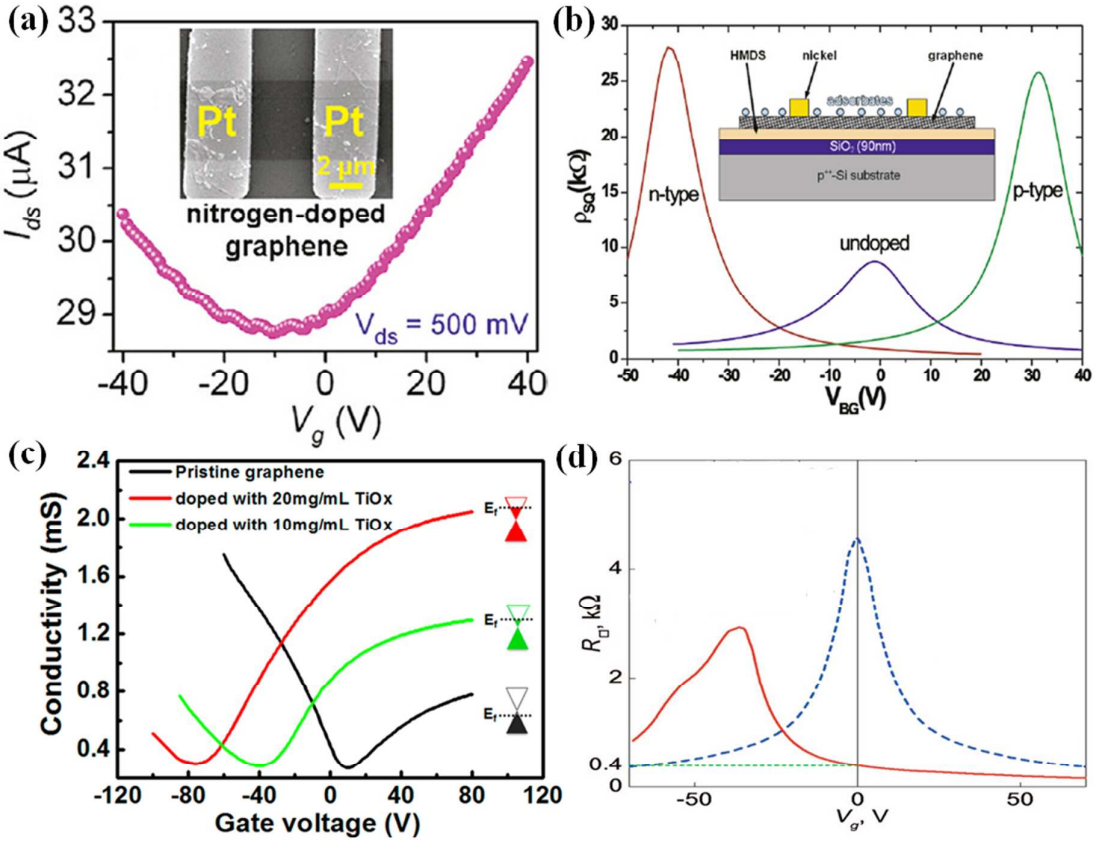

Fig. 3 (a) Source-drain current (I_{ds}) of a nitrogen doped graphene field effect transistor (GFET) as a function of the gate voltage (V_G). Inset: a top-view SEM image of the device.[161] (b) R_s of n-type, p-type, and undoped GFETs as a function of V_G. Inset: schematic diagram of the GFET.[167] (c) Conductivity of undoped or TiOx-doped GFETs as a function of V_G.[168] (d) R_s of undoped or PVA doped GFETs as a function of V_G.[57]

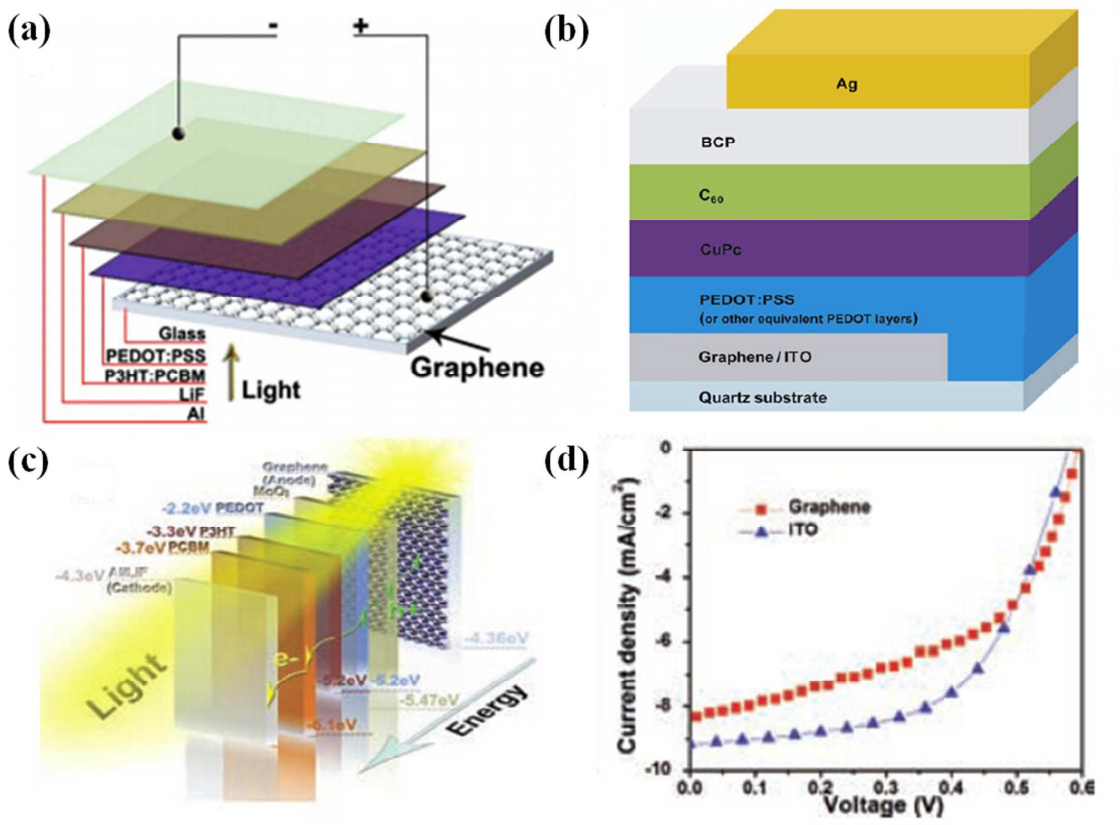

Fig. 4 (a) Schematic of an OPV with a PBASE-doped graphene anode.[185] (b) Schematic of OPVs with an $AuCl_3$ doped graphene anode.[186] (c) Schematic and (d) *J-V* characteristics of an OPV with the structure of graphene/MoO_3/PEDOT:PSS/P3HT:PCBM/LiF/Al and a control device with an ITO transparent electrode.[187]

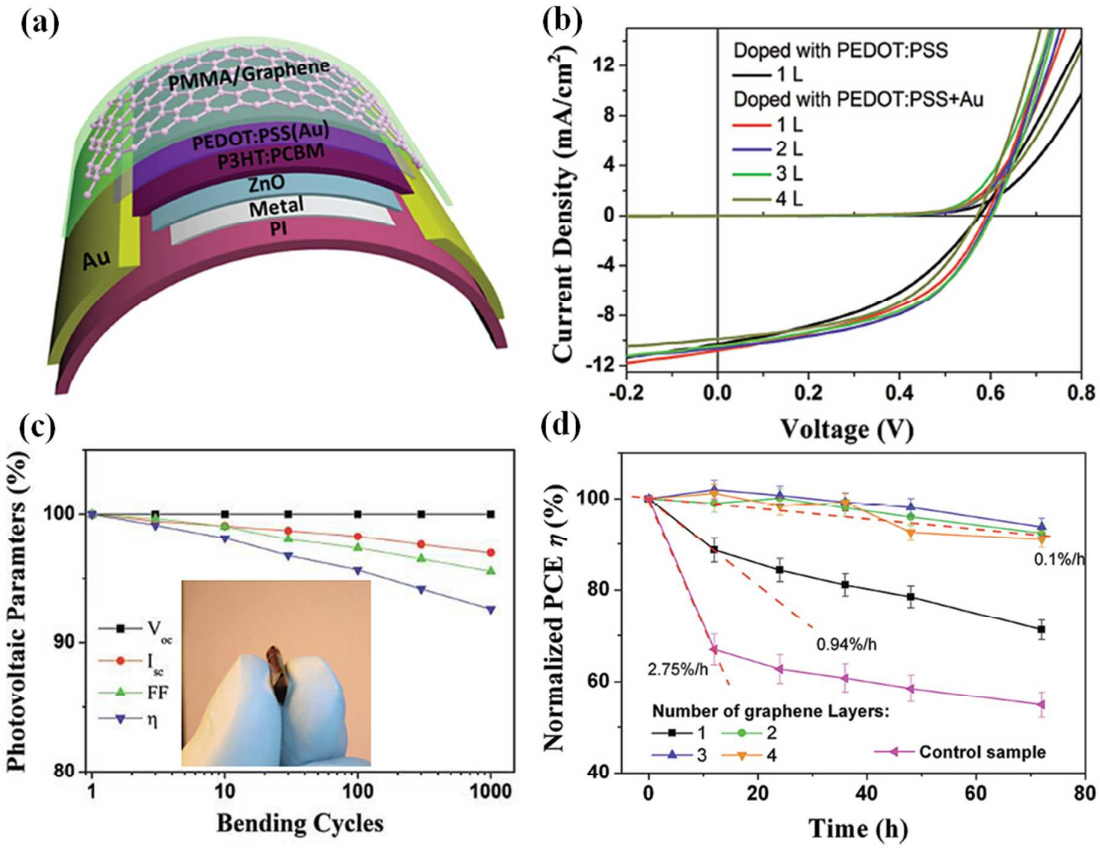

Fig. 5 (a) Schematic of a flexible OPV with an inverted structure of PI/Ag/ZnO/P3HT:PCBM/PEDOT:PSS/Graphene/PMMA. (b) *J*−*V* characteristics of OPVs with different number of layers of graphene anode doped with PEDOT:PSS and Au NPs or PEDOT:PSS only. (c) Bending performances of a flexible OPV with graphene anode. Inset: photograph of the device under bending condition. (d) Evolution of PCEs of package-free OPVs with 1 to 4 layers of graphene or Au top electrodes measured in air.[194]

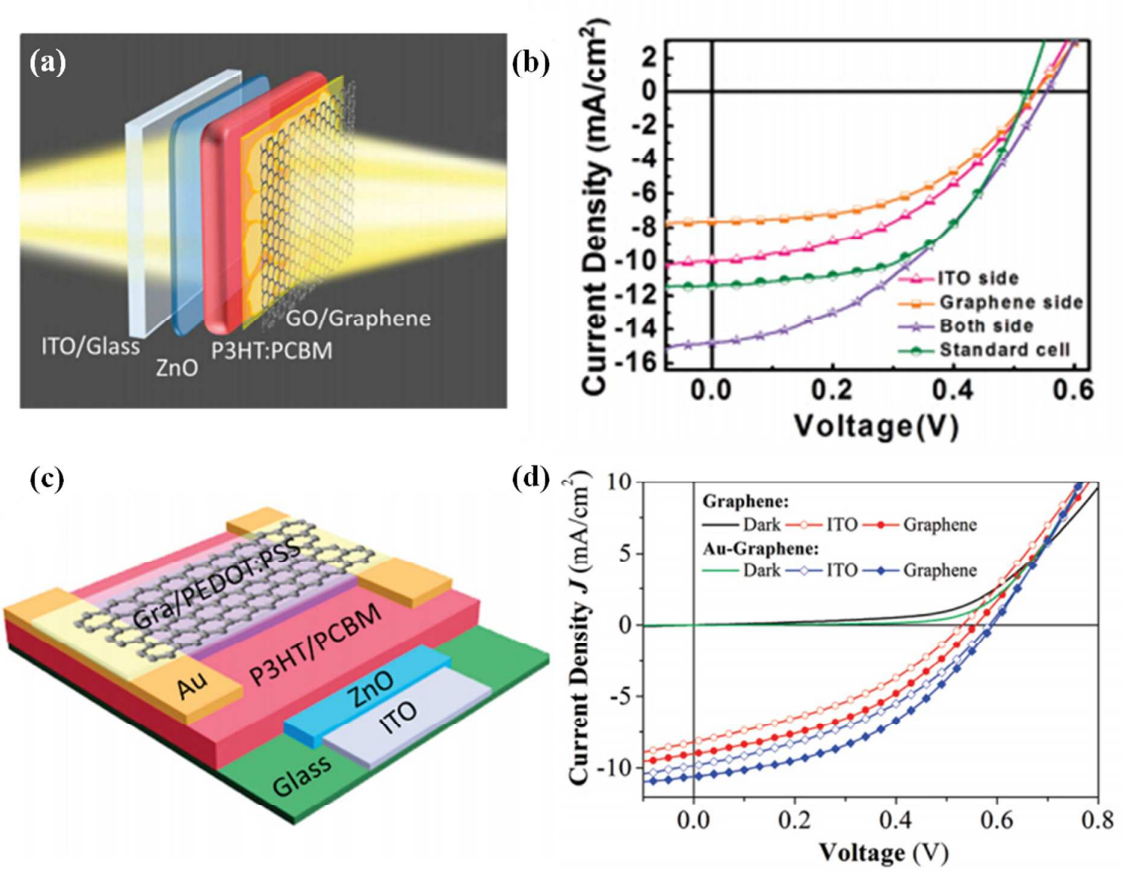

Fig. 6 (a) Schematic of a semitransparent inverted OPV with a structure of ITO/ZnO/P3HT:PCBM/GO/graphene, and (b) *J-V* characteristics of a standard OPV and semitransparent OPV consisting of eight layers of graphene illuminated from ITO side or graphene side.[199] (c) Schematic of a semitransparent inverted OPV with a structure of ITO/ZnO/P3HT:PCBM/PEDOT:PSS/graphene, and (d) *J-V* characteristics of semitransparent OPVs with PEDOT:PSS doped or Au/PEDOT:PSS codoped graphene top electrodes illuminated from ITO side or graphene side.[200]

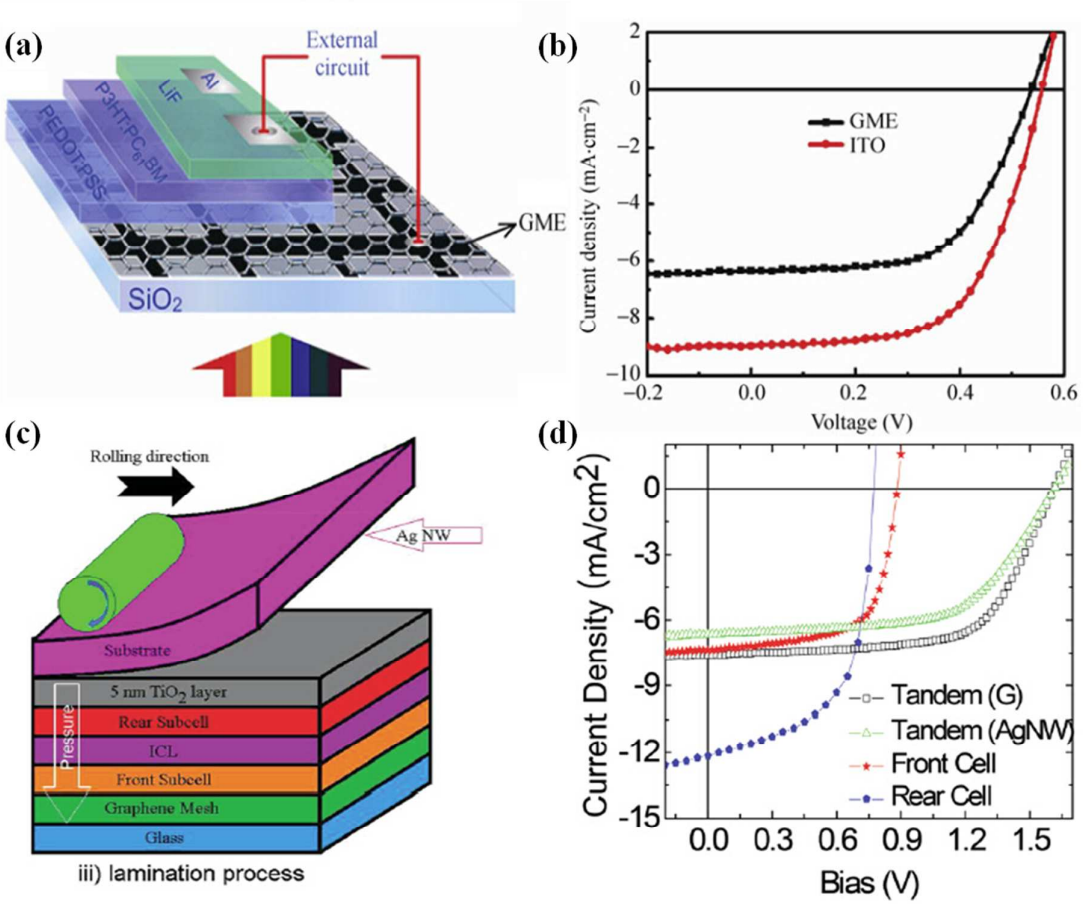

Fig. 7 (a) Schematic of an OPV with a structure of GME/PEDOT:PSS/P3HT:PCBM/LiF/Al, and (b) *J-V* characteristics of OPVs with ITO (red) or GME (black) anodes.[206] (c) Schematic of a tandem cell with graphene mesh bottom electrode and Ag nanowire top electrode, and (d) *J-V* characteristics of front, rear, and tandem cells (light projected from graphene mesh or AgNW).[207]

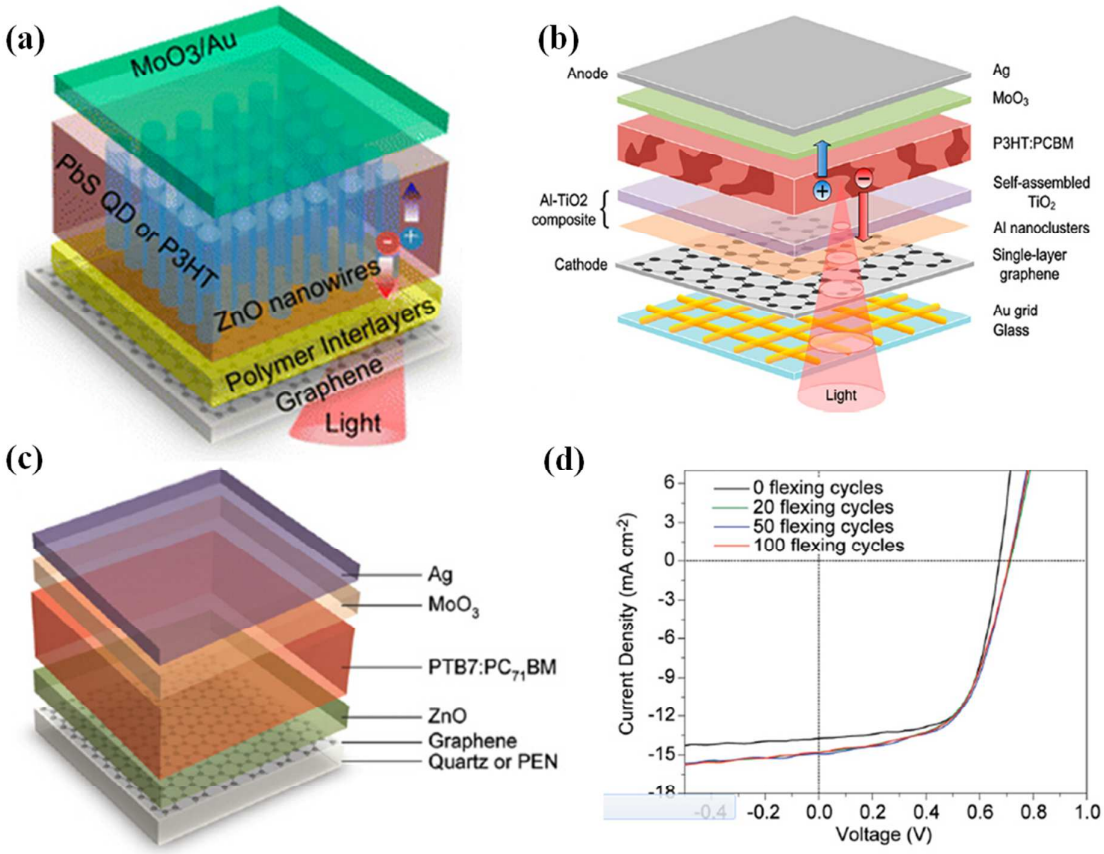

Fig. 8 (a) Schematic of P3HT:ZnO hybrid solar cells with graphene cathode and PEDOT:PEG interlayer.[209] (b) Schematic of an inverted P3HT:PCBM solar cell with Al modified graphene cathode.[210] (c) Schematic of a flexible PTB7:PCBM solar cell with graphene cathode on a FEN substrate.[198] (d) *J-V* characteristics of the champion flexible PTB7:$PC_{71}BM$ device before and after different flexing cycles.[198]

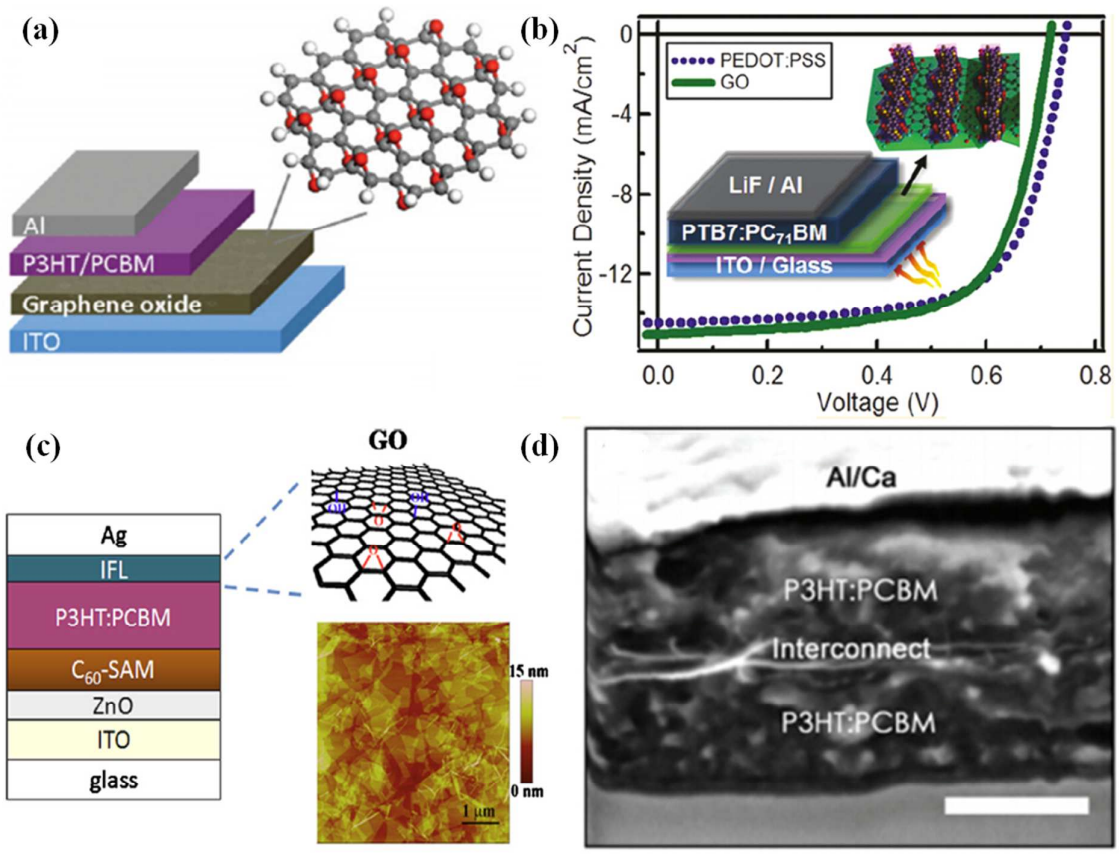

Fig. 9 (a) Schematic of an OPV with a normal structure of ITO/GO/P3HT:PCBM/Al.[211] (b) *J-V* characteristics of OPVs with PEDOT:PSS or GO as HTL. Inset: schematic of an OPV with GO as HTL.[221] (c) Schematic of an OPV with an inverted structure of ITO/ZnO/C_{60}-SAM/P3HT:PCBM/IFL(GO)/Ag, (C_{60}-SAM: fullerence-containing self-assembled monolayer, IFL: interfacial layer). the right images show the schematic structure of GO and the AFM topography image of GO nanosheets on a silicon substrate.[229] (d) Cross-sectional SEM image of a tandem device with GO/PEDOT as an interconnect layer.[181]

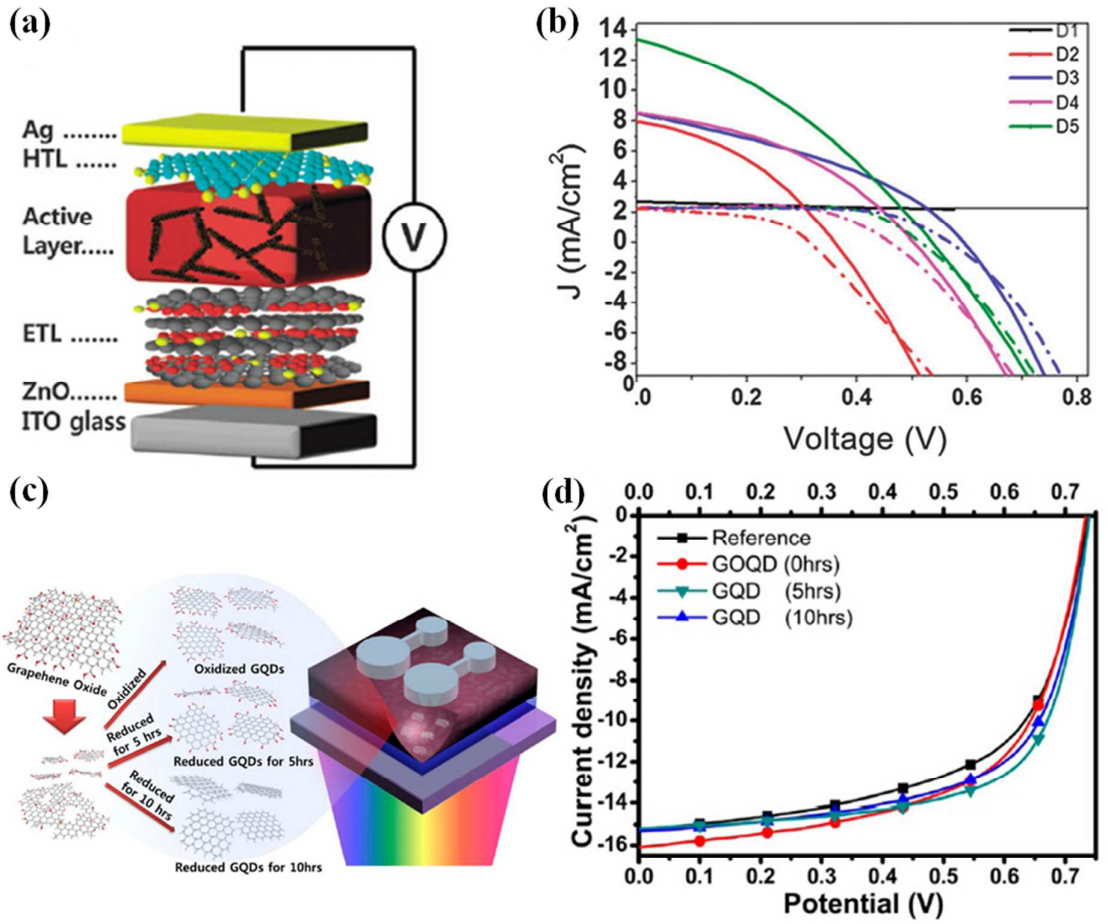

Fig. 10 (a) Schematic of an inverted OPV with GO HTL and PCA-rGO in the active layer and ETL.[251] (b) *J-V* characteristics of the OPVs with different structures.[251] D1: Glass/ITO/ZnO/P3HT/PEDOT:PSS/Ag, D2:Glass/ITO/ZnO/P3HT:rGO/PEDOT:PSS/Ag, D3: Glass/ITO/ZnO/P3HT:PCA-rGO/PEDOT:PSS/Ag, D4:Glass/ITO/ZnO/P3HT:PCA-rGO/GO /Ag, D5:Glass/ITO/ZnO/PCA-rGO/P3HT:PCA-rGO/GO/Ag, (PCA:1-pyrenecarboxylic acid). (c) Schematic of an OPV added three different types of GQDs in active layers, the edge functional groups of GQDs were tuned by different thermal reduction time.[253] (d) *J-V* characteristics of the reference device and three devices added with GQDs reduced for different period (0, 5 and 10 hours).[253]

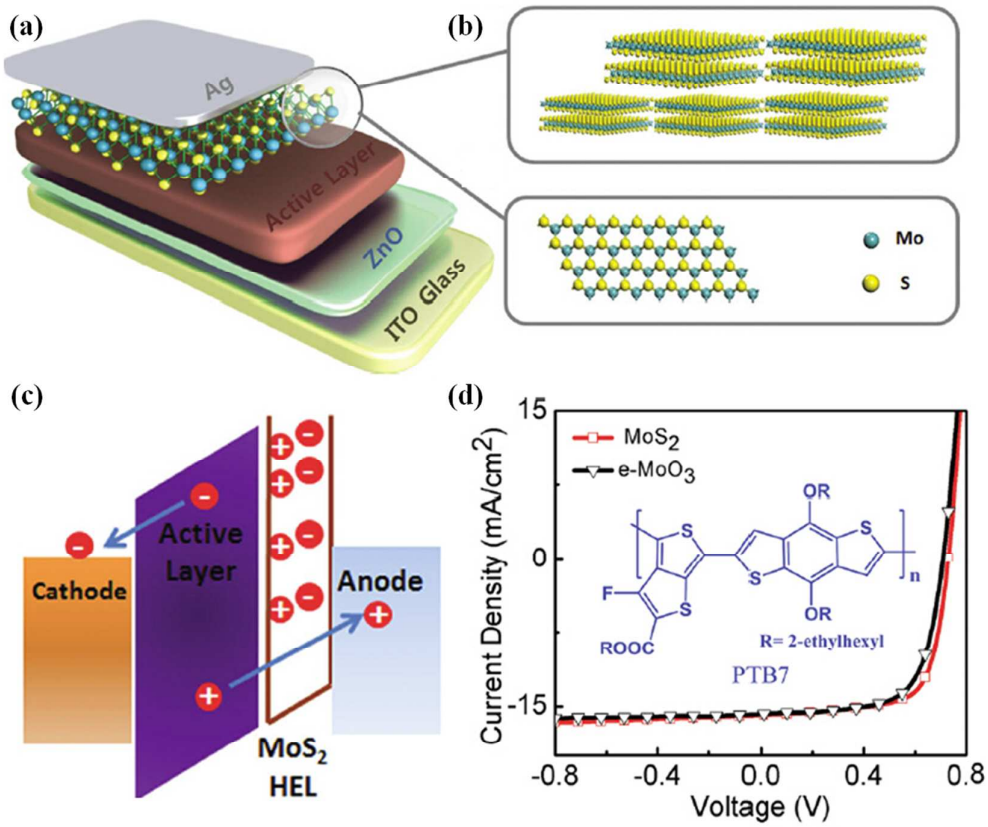

Fig. 11 (a) Schematic of an OPV with MoS_2 nanosheets as HTL.[35] (b) Schematic of the thin MoS_2 layer (side view) and the MoS_2 monolayer along the [0001] (top view).[35] (c) Schematic of the energy band structure of the OPV with MoS_2 HTL under short-circuit conditions based on the probed surface dipole.[35] (d) *J-V* characteristics of OPVs based PTB7:$PC_{71}BM$ with MoS_2 or e-MoO_3 as HTLs.[35]

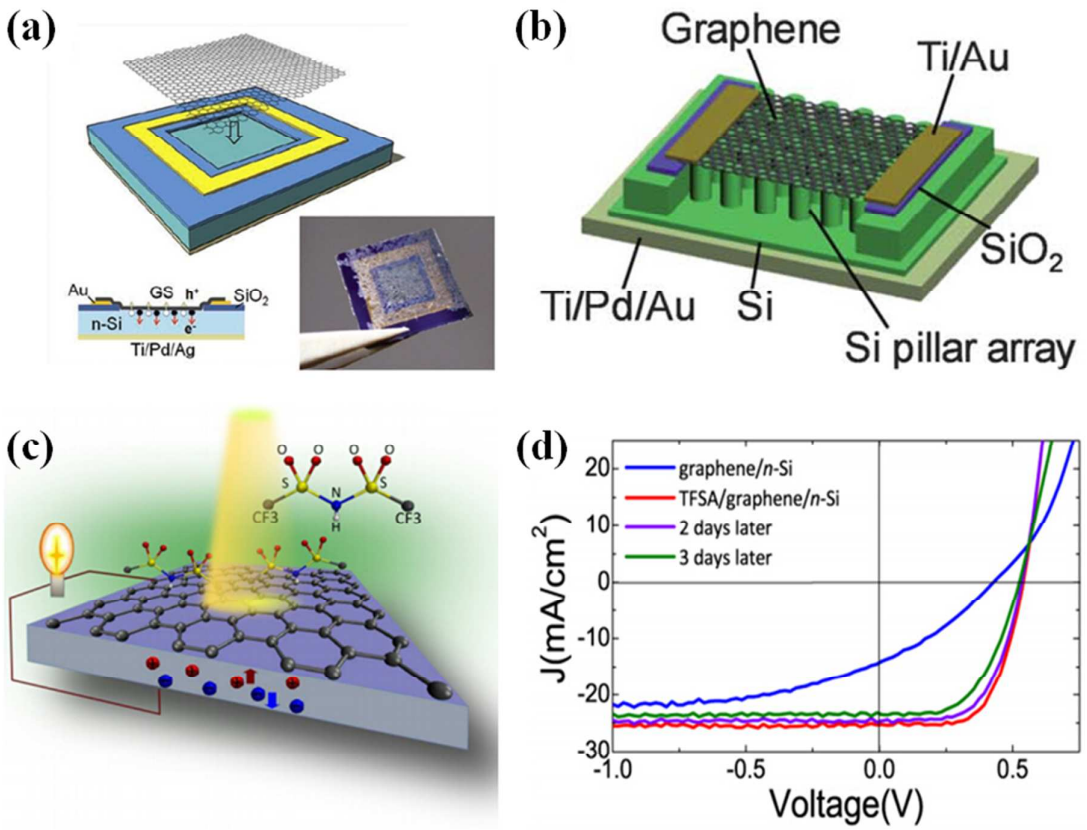

Fig. 12 (a) Schematic and photograph of a graphene/Si Schottky junction solar cell.[269] (b) Schematic of a HNO_3 doped graphene/Si-pillar-array Schottky junction solar cell.[273] (c) Schematic of a TFSA doped graphene/n-Si Schottky junction solar cell and (d) *J-V* characteristics of the TFSA undoped and doped graphene/n-Si Schottky junction solar cells under illumination with different periods.[281]

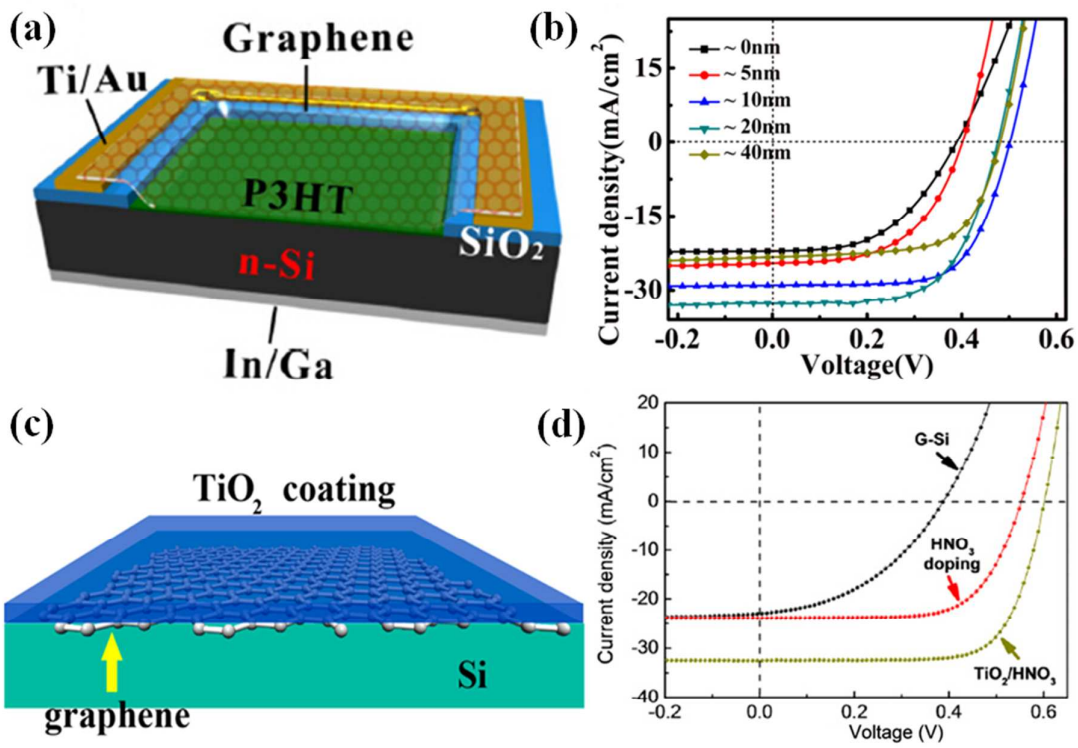

Fig. 13 (a) Schematic of few layer graphene (FLG)/Si Schottky junction solar cell with a layer of P3HT inserted between FLG film and Si, and (b) *J-V* characteristics of FLG/Si Schottky junction solar cells with different P3HT layer thicknesses.[284] (c) Schematic of graphene/Si Schottky junction solar cell with a layer of TiO_2 coated on graphene film, and (d) *J-V* characteristics of an as-fabricated graphene/Si Schottky junction solar cell, after HNO_3 vapor doping, and after TiO_2 coating (combined with HNO_3 doping), respectively.[288]

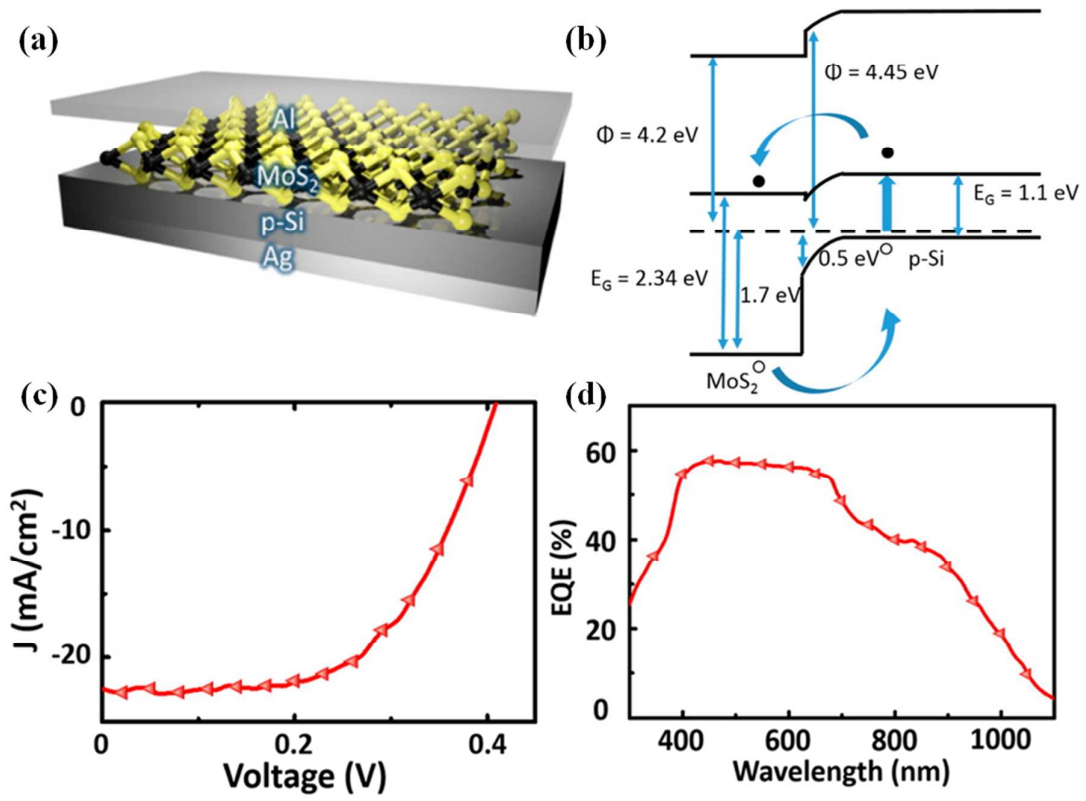

Fig. 14 (a) Schematic diagram; (b) Band structure; (c) *J-V* characteristic and (d) EQE spectrum of a MoS_2/p-Si heterojunction solar cell.[295]

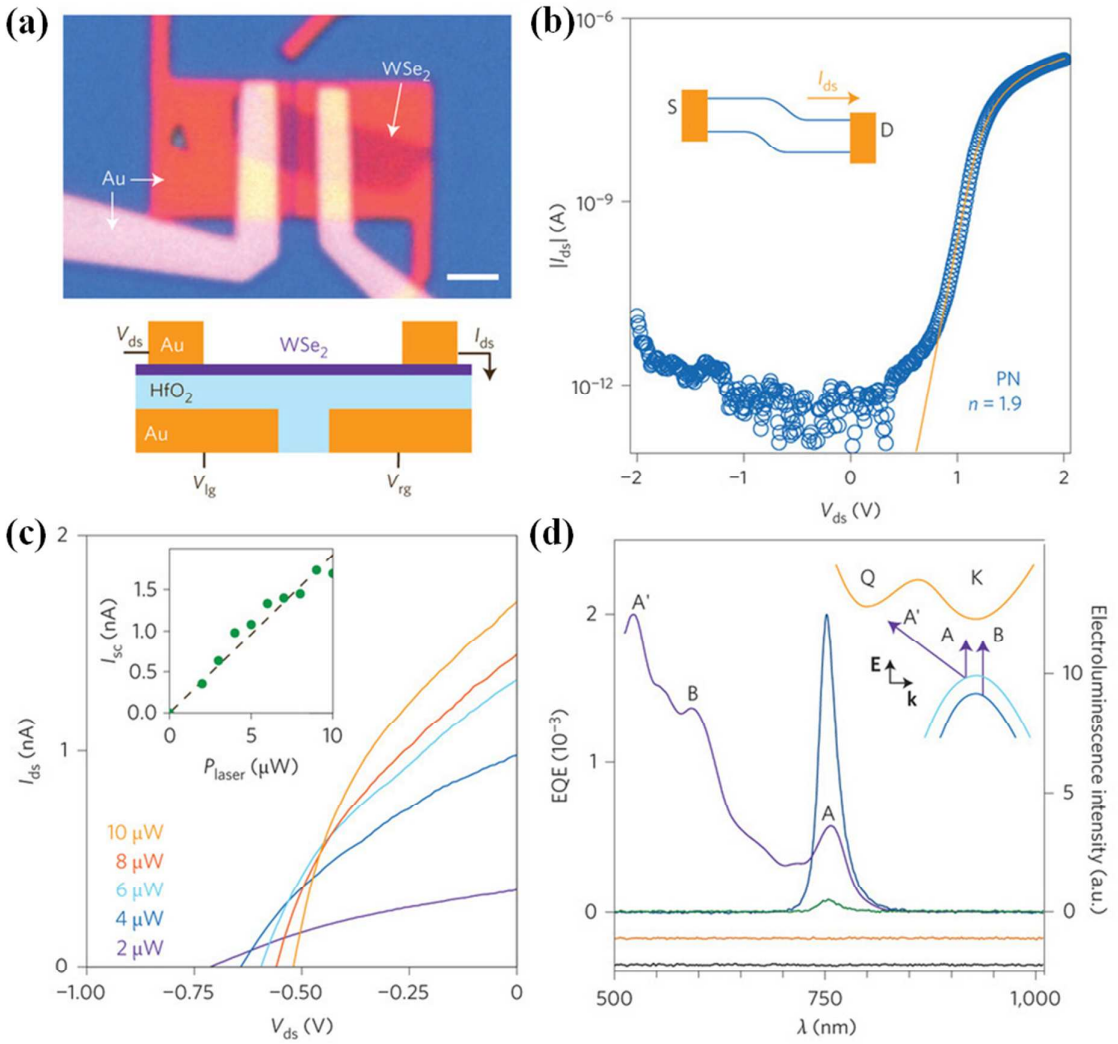

Fig. 15 Gate-controlled monolayer WSe_2 *p-n* junctions. (a) Top: Optical micrograph of a monolayer WSe_2 device controlled by two gates. WSe_2 is in contact with gold electrodes. Scale bar: 2 mm. Bottom: Schematic side view of the device including electrical connections. (b) Semi-logarithmic plots of I_{ds} through the *p-n* junction as a function of V_{ds}. The yellow fit line gives a diode ideality of n=1.9. Insets: Schematic band diagram of the device in forward bias. (c) Photovoltaic response of the WSe_2 *p-n* junction under the illumination of laser powers 2-10 mW (wavelength 700 nm). Inset: Short-circuit current (green dots) versus laser power with a linear fit (black dashed line). (d) EQE as a function of wavelength at a constant laser power of 2 mW in the WSe_2 *p-n* junction (purple line). Peaks in the EQEs correspond to exciton transitions A, B and A′, as labelled. Inset: Diagram of the band structure around the K and Q points, with arrows indicating the lowest-energy exciton transitions for monolayer WSe_2.[302]

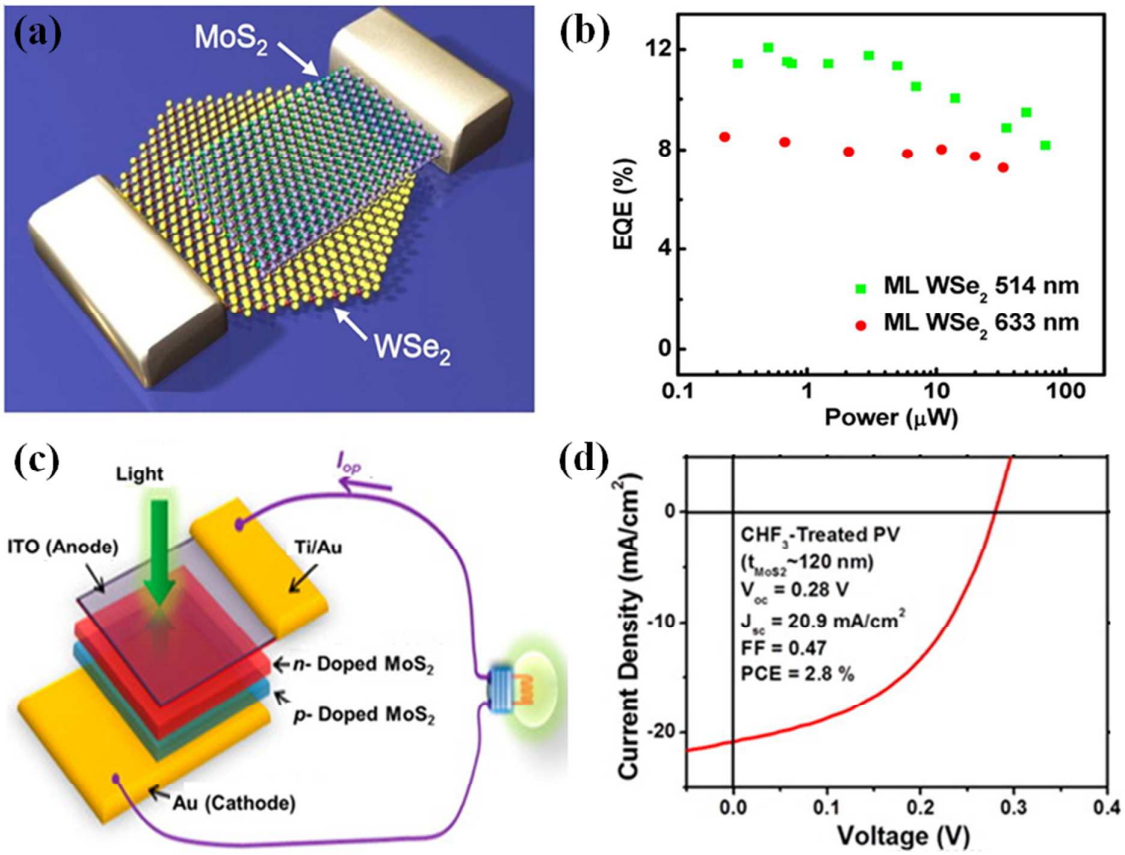

Fig. 16 (a) Schematic and (b) EQE spectra of a MoS_2/WSe_2 heterojunction solar cell under 514 and 633 nm laser illumination.[306] (c) Schematic and (d) *J-V* characteristics of a MoS_2 based *p-n* junction solar cell with CHF_3 Plasma-treatment.[307]

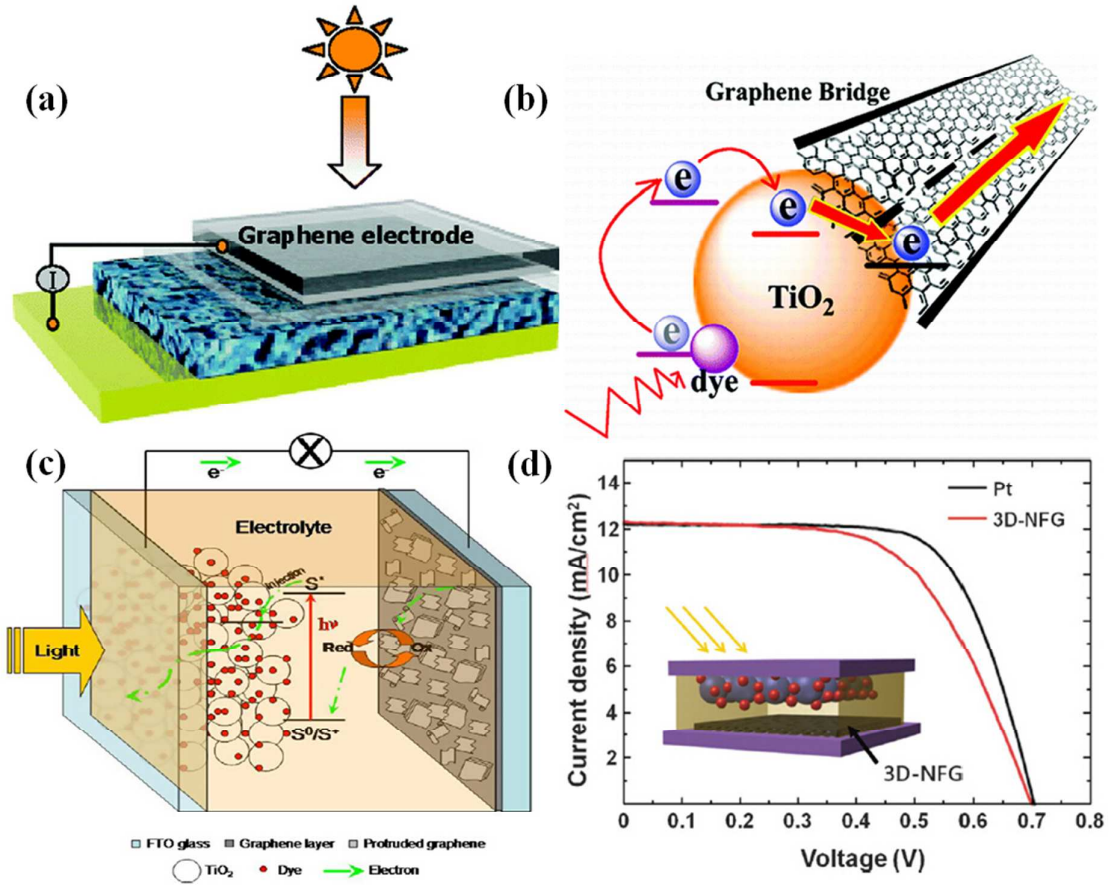

Fig. 17 (a) Schematic of a DSSC with graphene photoanode. The four layers from bottom to top are Au, dye-sensitized heterojunction, compact TiO_2, and graphene film.[315] (b) The transmission route of photoexcited electrons in TiO_2/GO composited material.[314] (c) Schematic of a DSSC with graphene nanosheets as CE.[325] (d) *J-V* characteristics and schematic (inset) of DSSCs with 3D graphene or Pt as CE.[51]

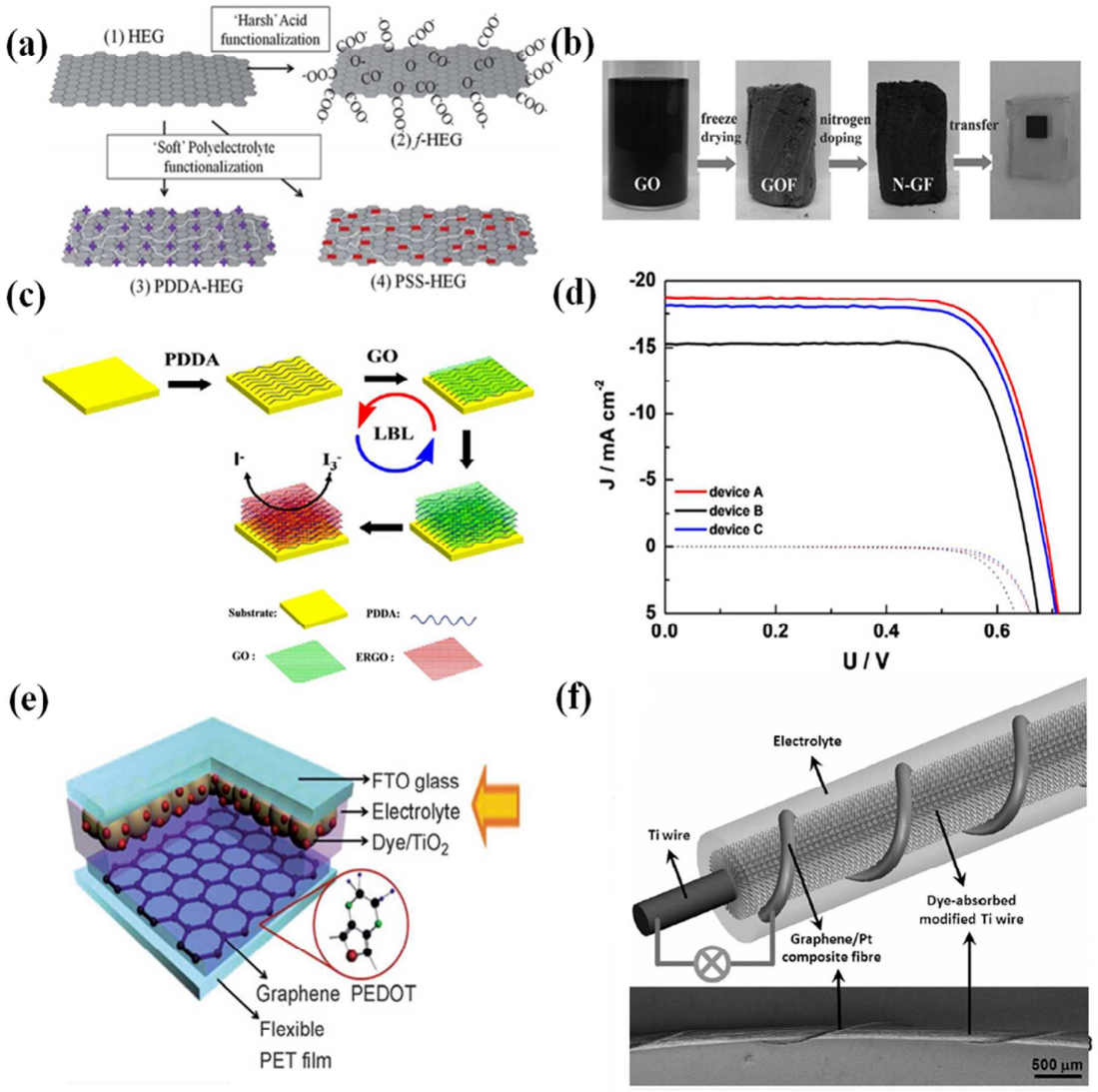

Fig. 18 (a) The functional processes of the harsh acid and soft polyelectrolyte on graphene.[338] (b) Preparation route of the N doped graphene foam CE.[149] (c) The decorating processes of a cationic polymer (PDDA) on graphene films by layer-by-layer assembling technique.[350] (d) *J-V* characteristics of DSSCs. Device A: electrolyte Z946 with PDDA/GO/ITO CE; Device B: electrolyte Z952 with PDDA/GO/ITO CE; Device C: Z946 with Pt/FTO CE.[350] (e) Schematic of flexible DSSC with PEDOT functionalized graphene CE.[364] (f) Schematic and photograph of a wire-shaped DSSC with Pt NPs/graphene CE and a titanium wire impregnated with titania nanotubes as the working electrode.[366]

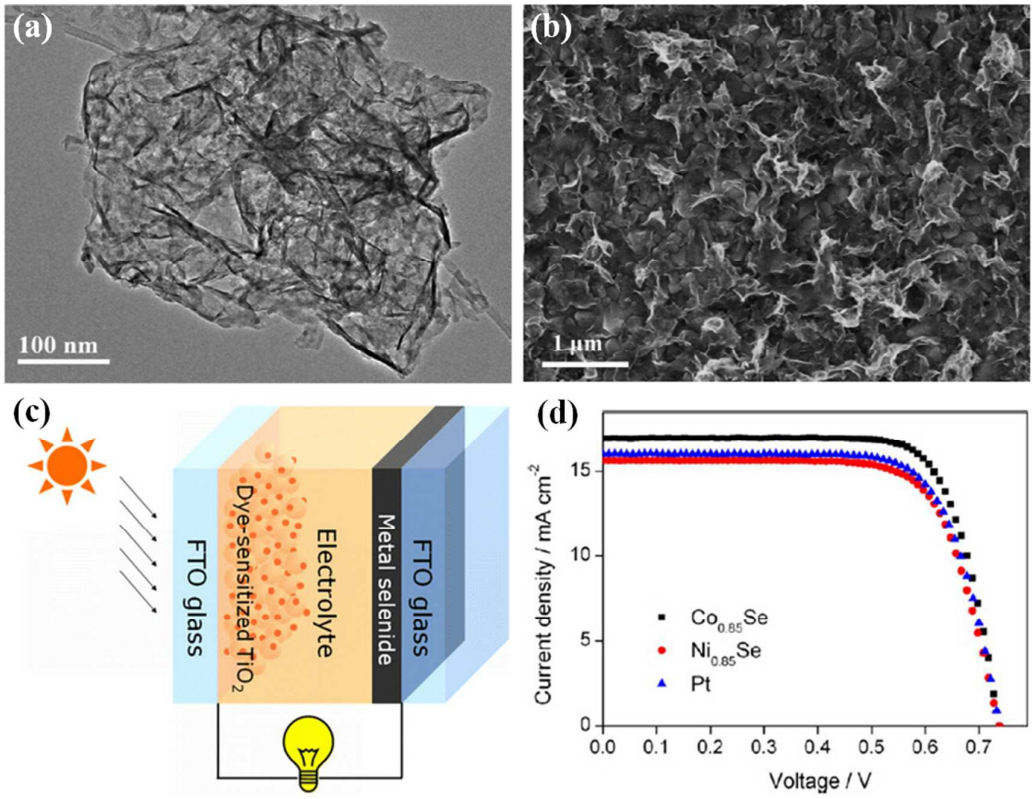

Fig. 19 (a) High-resolution transmission electron microscopy (HRTEM) image of as-synthesized $Co_{0.85}Se$ nanosheets.[372] (b) Field emission scanning electron microscopy (FESEM) image of $Co_{0.85}Se$ nanosheets grown on FTO glass.[372] (c) Schematic of DSSC with metal selenide ($Co_{0.85}Se$ or $Ni_{0.85}Se$) nanosheets as CE.[372] (d) *J-V* characteristics of DSSCs with different CEs, including $Co_{0.85}Se$, $Ni_{0.85}Se$ and Pt.[372]

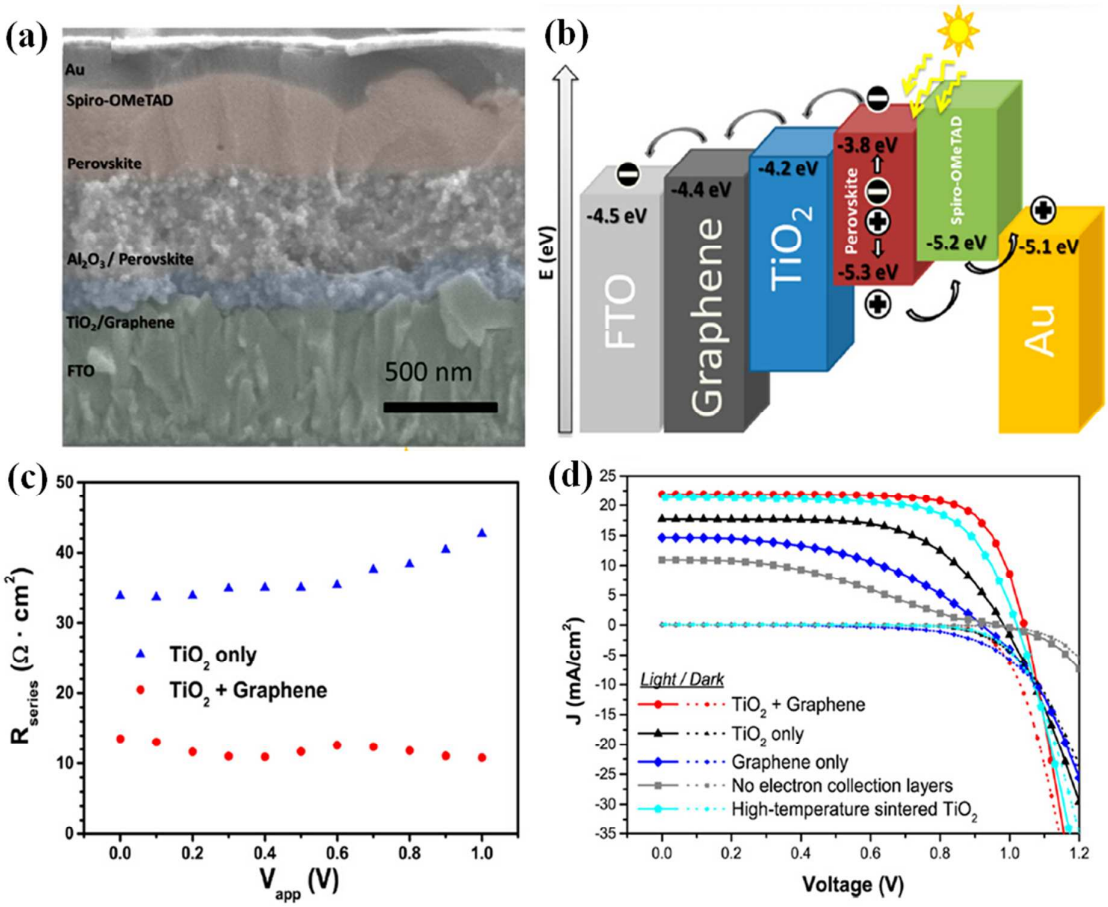

Fig. 20 (a) Cross-sectional SEM image and (b) energy levels of the perovskite solar cell with graphene/TiO_2 composite as ETL. (c) Series resistance (R_{series}) of the perovskite solar cells with graphene/TiO_2 composite or TiO_2 only as ETL. (d) *J-V* characteristics of the perovskite solar cells with different electron collection layers under solar irradiation (solid line) and in the dark (dotted line). [394]

Reference:

1. M. I. Hoffert, K. Caldeira, A. K. Jain, E. F. Haites, L. D. D. Harvey, S. D. Potter, M. E. Schlesinger, S. H. Schneider, R. G. Watts, T. M. L. Wigley and D. J. Wuebbles, *Nature*, 1998, **395**, 881-884.
2. M. A. Green, *Prog. Photovoltaics Rer. Appl.*, 2009, **17**, 183-189.
3. A. M. Bagher, *Sust. Energ.*, 2014, **2**, 85-90.
4. K. S. Novoselov, A. K. Geim, S. V. Morozov, D. Jiang, Y. Zhang, S. V. Dubonos, I. V. Grigorieva and A. A. Firsov, *Science*, 2004, **306**, 666-669.
5. A. K. Geim, *Science*, 2009, **324**, 1530-1534.
6. A. K. Geim and I. V. Grigorieva, *Nature*, 2013, **499**, 419-425.
7. P. Miro, M. Audiffred and T. Heine, *Chem. Soc. Rev.*, 2014, **43**, 6537-6554.
8. M. Xu, T. Liang, M. Shi and H. Chen, *Chem. Rev.*, 2013, **113**, 3766-3798.
9. D. Jariwala, V. K. Sangwan, L. J. Lauhon, T. J. Marks and M. C. Hersam, *ACS Nano*, 2014, **8**, 1102-1120.
10. Q. H. Wang, K. Kalantar-Zadeh, A. Kis, J. N. Coleman and M. S. Strano, *Nat. Nanotechnol.*, 2012, **7**, 699-712.
11. M. M. Benameur, B. Radisavljevic, J. S. Héron, S. Sahoo, H. Berger and A. Kis, *Nanotechnology*, 2011, **22**, 125706.
12. H. Liu, Y. Du, Y. Deng and P. D. Ye, *Chem. Soc. Rev.*, 2015, DOI: 10.1039/C1034CS00257A.
13. Y. Li and X. Chen, *2D Materials*, 2014, **1**, 031002.
14. E. Kan, M. Li, S. Hu, C. Xiao, H. Xiang and K. Deng, *J. Phys. Chem. Lett.*, 2013, **4**, 1120-1125.
15. D. Jose and A. Datta, *Acc. Chem. Res.*, 2013, **47**, 593-602.
16. A. O'Hare, F. V. Kusmartsev and K. I. Kugel, *Nano Lett.*, 2012, **12**, 1045-1052.
17. W. Niu, A. Eiden, G. Vijaya Prakash and J. J. Baumberg, *Appl. Phys. Lett.*, 2014, **104**, 171111.
18. A. C. Ferrari and D. M. Basko, *Nat. Nanotechnol.*, 2013, **8**, 235-246.
19. C. N. R. Rao, H. S. S. Ramakrishna Matte and U. Maitra, *Angew. Chem. Int. Ed. Engl.*, 2013, **52**, 13162-13185.
20. Y. Zhao, Y. Xie, Z. Liu, X. Wang, Y. Chai and F. Yan, *Small*, 2014, **10**, 4521-4542.
21. M. Chhowalla, H. S. Shin, G. Eda, L.-J. Li, K. P. Loh and H. Zhang, *Nat. Chem.*, 2013, **5**, 263-275.
22. Q. Bao and K. P. Loh, *ACS Nano*, 2012, **6**, 3677-3694.
23. H. Chang and H. Wu, *Adv. Funct. Mater.*, 2013, **23**, 1984-1997.
24. J. Li, L. Niu, Z. Zheng and F. Yan, *Adv. Mater.*, 2014, **26**, 5239-5273.
25. F. Bonaccorso, Z. Sun, T. Hasan and A. C. Ferrari, *Nat. Photon.*, 2010, **4**, 611-622.
26. F. Schwierz, *Nat. Nanotechnol.*, 2010, **5**, 487-496.
27. C. Huang, C. Li and G. Shi, *Energ. Environ. Sci.*, 2012, **5**, 8848-8868.
28. B. Luo, S. Liu and L. Zhi, *Small*, 2012, **8**, 630-646.
29. Y. Liu, X. Dong and P. Chen, *Chem. Soc. Rev.*, 2012, **41**, 2283-2307.
30. L. Feng, L. Wu and X. Qu, *Adv. Mater.*, 2013, **25**, 168-186.
31. F. Yan, M. Zhang and J. Li, *Adv. Healthc. Mater.*, 2014, **3**, 313-331.
32. Z. Yin, J. Zhu, Q. He, X. Cao, C. Tan, H. Chen, Q. Yan and H. Zhang, *Adv. Energy Mater.*, 2014, **4**, 1300574.
33. J. Du, S. Pei, L. Ma and H.-M. Cheng, *Adv. Mater.*, 2014, **26**, 1958-1991.
34. C.-H. Lee, G.-H. Lee, A. M. van der Zande, W. Chen, Y. Li, M. Han, X. Cui, G. Arefe, C. Nuckolls, T. F. Heinz, J. Guo, J. Hone and P. Kim, *Nat. Nanotechnol.*, 2014, **9**, 676-681.

35. X. Gu, W. Cui, H. Li, Z. Wu, Z. Zeng, S.-T. Lee, H. Zhang and B. Sun, *Adv. Energy Mater.*, 2013, **3**, 1262-1268.
36. A. K. Geim and K. S. Novoselov, *Nat. Mater.*, 2007, **6**, 183-191.
37. Z. Yin, H. Li, H. Li, L. Jiang, Y. Shi, Y. Sun, G. Lu, Q. Zhang, X. Chen and H. Zhang, *ACS Nano*, 2011, **6**, 74-80.
38. K. F. Mak, C. Lee, J. Hone, J. Shan and T. F. Heinz, *Phys. Rev. Lett.*, 2010, **105**, 136805.
39. Radisavljevic B, Radenovic A, Brivio J, Giacometti V and Kis A, *Nat. Nanotechnol.*, 2011, **6**, 147-150.
40. S. Stankovich, D. A. Dikin, R. D. Piner, K. A. Kohlhaas, A. Kleinhammes, Y. Jia, Y. Wu, S. T. Nguyen and R. S. Ruoff, *Carbon*, 2007, **45**, 1558-1565.
41. L. J. Cote, F. Kim and J. Huang, *J. Am. Chem. Soc.*, 2008, **131**, 1043-1049.
42. S. Stankovich, R. D. Piner, X. Chen, N. Wu, S. T. Nguyen and R. S. Ruoff, *J. Mater. Chem.*, 2006, **16**, 155-158.
43. B. Brodie, *Ann. Chim. Phys*, 1860, **59**, 466-472.
44. Y. Zhu, D. K. James and J. M. Tour, *Adv. Mater.*, 2012, **24**, 4924-4955.
45. K.-S. Shin, H. Jo, H.-J. Shin, W. M. Choi, J.-Y. Choi and S.-W. Kim, *J. Mater. Chem.*, 2012, **22**, 13032-13038.
46. S. Park and R. S. Ruoff, *Nat. Nanotechnol.*, 2009, **4**, 217-224.
47. H. A. Becerril, J. Mao, Z. Liu, R. M. Stoltenberg, Z. Bao and Y. Chen, *ACS Nano*, 2008, **2**, 463-470.
48. S.-Y. Bae, I.-Y. Jeon, J. Yang, N. Park, H. S. Shin, S. Park, R. S. Ruoff, L. Dai and J.-B. Baek, *ACS Nano*, 2011, **5**, 4974-4980.
49. F. Torrisi, T. Hasan, W. Wu, Z. Sun, A. Lombardo, T. S. Kulmala, G.-W. Hsieh, S. Jung, F. Bonaccorso, P. J. Paul, D. Chu and A. C. Ferrari, *ACS Nano*, 2012, **6**, 2992-3006.
50. S. Gilje, S. Han, M. Wang, K. L. Wang and R. B. Kaner, *Nano Lett.*, 2007, **7**, 3394-3398.
51. G. Wang, J. Yang, J. Park, X. Gou, B. Wang, H. Liu and J. Yao, *J. Phys. Chem. C*, 2008, **112**, 8192-8195.
52. V. Dua, S. P. Surwade, S. Ammu, S. R. Agnihotra, S. Jain, K. E. Roberts, S. Park, R. S. Ruoff and S. K. Manohar, *Angew. Chem. Int. Ed. Engl.*, 2010, **49**, 2154-2157.
53. G. Eda, H. Yamaguchi, D. Voiry, T. Fujita, M. Chen and M. Chhowalla, *Nano Lett.*, 2011, **11**, 5111-5116.
54. X. Li, G. Zhang, X. Bai, X. Sun, X. Wang, E. Wang and H. Dai, *Nat. Nanotechnol.*, 2008, **3**, 538-542.
55. Y. Hernandez, V. Nicolosi, M. Lotya, F. M. Blighe, Z. Sun, S. De, I. T. McGovern, B. Holland, M. Byrne, Y. K. Gun'Ko, J. J. Boland, P. Niraj, G. Duesberg, S. Krishnamurthy, R. Goodhue, J. Hutchison, V. Scardaci, A. C. Ferrari and J. N. Coleman, *Nat. Nanotechnol.*, 2008, **3**, 563-568.
56. M. Lotya, Y. Hernandez, P. J. King, R. J. Smith, V. Nicolosi, L. S. Karlsson, F. M. Blighe, S. De, Z. Wang, I. T. McGovern, G. S. Duesberg and J. N. Coleman, *J. Am. Chem. Soc.*, 2009, **131**, 3611-3620.
57. P. Blake, P. D. Brimicombe, R. R. Nair, T. J. Booth, D. Jiang, F. Schedin, L. A. Ponomarenko, S. V. Morozov, H. F. Gleeson, E. W. Hill, A. K. Geim and K. S. Novoselov, *Nano Lett.*, 2008, **8**, 1704-1708.
58. N. Behabtu, J. R. Lomeda, M. J. Green, A. L. Higginbotham, A. Sinitskii, D. V. Kosynkin, D. Tsentalovich, A. N. G. Parra-Vasquez, J. Schmidt, E. Kesselman, Y. Cohen, Y. Talmon, J. M. Tour and M. Pasquali, *Nat. Nanotechnol.*, 2010, **5**, 406-411.
59. N. Liu, F. Luo, H. Wu, Y. Liu, C. Zhang and J. Chen, *Adv. Funct. Mater.*, 2008, **18**, 1518-1525.

60. C.-Y. Su, A.-Y. Lu, Y. Xu, F.-R. Chen, A. N. Khlobystov and L.-J. Li, *ACS Nano*, 2011, **5**, 2332-2339.
61. Z. Zeng, Z. Yin, X. Huang, H. Li, Q. He, G. Lu, F. Boey and H. Zhang, *Angew. Chem. Int. Ed. Engl.*, 2011, **50**, 11093-11097.
62. K. S. Kim, Y. Zhao, H. Jang, S. Y. Lee, J. M. Kim, J. H. Ahn, P. Kim, J. Y. Choi and B. H. Hong, *Nature*, 2009, **457**, 706-710.
63. X. Li, W. Cai, J. An, S. Kim, J. Nah, D. Yang, R. Piner, A. Velamakanni, I. Jung, E. Tutuc, S. K. Banerjee, L. Colombo and R. S. Ruoff, *Science*, 2009, **324**, 1312-1314.
64. B. J. Kang, J. H. Mun, C. Y. Hwang and B. J. Cho, *J. Appl. Phys.*, 2009, **106**, 104309.
65. P. W. Sutter, J.-I. Flege and E. A. Sutter, *Nat. Mater.*, 2008, **7**, 406-411.
66. J. Coraux, A. T. N'Diaye, C. Busse and T. Michely, *Nano Lett.*, 2008, **8**, 565-570.
67. P. R. Somani, S. P. Somani and M. Umeno, *Chem. Phys. Lett.*, 2006, **430**, 56-59.
68. Q. Yu, J. Lian, S. Siriponglert, H. Li, Y. P. Chen and S.-S. Pei, *Appl. Phys. Lett.*, 2008, **93**, 113103.
69. Y. Zhang, L. Gomez, F. N. Ishikawa, A. Madaria, K. Ryu, C. Wang, A. Badmaev and C. Zhou, *J. Phys. Chem. Lett.*, 2010, **1**, 3101-3107.
70. X. Li, Y. Zhu, W. Cai, M. Borysiak, B. Han, D. Chen, R. D. Piner, L. Colombo and R. S. Ruoff, *Nano Lett.*, 2009, **9**, 4359-4363.
71. L. Gao, W. Ren, H. Xu, L. Jin, Z. Wang, T. Ma, L.-P. Ma, Z. Zhang, Q. Fu, L.-M. Peng, X. Bao and H.-M. Cheng, *Nat. Commun.*, 2012, **3**, 699.
72. Z. Yan, Z. Peng, Z. Sun, J. Yao, Y. Zhu, Z. Liu, P. M. Ajayan and J. M. Tour, *ACS Nano*, 2011, **5**, 8187-8192.
73. K. V. Emtsev, A. Bostwick, K. Horn, J. Jobst, G. L. Kellogg, L. Ley, J. L. McChesney, T. Ohta, S. A. Reshanov, J. Rohrl, E. Rotenberg, A. K. Schmid, D. Waldmann, H. B. Weber and T. Seyller, *Nat. Mater.*, 2009, **8**, 203-207.
74. C. Berger, Z. Song, X. Li, X. Wu, N. Brown, C. Naud, D. Mayou, T. Li, J. Hass, A. N. Marchenkov, E. H. Conrad, P. N. First and W. A. de Heer, *Science*, 2006, **312**, 1191-1196.
75. S. Bae, H. Kim, Y. Lee, X. Xu, J.-S. Park, Y. Zheng, J. Balakrishnan, T. Lei, H. Ri Kim, Y. I. Song, Y.-J. Kim, K. S. Kim, B. Ozyilmaz, J.-H. Ahn, B. H. Hong and S. Iijima, *Nat. Nanotechnol.*, 2010, **5**, 574-578.
76. D.-Y. Wang, I. S. Huang, P.-H. Ho, S.-S. Li, Y.-C. Yeh, D.-W. Wang, W.-L. Chen, Y.-Y. Lee, Y.-M. Chang, C.-C. Chen, C.-T. Liang and C.-W. Chen, *Adv. Mater.*, 2013, **25**, 4521-4526.
77. X. Wan, G. Long, L. Huang and Y. Chen, *Adv. Mater.*, 2011, **23**, 5342-5358.
78. A. Reina, X. Jia, J. Ho, D. Nezich, H. Son, V. Bulovic, M. S. Dresselhaus and J. Kong, *Nano Lett.*, 2008, **9**, 30-35.
79. C. Mattevi, H. Kim and M. Chhowalla, *J. Mater. Chem.*, 2011, **21**, 3324-3334.
80. Y. Zhan, Z. Liu, S. Najmaei, P. M. Ajayan and J. Lou, *Small*, 2012, **8**, 966-971.
81. X. Wang, H. Feng, Y. Wu and L. Jiao, *J. Am. Chem. Soc.*, 2013, **135**, 5304-5307.
82. K.-K. Liu, W. Zhang, Y.-H. Lee, Y.-C. Lin, M.-T. Chang, C.-Y. Su, C.-S. Chang, H. Li, Y. Shi, H. Zhang, C.-S. Lai and L.-J. Li, *Nano Lett.*, 2012, **12**, 1538-1544.
83. Y.-H. Lee, X.-Q. Zhang, W. Zhang, M.-T. Chang, C.-T. Lin, K.-D. Chang, Y.-C. Yu, J. T.-W. Wang, C.-S. Chang, L.-J. Li and T.-W. Lin, *Adv. Mater.*, 2012, **24**, 2320-2325.
84. Y. Shi, H. Li and L.-J. Li, *Chem. Soc. Rev.*, 2015, DOI: 10.1039/C1034CS00256C.
85. S. V. Morozov, K. S. Novoselov, M. I. Katsnelson, F. Schedin, D. C. Elias, J. A. Jaszczak and A. K. Geim, *Phys. Rev. Lett.*, 2008, **100**, 016602.
86. J.-H. Chen, C. Jang, S. Xiao, M. Ishigami and M. S. Fuhrer, *Nat. Nanotechnol.*, 2008, **3**, 206-209.
87. K. I. Bolotin, K. J. Sikes, Z. Jiang, M. Klima, G. Fudenberg, J. Hone, P. Kim and H. L. Stormer, *Solid State Commun.*, 2008, **146**, 351-355.

88. V. Podzorov, M. E. Gershenson, C. Kloc, R. Zeis and E. Bucher, *Appl. Phys. Lett.*, 2004, **84**, 3301-3303.
89. N. R. Pradhan, D. Rhodes, Y. Xin, S. Memaran, L. Bhaskaran, M. Siddiq, S. Hill, P. M. Ajayan and L. Balicas, *ACS Nano*, 2014, **8**, 7923-7929.
90. D. Ovchinnikov, A. Allain, Y.-S. Huang, D. Dumcenco and A. Kis, *ACS Nano*, 2014, **8**, 8174-8181.
91. L. Li, Y. Yu, G. J. Ye, Q. Ge, X. Ou, H. Wu, D. Feng, X. H. Chen and Y. Zhang, *Nat. Nanotechnol.*, 2014, **9**, 372-377.
92. A. B. Kuzmenko, E. van Heumen, F. Carbone and D. van der Marel, *Phys. Rev. Lett.*, 2008, **100**, 117401.
93. R. R. Nair, P. Blake, A. N. Grigorenko, K. S. Novoselov, T. J. Booth, T. Stauber, N. M. R. Peres and A. K. Geim, *Science*, 2008, **320**, 1308-1308.
94. K. F. Mak, M. Y. Sfeir, Y. Wu, C. H. Lui, J. A. Misewich and T. F. Heinz, *Phys. Rev. Lett.*, 2008, **101**, 196405.
95. M. Bernardi, M. Palummo and J. C. Grossman, *Nano Lett.*, 2013, **13**, 3664-3670.
96. J. Wu, M. Agrawal, H. A. Becerril, Z. Bao, Z. Liu, Y. Chen and P. Peumans, *ACS Nano*, 2009, **4**, 43-48.
97. S. Bhattacharyya and A. K. Singh, *Phys. Rev. B.*, 2012, **86**, 075454.
98. C. Lee, X. Wei, J. W. Kysar and J. Hone, *Science*, 2008, **321**, 385-388.
99. S. Bertolazzi, J. Brivio and A. Kis, *ACS Nano*, 2011, **5**, 9703-9709.
100. R. C. Cooper, C. Lee, C. A. Marianetti, X. Wei, J. Hone and J. W. Kysar, *Phys. Rev. B.*, 2013, **87**, 035423.
101. Y. Zhu, S. Murali, W. Cai, X. Li, J. W. Suk, J. R. Potts and R. S. Ruoff, *Adv. Mater.*, 2010, **22**, 3906-3924.
102. G. Zhu, T. Xu, T. Lv, L. Pan, Q. Zhao and Z. Sun, *J. Electroanal. Chem.*, 2011, **650**, 248-251.
103. S. Wang, F. Tristan, D. Minami, T. Fujimori, R. Cruz-Silva, M. Terrones, K. Takeuchi, K. Teshima, F. Rodríguez-Reinoso, M. Endo and K. Kaneko, *Carbon*, 2014, **76**, 220-231.
104. P. Afanasiev, G.-F. Xia, G. Berhault, B. Jouguet and M. Lacroix, *Chem. Mater.*, 1999, **11**, 3216-3219.
105. DasA, PisanaS, ChakrabortyB, PiscanecS, S. K. Saha, U. V. Waghmare, K. S. Novoselov, H. R. Krishnamurthy, A. K. Geim, A. C. Ferrari and A. K. Sood, *Nat. Nanotechnol.*, 2008, **3**, 210-215.
106. X. Wang, X. Li, L. Zhang, Y. Yoon, P. K. Weber, H. Wang, J. Guo and H. Dai, *Science*, 2009, **324**, 768-771.
107. X. Wang, L. Zhi and K. Müllen, *Nano Lett.*, 2007, **8**, 323-327.
108. F. Kurdesau, G. Khripunov, A. F. da Cunha, M. Kaelin and A. N. Tiwari, *J. Non-Cryst. Solids*, 2006, **352**, 1466-1470.
109. S. Pang, Y. Hernandez, X. Feng and K. Müllen, *Adv. Mater.*, 2011, **23**, 2779-2795.
110. D. S. Hecht, L. Hu and G. Irvin, *Adv. Mater.*, 2011, **23**, 1482-1513.
111. M.-G. Kang, M.-S. Kim, J. Kim and L. J. Guo, *Adv. Mater.*, 2008, **20**, 4408-4413.
112. S. H. Ahn and L. J. Guo, *Nano Lett.*, 2010, **10**, 4228-4234.
113. S. De, T. M. Higgins, P. E. Lyons, E. M. Doherty, P. N. Nirmalraj, W. J. Blau, J. J. Boland and J. N. Coleman, *ACS Nano*, 2009, **3**, 1767-1774.
114. J.-Y. Lee, S. T. Connor, Y. Cui and P. Peumans, *Nano Lett.*, 2008, **8**, 689-692.
115. Y.-M. Chang, L. Wang and W.-F. Su, *Org. Electron.*, 2008, **9**, 968-973.
116. S.-I. Na, S.-S. Kim, J. Jo and D.-Y. Kim, *Adv. Mater.*, 2008, **20**, 4061-4067.
117. S. Kirchmeyer and K. Reuter, *J. Mater. Chem.*, 2005, **15**, 2077-2088.

118. Z. Wu, Z. Chen, X. Du, J. M. Logan, J. Sippel, M. Nikolou, K. Kamaras, J. R. Reynolds, D. B. Tanner, A. F. Hebard and A. G. Rinzler, *Science*, 2004, **305**, 1273-1276.
119. A. D. Pasquier, H. E. Unalan, A. Kanwal, S. Miller and M. Chhowalla, *Appl. Phys. Lett.*, 2005, **87**, 203511.
120. H.-Z. Geng, K. K. Kim, K. P. So, Y. S. Lee, Y. Chang and Y. H. Lee, *J. Am. Chem. Soc.*, 2007, **129**, 7758-7759.
121. Y. Zhu, Z. Sun, Z. Yan, Z. Jin and J. M. Tour, *ACS Nano*, 2011, **5**, 6472-6479.
122. C. Jeong, P. Nair, M. Khan, M. Lundstrom and M. A. Alam, *Nano Lett.*, 2011, **11**, 5020-5025.
123. E. C. Garnett, W. Cai, J. J. Cha, F. Mahmood, S. T. Connor, M. Greyson Christoforo, Y. Cui, M. D. McGehee and M. L. Brongersma, *Nat. Mater.*, 2012, **11**, 241-249.
124. L. Hu, H. S. Kim, J. Y. Lee, P. Peumans and Y. Cui, *ACS Nano*, 2010, **4**, 2955-2963.
125. H. Wu, L. Hu, M. W. Rowell, D. Kong, J. J. Cha, J. R. McDonough, J. Zhu, Y. Yang, M. D. McGehee and Y. Cui, *Nano Lett.*, 2010, **10**, 4242-4248.
126. P. E. Lyons, S. De, J. Elias, M. Schamel, L. Philippe, A. T. Bellew, J. J. Boland and J. N. Coleman, *J. Phys. Chem. Lett.*, 2011, **2**, 3058-3062.
127. M. Song, D. S. You, K. Lim, S. Park, S. Jung, C. S. Kim, D.-H. Kim, D.-G. Kim, J.-K. Kim, J. Park, Y.-C. Kang, J. Heo, S.-H. Jin, J. H. Park and J.-W. Kang, *Adv. Funct. Mater.*, 2013, **23**, 4177-4184.
128. W. Zhang, B. Zhao, Z. He, X. Zhao, H. Wang, S. Yang, H. Wu and Y. Cao, *Energ. Environ. Sci.*, 2013, **6**, 1956-1964.
129. P. Matyba, H. Yamaguchi, M. Chhowalla, N. D. Robinson and L. Edman, *ACS Nano*, 2010, **5**, 574-580.
130. J. Li, L. Hu, L. Wang, Y. Zhou, G. Gruner and T. J. Marks, *Nano Lett*, 2006, **6**, 2472-2477.
131. D. Zhang, K. Ryu, X. Liu, E. Polikarpov, J. Ly, M. E. Tompson and C. Zhou, *Nano Lett.*, 2006, **6**, 1880-1886.
132. M. W. Rowell, M. A. Topinka, M. D. McGehee, H.-J. Prall, G. Dennler, N. S. Sariciftci, L. Hu and G. Gruner, *Appl. Phys. Lett.*, 2006, **88**, 233506.
133. K. Jiang, J. Wang, Q. Li, L. Liu, C. Liu and S. Fan, *Adv. Mater.*, 2011, **23**, 1154-1161.
134. J. Wang, *Electroanalysis*, 2005, **17**, 7-14.
135. J. Liu, Z. Yin, X. Cao, F. Zhao, A. Lin, L. Xie, Q. Fan, F. Boey, H. Zhang and W. Huang, *ACS Nano*, 2010, **4**, 3987-3992.
136. S. T. Han, Y. Zhou, C. Wang, L. He, W. Zhang and V. A. Roy, *Adv. Mater.*, 2013, **25**, 872-877.
137. K. K. Manga, J. Wang, M. Lin, J. Zhang, M. Nesladek, V. Nalla, W. Ji and K. P. Loh, *Adv. Mater.*, 2012, **24**, 1697-1702.
138. B. Chitara, L. S. Panchakarla, S. B. Krupanidhi and C. N. Rao, *Adv. Mater.*, 2011, **23**, 5419-5424.
139. S. Mao, G. Lu, K. Yu, Z. Bo and J. Chen, *Adv. Mater.*, 2010, **22**, 3521-3626.
140. O. S. Kwon, S. H. Lee, S. J. Park, J. H. An, H. S. Song, T. Kim, J. H. Oh, J. Bae, H. Yoon, T. H. Park and J. Jang, *Adv. Mater.*, 2013, **25**, 4177-4185.
141. S. Lee, G. Jo, S. J. Kang, G. Wang, M. Choe, W. Park, D. Y. Kim, Y. H. Kahng and T. Lee, *Adv. Mater.*, 2011, **23**, 100-105.
142. J. M. Lee, J. W. Choung, J. Yi, D. H. Lee, M. Samal, D. K. Yi, C. H. Lee, G. C. Yi, U. Paik, J. A. Rogers and W. I. Park, *Nano Lett.*, 2010, **10**, 2783-2788.
143. D. Chen, H. Feng and J. Li, *Chem. Rev.*, 2012, **112**, 6027-6053.
144. Z. Sun, Z. Yan, J. Yao, E. Beitler, Y. Zhu and J. M. Tour, *Nature*, 2010, **468**, 549-552.
145. R. A. Nistor, D. M. Newns and G. J. Martyna, *ACS Nano*, 2011, **5**, 3096-3103.
146. I. Gierz, C. Riedl, U. Starke, C. R. Ast and K. Kern, *Nano Lett.*, 2008, **8**, 4603-4607.

147. A. Kasry, M. A. Kuroda, G. J. Martyna, G. S. Tulevski and A. A. Bol, *ACS Nano*, 2010, **4**, 3839-3844.
148. Y. J. Yu, Y. Zhao, S. Ryu, L. E. Brus, K. S. Kim and P. Kim, *Nano Lett.*, 2009, **9**, 3430-3434.
149. S. Huh, J. Park, K. S. Kim, B. H. Hong and S. B. Kim, *ACS Nano*, 2011, **5**, 3639-3644.
150. G. Giovannetti, P. A. Khomyakov, G. Brocks, V. M. Karpan, J. van den Brink and P. J. Kelly, *Phys. Rev. Lett.*, 2008, **101**, 026803.
151. P. Huang, H. Zhu, L. Jing, Y. Zhao and X. Gao, *ACS Nano*, 2011, **5**, 7945-7949.
152. T. O. Wehling, K. S. Novoselov, S. V. Morozov, E. E. Vdovin, M. I. Katsnelson, A. K. Geim and A. I. Lichtenstein, *Nano Lett.*, 2008, **8**, 173-177.
153. C.-L. Hsu, C.-T. Lin, J.-H. Huang, C.-W. Chu, K.-H. Wei and L.-J. Li, *ACS Nano*, 2012, **6**, 5031-5039.
154. X. C. Dong, D. L. Fu, W. J. Fang, Y. M. Shi, P. Chen and L. J. Li, *Small*, 2009, **5**, 1422-1426.
155. S. Pei, J. Zhao, J. Du, W. Ren and H.-M. Cheng, *Carbon*, 2010, **48**, 4466-4474.
156. W. J. Yu, L. Liao, S. H. Chae, Y. H. Lee and X. Duan, *Nano Lett.*, 2011, **11**, 4759-4763.
157. K. K. Kim, A. Reina, Y. Shi, H. Park, L.-J. Li, Y. H. Lee and J. Kong, *Nanotechnology*, 2010, **21**, 285205.
158. W. H. Lee, J. W. Suk, J. Lee, Y. Hao, J. Park, J. W. Yang, H.-W. Ha, S. Murali, H. Chou, D. Akinwande, K. S. Kim and R. S. Ruoff, *ACS Nano*, 2012, **6**, 1284-1290.
159. G.-X. Ni, Y. Zheng, S. Bae, C. Y. Tan, O. Kahya, J. Wu, B. H. Hong, K. Yao and B. Özyilmaz, *ACS Nano*, 2012, **6**, 3935-3942.
160. S.-H. Bae, O. Kahya, B. K. Sharma, J. Kwon, H. J. Cho, B. Özyilmaz and J.-H. Ahn, *ACS Nano*, 2013, **7**, 3130-3138.
161. Z. Jin, J. Yao, C. Kittrell and J. M. Tour, *ACS Nano*, 2011, **5**, 4112-4117.
162. M. Bokdam, P. A. Khomyakov, G. Brocks, Z. Zhong and P. J. Kelly, *Nano Lett.*, 2011, **11**, 4631-4635.
163. B. Guo, Q. Liu, E. Chen, H. Zhu, L. Fang and J. R. Gong, *Nano Lett.*, 2010, **10**, 4975-4980.
164. D. Wei, Y. Liu, Y. Wang, H. Zhang, L. Huang and G. Yu, *Nano Lett.*, 2009, **9**, 1752-1758.
165. K. C. Kwon, K. S. Choi, B. J. Kim, J.-L. Lee and S. Y. Kim, *J. Phys. Chem. C*, 2012, **116**, 26586-26591.
166. J. H. Huang, J. H. Fang, C. C. Liu and C. W. Chu, *ACS Nano*, 2011, **5**, 6262-6271.
167. B. N. Szafranek, D. Schall, M. Otto, D. Neumaier and H. Kurz, *Nano Lett.*, 2011, **11**, 2640-2643.
168. P.-H. Ho, Y.-C. Yeh, D.-Y. Wang, S.-S. Li, H.-A. Chen, Y.-H. Chung, C.-C. Lin, W.-H. Wang and C.-W. Chen, *ACS Nano*, 2012, **6**, 6215-6221.
169. Z. Yan, J. Yao, Z. Z. Sun, Y. Zhu and J. M. Tour, *Small*, 2012, **8**, 59-62.
170. Y. Zhou, C. Fuentes-Hernandez, J. Shim, J. Meyer, A. J. Giordano, H. Li, P. Winget, T. Papadopoulos, H. Cheun, J. Kim, M. Fenoll, A. Dindar, W. Haske, E. Najafabadi, T. M. Khan, H. Sojoudi, S. Barlow, S. Graham, J.-L. Brédas, S. R. Marder, A. Kahn and B. Kippelen, *Science*, 2012, **336**, 327-332.
171. G. Jo, S.-I. Na, S.-H. Oh, S. Lee, T.-S. Kim, G. Wang, M. Choe, W. Park, J. Yoon, D.-Y. Kim, Y. H. Kahng and T. Lee, *Appl. Phys. Lett.*, 2010, **97**, 213301.
172. K.-W. Seo, J.-H. Lee, N. G. Cho, S. J. Kang, H.-K. Kim, S.-I. Na, H.-W. Koo and T.-W. Kim, *J. Vac. Sci. Technol., A*, 2014, **32**, 061201.
173. M.-S. Lee, K. Lee, S.-Y. Kim, H. Lee, J. Park, K.-H. Choi, H.-K. Kim, D.-G. Kim, D.-Y. Lee, S. Nam and J.-U. Park, *Nano Lett.*, 2013, **13**, 2814-2821.

174. D. Lee, H. Lee, Y. Ahn, Y. Jeong, D.-Y. Lee and Y. Lee, *Nanoscale*, 2013, **5**, 7750-7755.
175. I. N. Kholmanov, C. W. Magnuson, A. E. Aliev, H. Li, B. Zhang, J. W. Suk, L. L. Zhang, E. Peng, S. H. Mousavi, A. B. Khanikaev, R. Piner, G. Shvets and R. S. Ruoff, *Nano Lett.*, 2012, **12**, 5679-5683.
176. V. C. Tung, L. M. Chen, M. J. Allen, J. K. Wassei, K. Nelson, R. B. Kaner and Y. Yang, *Nano Lett.*, 2009, **9**, 1949-1955.
177. P. J. King, U. Khan, M. Lotya, S. De and J. N. Coleman, *ACS Nano*, 2010, **4**, 4238-4246.
178. P. Lin and F. Yan, *Adv. Mater.*, 2012, **24**, 34-51.
179. C. Liao and F. Yan, *Polym. Rev.*, 2013, **53**, 352-406.
180. H. Chang, G. Wang, A. Yang, X. Tao, X. Liu, Y. Shen and Z. Zheng, *Adv. Funct. Mater.*, 2010, **20**, 2893-2902.
181. V. C. Tung, J. Kim, L. J. Cote and J. Huang, *J. Am. Chem. Soc.*, 2011, **133**, 9262-9265.
182. G. Li, V. Shrotriya, J. Huang, Y. Yao, T. Moriarty, K. Emery and Y. Yang, *Nat. Mater.*, 2005, **4**, 864-868.
183. Z. He, C. Zhong, S. Su, M. Xu, H. Wu and Y. Cao, *Nat. Photon.*, 2012, **6**, 591-595.
184. J. You, L. Dou, K. Yoshimura, T. Kato, K. Ohya, T. Moriarty, K. Emery, C.-C. Chen, J. Gao, G. Li and Y. Yang, *Nat. Commun.*, 2013, **4**, 1446.
185. Y. Wang, X. Chen, Y. Zhong, F. Zhu and K. P. Loh, *Appl. Phys. Lett.*, 2009, **95**, 063302.
186. H. Park, J. A. Rowehl, K. K. Kim, V. Bulovic and J. Kong, *Nanotechnology*, 2010, **21**, 505204.
187. Y. Wang, S. W. Tong, X. F. Xu, B. Ozyilmaz and K. P. Loh, *Adv. Mater.*, 2011, **23**, 1514-1518.
188. H. Park, R. M. Howden, M. C. Barr, V. Bulovic, K. Gleason and J. Kong, *ACS Nano*, 2012, **6**, 6370-6377.
189. H. Park, S. Chang, M. Smith, S. Gradecak and J. Kong, *Sci. Rep.*, 2013, **3**, 1581.
190. H. Park, Y. Shi and J. Kong, *Nanoscale*, 2013, **5**, 8934-8939.
191. H. Park and J. Kong, *Adv. Energy Mater.*, 2014, **4**, 1301280.
192. L. Gomez De Arco, Y. Zhang, C. W. Schlenker, K. Ryu, M. E. Thompson and C. Zhou, *ACS Nano*, 2010, **4**, 2865-2873.
193. S. Lee, J. S. Yeo, Y. Ji, C. Cho, D. Y. Kim, S. I. Na, B. H. Lee and T. Lee, *Nanotechnology*, 2012, **23**, 344013.
194. Z. Liu, J. Li and F. Yan, *Adv. Mater.*, 2013, **25**, 4296-4301.
195. D. Liu, Y. Li, S. Zhao, A. Cao, C. Zhang, Z. Liu, Z. Bian, Z. Liu and C. Huang, *RSC Adv.*, 2013, **3**, 13720-13727.
196. B. H. Lee, J.-H. Lee, Y. H. Kahng, N. Kim, Y. J. Kim, J. Lee, T. Lee and K. Lee, *Adv. Funct. Mater.*, 2014, **24**, 1847-1856.
197. K. Kim, S.-H. Bae, C. T. Toh, H. Kim, J. H. Cho, D. Whang, T.-W. Lee, B. Özyilmaz and J.-H. Ahn, *ACS Appl. Mater. Interfaces*, 2014, **6**, 3299-3304.
198. H. Park, S. Chang, X. Zhou, J. Kong, T. Palacios and S. Gradečak, *Nano Lett.*, 2014, **14**, 5148-5154.
199. Y. Y. Lee, K. H. Tu, C. C. Yu, S. S. Li, J. Y. Hwang, C. C. Lin, K. H. Chen, L. C. Chen, H. L. Chen and C. W. Chen, *ACS Nano*, 2011, **5**, 6564-6570.
200. Z. Liu, J. Li, Z. H. Sun, G. Tai, S. P. Lau and F. Yan, *ACS Nano*, 2012, **6**, 810-818.
201. P. Lin, W. C. H. Choy, D. Zhang, F. Xie, J. Xin and C. W. Leung, *Appl. Phys. Lett.*, 2013, **102**, 113303.
202. X. Wang, L. Zhi, N. Tsao, Ž. Tomović, J. Li and K. Müllen, *Angew. Chem. Int. Ed. Engl.*, 2008, **47**, 2990-2992.

203. Q. Su, S. Pang, V. Alijani, C. Li, X. Feng and K. Müllen, *Adv. Mater.*, 2009, **21**, 3191-3195.
204. J. Wu, H. A. Becerril, Z. Bao, Z. Liu, Y. Chen and P. Peumans, *Appl. Phys. Lett.*, 2008, **92**, 263302.
205. E. Kymakis, K. Savva, M. M. Stylianakis, C. Fotakis and E. Stratakis, *Adv. Funct. Mater.*, 2013, **23**, 2742-2749.
206. Q. Zhang, X. Wan, F. Xing, L. Huang, G. Long, N. Yi, W. Ni, Z. Liu, J. Tian and Y. Chen, *Nano Res.*, 2013, **6**, 478-484.
207. A. R. b. M. Yusoff, S. J. Lee, F. K. Shneider, W. J. da Silva and J. Jang, *Adv. Energy Mater.*, 2014, **4**, DOI: 10.1002/aenm.201301989.
208. Z. Yin, S. Sun, T. Salim, S. Wu, X. Huang, Q. He, Y. M. Lam and H. Zhang, *ACS Nano*, 2010, **4**, 5263-5268.
209. H. Park, S. Chang, J. Jean, J. J. Cheng, P. T. Araujo, M. Wang, M. G. Bawendi, M. S. Dresselhaus, V. Bulovic, J. Kong and S. Gradecak, *Nano Lett.*, 2013, **13**, 233-239.
210. D. Zhang, F. Xie, P. Lin and W. C. H. Choy, *ACS Nano*, 2013, **7**, 1740-1747.
211. S.-S. Li, K.-H. Tu, C.-C. Lin, C.-W. Chen and M. Chhowalla, *ACS Nano*, 2010, **4**, 3169-3174.
212. S.-H. Lee, D.-H. Kim, J.-H. Kim, G.-S. Lee and J.-G. Park, *J. Phys. Chem. C*, 2009, **113**, 21915-21920.
213. V. Shrotriya, G. Li, Y. Yao, C.-W. Chu and Y. Yang, *Appl. Phys. Lett.*, 2006, **88**, 073508.
214. A. Hadipour, D. Cheyns, P. Heremans and B. P. Rand, *Adv. Energy Mater.*, 2011, **1**, 930-935.
215. M. D. Irwin, D. B. Buchholz, A. W. Hains, R. P. H. Chang and T. J. Marks, *PNAS*, 2008, **105**, 2783-2787.
216. J.-M. Yun, J.-S. Yeo, J. Kim, H.-G. Jeong, D.-Y. Kim, Y.-J. Noh, S.-S. Kim, B.-C. Ku and S.-I. Na, *Adv. Mater.*, 2011, **23**, 4923-4928.
217. J. Liu, G.-H. Kim, Y. Xue, J. Y. Kim, J.-B. Baek, M. Durstock and L. Dai, *Adv. Mater.*, 2014, **26**, 786-790.
218. M. Li, W. Ni, B. Kan, X. Wan, L. Zhang, Q. Zhang, G. Long, Y. Zuo and Y. Chen, *Phys. Chem. Chem. Phys.*, 2013, **15**, 18973-18978.
219. C. T. G. Smith, R. W. Rhodes, M. J. Beliatis, K. D. G. Imalka Jayawardena, L. J. Rozanski, C. A. Mills and S. R. P. Silva, *Appl. Phys. Lett.*, 2014, **105**, 073304.
220. J.-S. Yeo, J.-M. Yun, Y.-S. Jung, D.-Y. Kim, Y.-J. Noh, S.-S. Kim and S.-I. Na, *J. Mater. Chem. A*, 2014, **2**, 292-298.
221. I. P. Murray, S. J. Lou, L. J. Cote, S. Loser, C. J. Kadleck, T. Xu, J. M. Szarko, B. S. Rolczynski, J. E. Johns, J. Huang, L. Yu, L. X. Chen, T. J. Marks and M. C. Hersam, *J. Phys. Chem. Lett.*, 2011, **2**, 3006-3012.
222. J. Kim, V. C. Tung and J. Huang, *Adv. Energy Mater.*, 2011, **1**, 1052-1057.
223. J. Liu, Y. Xue and L. Dai, *J. Phys. Chem. Lett.*, 2012, **3**, 1928-1933.
224. D. D. Nguyen, N. H. Tai, Y. L. Chueh, S. Y. Chen, Y. J. Chen, W. S. Kuo, T. W. Chou, C. S. Hsu and L. J. Chen, *Nanotechnology*, 2011, **22**, 295606.
225. B. Yin, Q. Liu, L. Y. Yang, X. M. Wu, Z. F. Liu, Y. L. Hua, S. G. Yin and Y. S. Chen, *J. Nanosci. Nanotechnol.*, 2010, **10**, 1934-1938.
226. J. C. Yu, J. I. Jang, B. R. Lee, G.-W. Lee, J. T. Han and M. H. Song, *ACS Appl. Mater. Interfaces*, 2014, **6**, 2067-2073.
227. Y.-H. Chao, J.-S. Wu, C.-E. Wu, J.-F. Jheng, C.-L. Wang and C.-S. Hsu, *Adv. Energy Mater.*, 2013, **3**, 1279-1285.
228. J. J. Intemann, K. Yao, Y.-X. Li, H.-L. Yip, Y.-X. Xu, P.-W. Liang, C.-C. Chueh, F.-Z. Ding, X. Yang, X. Li, Y. Chen and A. K. Y. Jen, *Adv. Funct. Mater.*, 2014, **24**, 1465-1473.

229. Y. Gao, H.-L. Yip, S. K. Hau, K. M. O'Malley, N. C. Cho, H. Chen and A. K.-Y. Jen, *Appl. Phys. Lett.*, 2010, **97**, 203306.
230. S. S. Li, K. H. Tu, C. C. Lin, C. W. Chen and M. Chhowalla, *ACS Nano*, 2010, **4**, 3169-3174.
231. Y. Gao, H. L. Yip, K. S. Chen, K. M. O'Malley, O. Acton, Y. Sun, G. Ting, H. Chen and A. K. Jen, *Adv. Mater.*, 2011, **23**, 1903-1908.
232. A. R. b. Mohd Yusoff, H. P. Kim and J. Jang, *Nanoscale*, 2014, **6**, 1537-1544.
233. D. Yang, L. Zhou, L. Chen, B. Zhao, J. Zhang and C. Li, *Chem. Commun.*, 2012, **48**, 8078-8080.
234. E. Stratakis, K. Savva, D. Konios, C. Petridis and E. Kymakis, *Nanoscale*, 2014, **6**, 6925-6931.
235. S.-H. Kim, C.-H. Lee, J.-M. Yun, Y.-J. Noh, S.-S. Kim, S. Lee, S. M. Jo, H.-I. Joh and S.-I. Na, *Nanoscale*, 2014, **6**, 7183-7187.
236. D. Yang, L. Zhou, W. Yu, J. Zhang and C. Li, *Adv. Energy Mater.*, 2014, **4**, 1400591.
237. J. Liu, Y. Xue, Y. Gao, D. Yu, M. Durstock and L. Dai, *Adv. Mater.*, 2012, **24**, 2228-2233.
238. H. B. Yang, Y. Q. Dong, X. Wang, S. Y. Khoo and B. Liu, *ACS Appl. Mater. Interfaces*, 2013, **6**, 1092-1099.
239. S. Qu, M. Li, L. Xie, X. Huang, J. Yang, N. Wang and S. Yang, *ACS Nano*, 2013, **7**, 4070-4081.
240. M. J. Beliatis, K. K. Gandhi, L. J. Rozanski, R. Rhodes, L. McCafferty, M. R. Alenezi, A. S. Alshammari, C. A. Mills, K. D. G. I. Jayawardena, S. J. Henley and S. R. P. Silva, *Adv. Mater.*, 2014, **26**, 2078-2083.
241. K. D. G. I. Jayawardena, R. Rhodes, K. K. Gandhi, M. R. R. Prabhath, G. D. M. R. Dabera, M. J. Beliatis, L. J. Rozanski, S. J. Henley and S. R. P. Silva, *J. Mater. Chem. A*, 2013, **1**, 9922-9927.
242. D. H. Wang, J. K. Kim, J. H. Seo, I. Park, B. H. Hong, J. H. Park and A. J. Heeger, *Angew. Chem. Int. Ed. Engl.*, 2013, **52**, 2874-2880.
243. S. W. Tong, Y. Wang, Y. Zheng, M.-F. Ng and K. P. Loh, *Adv. Funct. Mater.*, 2011, **21**, 4430-4435.
244. V. C. Tung, J. Kim and J. Huang, *Adv. Energy Mater.*, 2012, **2**, 299-303.
245. Y. Chen, W.-C. Lin, J. Liu and L. Dai, *Nano Lett.*, 2014, **14**, 1467-1471.
246. Z. Liu, Q. Liu, Y. Huang, Y. Ma, S. Yin, X. Zhang, W. Sun and Y. Chen, *Adv. Mater.*, 2008, **20**, 3924-3930.
247. V. Gupta, N. Chaudhary, R. Srivastava, G. D. Sharma, R. Bhardwaj and S. Chand, *J. Am. Chem. Soc.*, 2011, **133**, 9960-9963.
248. Y. Li, Y. Hu, Y. Zhao, G. Shi, L. Deng, Y. Hou and L. Qu, *Adv. Mater.*, 2011, **23**, 776-780.
249. D. Yu, Y. Yang, M. Durstock, J. B. Baek and L. Dai, *ACS Nano*, 2010, **4**, 5633-5640.
250. D. Yu, K. Park, M. Durstock and L. Dai, *J. Phys. Chem. Lett.*, 2011, **2**, 1113-1118.
251. T. Mahmoudi, W.-Y. Rho, H.-Y. Yang, S. R. P. Silva and Y.-B. Hahn, *Chem. Commun.*, 2014, **50**, 8705-8708.
252. G. H. Jun, S. H. Jin, B. Lee, B. H. Kim, W.-S. Chae, S. H. Hong and S. Jeon, *Energ. Environ. Sci.*, 2013, **6**, 3000-3006.
253. J. K. Kim, M. J. Park, S. J. Kim, D. H. Wang, S. P. Cho, S. Bae, J. H. Park and B. H. Hong, *ACS Nano*, 2013, **7**, 7207-7212.
254. S. Günes, H. Neugebauer and N. S. Sariciftci, *Chem. Rev.*, 2007, **107**, 1324-1338.
255. M. Shanmugam, T. Bansal, C. A. Durcan and B. Yu, *Appl. Phys. Lett.*, 2012, **100**, 153901.
256. M. Shanmugam, C. A. Durcan, R. Jacobs-Gedrim and B. Yu, *Nano Energy*, 2013, **2**, 419-424.

257. W. Liu, X. Yang, Y. Zhang, M. Xu and H. Chen, *RSC Adv.*, 2014, **4**, 32744-32748.
258. X. Yang, W. Fu, W. Liu, J. Hong, Y. Cai, C. Jin, M. Xu, H. Wang, D. Yang and H. Chen, *J. Mater. Chem. A*, 2014, **2**, 7727-7733.
259. Q. V. Le, T. P. Nguyen and S. Y. Kim, *Phys. Status Solidi-Rapid Res. Lett.*, 2014, **8**, 390-394.
260. X. Gu, W. Cui, T. Song, C. Liu, X. Shi, S. Wang and B. Sun, *ChemSusChem*, 2014, **7**, 416-420.
261. Q. V. Le, T. P. Nguyen, K. S. Choi, Y.-H. Cho, Y. J. Hong and S. Y. Kim, *Phys. Chem. Chem. Phys.*, 2014, **16**, 25468-25472.
262. M. A. Ibrahem, T.-w. Lan, J. K. Huang, Y.-Y. Chen, K.-H. Wei, L.-J. Li and C. W. Chu, *RSC Adv.*, 2013, **3**, 13193-13202.
263. J.-M. Yun, Y.-J. Noh, J.-S. Yeo, Y.-J. Go, S.-I. Na, H.-G. Jeong, J. Kim, S. Lee, S.-S. Kim, H. Y. Koo, T.-W. Kim and D.-Y. Kim, *J. Mater. Chem. C*, 2013, **1**, 3777-3783.
264. V. Berry, *Carbon*, 2013, **62**, 1-10.
265. M. Topsakal, H. Şahin and S. Ciraci, *Phys. Rev. B.*, 2012, **85**, 155445.
266. H. Yamaguchi, J. Granstrom, W. Nie, H. Sojoudi, T. Fujita, D. Voiry, M. Chen, G. Gupta, A. D. Mohite, S. Graham and M. Chhowalla, *Adv. Energy Mater.*, 2014, **4**, DOI:10.1002/aenm.201300986.
267. T. Kim, J. H. Kang, S. J. Yang, S. J. Sung, Y. S. Kim and C. R. Park, *Energ. Environ. Sci.*, 2014, **7**, 3403-3411.
268. Y. F. Li, W. Yang, Z. Q. Tu, Z. C. Liu, F. Yang, L. Q. Zhang and R. Hatakeyama, *Appl. Phys. Lett.*, 2014, **104**, 043903.
269. X. Li, H. Zhu, K. Wang, A. Cao, J. Wei, C. Li, Y. Jia, Z. Li and D. Wu, *Adv. Mater.*, 2010, **22**, 2743-2748.
270. G. Fan, H. Zhu, K. Wang, J. Wei, X. Li, Q. Shu, N. Guo and D. Wu, *ACS Appl. Mater. Interfaces*, 2011, **3**, 721-725.
271. T. Feng, D. Xie, Y. Lin, Y. Zang, T. Ren, R. Song, H. Zhao, H. Tian, X. Li, H. Zhu and L. Liu, *Appl. Phys. Lett.*, 2011, **99**, 233505.
272. X. Li, L. Fan, Z. Li, K. Wang, M. Zhong, J. Wei, D. Wu and H. Zhu, *Adv. Energy Mater.*, 2012, **2**, 425-429.
273. Y. Lin, X. Li, D. Xie, T. Feng, Y. Chen, R. Song, H. Tian, T. Ren, M. Zhong, K. Wang and H. Zhu, *Energ. Environ. Sci.*, 2013, **6**, 108-115.
274. Y. Wu, X. Zhang, J. Jie, C. Xie, X. Zhang, B. Sun, Y. Wang and P. Gao, *J. Phys. Chem. C*, 2013, **117**, 11968-11976.
275. T. Cui, R. Lv, Z.-H. Huang, X. Gan, K. Wang, D. Wu, H. Zhu and F. Kang, *RSC Adv.*, 2013, **3**, 22295-22300.
276. T. Feng, D. Xie, Y. Lin, H. Zhao, Y. Chen, H. Tian, T. Ren, X. Li, Z. Li, K. Wang, D. Wu and H. Zhu, *Nanoscale*, 2012, **4**, 2130-2133.
277. C. Xie, P. Lv, B. Nie, J. Jie, X. Zhang, Z. Wang, P. Jiang, Z. Hu, L. Luo, Z. Zhu, L. Wang and C. Wu, *Appl. Phys. Lett.*, 2011, **99**, 133113.
278. T. Cui, R. Lv, Z.-H. Huang, S. Chen, Z. Zhang, X. Gan, Y. Jia, X. Li, K. Wang, D. Wu and F. Kang, *J. Mater. Chem. A*, 2013, **1**, 5736-5740.
279. H.-J. Shin, W. M. Choi, D. Choi, G. H. Han, S.-M. Yoon, H.-K. Park, S.-W. Kim, Y. W. Jin, S. Y. Lee, J. M. Kim, J.-Y. Choi and Y. H. Lee, *J. Am. Chem. Soc.*, 2010, **132**, 15603-15609.
280. X. An, F. Liu and S. Kar, *Carbon*, 2013, **57**, 329-337.
281. X. Miao, S. Tongay, M. K. Petterson, K. Berke, A. G. Rinzler, B. R. Appleton and A. F. Hebard, *Nano Lett.*, 2012, **12**, 2745-2750.
282. X. Li, D. Xie, H. Park, T. H. Zeng, K. Wang, J. Wei, M. Zhong, D. Wu, J. Kong and H. Zhu, *Adv. Energy Mater.*, 2013, **3**, 1029-1034.

283. X. Li, D. Xie, H. Park, M. Zhu, T. H. Zeng, K. Wang, J. Wei, D. Wu, J. Kong and H. Zhu, *Nanoscale*, 2013, **5**, 1945-1948.
284. C. Xie, X. Zhang, Y. Wu, X. Zhang, X. Zhang, Y. Wang, W. Zhang, P. Gao, Y. Han and J. Jie, *J. Mater. Chem. A*, 2013, **1**, 8567-8574.
285. V. V. Brus, M. A. Gluba, X. Zhang, K. Hinrichs, J. Rappich and N. H. Nickel, *Phys. Status. Solidi. A.*, 2014, **211**, 843-847.
286. C. Xie, X. Zhang, K. Ruan, Z. Shao, S. S. Dhaliwal, L. Wang, Q. Zhang, X. Zhang and J. Jie, *J. Mater. Chem. A*, 2013, **1**, 15348-15354.
287. X. Zhang, C. Xie, J. Jie, X. Zhang, Y. Wu and W. Zhang, *J. Mater. Chem. A*, 2013, **1**, 6593-6601.
288. E. Shi, H. Li, L. Yang, L. Zhang, Z. Li, P. Li, Y. Shang, S. Wu, X. Li, J. Wei, K. Wang, H. Zhu, D. Wu, Y. Fang and A. Cao, *Nano Lett.*, 2013, **13**, 1776-1781.
289. L. Yang, X. Yu, M. Xu, H. Chen and D. Yang, *J. Mater. Chem. A*, 2014, **2**, 16877-16883.
290. K. Jiao, X. Wang, Y. Wang and Y. Chen, *J. Mater. Chem. C*, 2014, **2**, 7715-7721.
291. Y. Ye, Y. Dai, L. Dai, Z. Shi, N. Liu, F. Wang, L. Fu, R. Peng, X. Wen, Z. Chen, Z. Liu and G. Qin, *ACS Appl. Mater. Interfaces*, 2010, **2**, 3406-3410.
292. Y. Ye, L. Gan, L. Dai, Y. Dai, X. Guo, H. Meng, B. Yu, Z. Shi, K. Shang and G. Qin, *Nanoscale*, 2011, **3**, 1477-1481.
293. L. Britnell, R. M. Ribeiro, A. Eckmann, R. Jalil, B. D. Belle, A. Mishchenko, Y.-J. Kim, R. V. Gorbachev, T. Georgiou, S. V. Morozov, A. N. Grigorenko, A. K. Geim, C. Casiraghi, A. H. C. Neto and K. S. Novoselov, *Science*, 2013, **340**, 1311-1314.
294. M. Shanmugam, C. A. Durcan and B. Yu, *Nanoscale*, 2012, **4**, 7399-7405.
295. M.-L. Tsai, S.-H. Su, J.-K. Chang, D.-S. Tsai, C.-H. Chen, C.-I. Wu, L.-J. Li, L.-J. Chen and J.-H. He, *ACS Nano*, 2014, **8**, 8317-8322.
296. B. Wang, J. Park, D. Su, C. Wang, H. Ahn and G. Wang, *J. Mater. Chem.*, 2012, **22**, 15750-15756.
297. C.-Y. Chen, Z.-Y. Shih, Z. Yang and H.-T. Chang, *J. Power Sources*, 2012, **215**, 43-47.
298. X. Fang, T. Song, R. Liu and B. Sun, *J. Phys. Chem. C*, 2014, **118**, 20238-20245.
299. J. R. Williams, L. DiCarlo and C. M. Marcus, *Science*, 2007, **317**, 638-641.
300. K. Yan, D. Wu, H. Peng, L. Jin, Q. Fu, X. Bao and Z. Liu, *Nat. Commun.*, 2012, **3**, 1280.
301. M. Buscema, D. J. Groenendijk, G. A. Steele, H. S. J. van der Zant and A. Castellanos-Gomez, *Nat. Commun.*, 2014, DOI: 10.1038/ncomms5651.
302. B. W. H. Baugher, H. O. H. Churchill, Y. Yang and P. Jarillo-Herrero, *Nat. Nanotechnol.*, 2014, **9**, 262-267.
303. A. Pospischil, M. M. Furchi and T. Mueller, *Nat. Nanotechnol.*, 2014, **9**, 257-261.
304. Y. Deng, Z. Luo, N. J. Conrad, H. Liu, Y. Gong, S. Najmaei, P. M. Ajayan, J. Lou, X. Xu and P. D. Ye, *ACS Nano*, 2014, **8**, 8292-8299.
305. X. Hong, J. Kim, S.-F. Shi, Y. Zhang, C. Jin, Y. Sun, S. Tongay, J. Wu, Y. Zhang and F. Wang, *Nat. Nanotechnol.*, 2014, **9**, 682-686.
306. R. Cheng, D. Li, H. Zhou, C. Wang, A. Yin, S. Jiang, Y. Liu, Y. Chen, Y. Huang and X. Duan, *Nano Lett.*, 2014, **14**, 5590-5597.
307. S. Wi, H. Kim, M. Chen, H. Nam, L. J. Guo, E. Meyhofer and X. Liang, *ACS Nano*, 2014, **8**, 5270-5281.
308. B. O'Regan and M. Gratzel, *Nature*, 1991, **353**, 737-740.
309. S. Yun, A. Hagfeldt and T. Ma, *Adv. Mater.*, 2014, **26**, 6210-6237.
310. J. D. Roy-Mayhew and I. A. Aksay, *Chem. Rev.*, 2014, **114**, 6323-6348.
311. Z. He, H. Phan, J. Liu, T.-Q. Nguyen and T. T. Y. Tan, *Adv. Mater.*, 2013, **25**, 6900-6904.

312. J. Fan, S. Liu and J. Yu, *J. Mater. Chem.*, 2012, **22**, 17027-17036.
313. T. Chen, W. Hu, J. Song, G. H. Guai and C. M. Li, *Adv. Funct. Mater.*, 2012, **22**, 5245-5250.
314. N. Yang, J. Zhai, D. Wang, Y. Chen and L. Jiang, *ACS Nano*, 2010, **4**, 887-894.
315. Y. Liu, Y. Cheng, W. Shu, Z. Peng, K. Chen, J. Zhou, W. Chen and G. S. Zakharova, *Nanoscale*, 2014, **6**, 6755-6762.
316. M. Wu and T. Ma, *ChemSusChem*, 2012, **5**, 1343-1357.
317. T. N. Murakami, S. Ito, Q. Wang, M. K. Nazeeruddin, T. Bessho, I. Cesar, P. Liska, R. Humphry-Baker, P. Comte, P. Péchy and M. Grätzel, *J. Electrochem. Soc.*, 2006, **153**, 2255-2261.
318. P. Joshi, L. Zhang, Q. Chen, D. Galipeau, H. Fong and Q. Qiao, *ACS Appl. Mater. Interfaces*, 2010, **2**, 3572-3577.
319. S. Pan, Z. Yang, P. Chen, X. Fang, G. Guan, Z. Zhang, J. Deng and H. Peng, *J. Phys. Chem. C*, 2013, **118**, 16419-16425.
320. K. S. Lee, W. J. Lee, N.-G. Park, S. O. Kim and J. H. Park, *Chem. Commun.*, 2011, **47**, 4264-4266.
321. M.-H. Yeh, L.-Y. Lin, C.-L. Sun, Y.-A. Leu, J.-T. Tsai, C.-Y. Yeh, R. Vittal and K.-C. Ho, *J. Phys. Chem. C*, 2014, **118**, 16626-16634.
322. M. Wu, X. Lin, T. Wang, J. Qiu and T. Ma, *Energ. Environ. Sci.*, 2011, **4**, 2308-2315.
323. Y. Xu, H. Bai, G. Lu, C. Li and G. Shi, *J. Am. Chem. Soc.*, 2008, **130**, 5856-5857.
324. W. Hong, Y. Xu, G. Lu, C. Li and G. Shi, *Electrochem. Commun.*, 2008, **10**, 1555-1558.
325. D. W. Zhang, X. D. Li, H. B. Li, S. Chen, Z. Sun, X. J. Yin and S. M. Huang, *Carbon*, 2011, **49**, 5382-5388.
326. J.-S. Lee, H.-J. Ahn, J.-C. Yoon and J.-H. Jang, *Phys. Chem. Chem. Phys.*, 2012, **14**, 7938-7943.
327. H. Wang, K. Sun, F. Tao, D. J. Stacchiola and Y. H. Hu, *Angew. Chem. Int. Ed. Engl.*, 2013, **52**, 9210-9214.
328. W. Wei, K. Sun and Y. H. Hu, *J. Mater. Chem. A*, 2014, **2**, 16842-16846.
329. C. Y. Neo, N. K. Gopalan and J. Ouyang, *J. Mater. Chem. A*, 2014, **2**, 9226-9235.
330. G. Zhu, L. Pan, T. Lu, T. Xu and Z. Sun, *J. Mater. Chem.*, 2011, **21**, 14869-14875.
331. M.-H. Yeh , L.-Y. Lin , J.-S. Su, Y.-A. Leu, R. Vittal, C.-L. Sun and K.-C. Ho, *ChemElectroChem*, 2014, **1**, 416-425.
332. K. Saranya, N. Sivasankar and A. Subramania, *RSC Adv.*, 2014, **4**, 36226-36233.
333. R. Cruz, J. P. Araujo, L. Andrade and A. Mendes, *J. Mater. Chem. A*, 2014, **2**, 2028-2032.
334. R. Bajpai, S. Roy, N. kulshrestha, J. Rafiee, N. Koratkar and D. S. Misra, *Nanoscale*, 2012, **4**, 926-930.
335. Q. Chang, Z. Wang, J. Wang, Y. Yan, Z. Ma, J. Zhu, W. Shi, Q. Chen, Q. Yu and L. Huang, *Nanoscale*, 2014, **6**, 5410-5415.
336. Z. Yang, M. Liu, C. Zhang, W. W. Tjiu, T. Liu and H. Peng, *Angew. Chem. Int. Ed. Engl.*, 2013, **52**, 3996-3999.
337. E. Bi, H. Chen, X. Yang, W. Peng, M. Gratzel and L. Han, *Energ. Environ. Sci.*, 2014, **7**, 2637-2641.
338. A. Kaniyoor and S. Ramaprabhu, *J. Mater. Chem.*, 2012, **22**, 8377-8384.
339. J. D. Roy-Mayhew, D. J. Bozym, C. Punckt and I. A. Aksay, *ACS Nano*, 2010, **4**, 6203-6211.
340. S. Das, P. Sudhagar, E. Ito, D.-y. Lee, S. Nagarajan, S. Y. Lee, Y. S. Kang and W. Choi, *J. Mater. Chem.*, 2012, **22**, 20490-20497.
341. L. Song, Q. Luo, F. Zhao, Y. Li, H. Lin, L. Qu and Z. Zhang, *Phys. Chem. Chem. Phys.*, 2014, **16**, 21820-21826.

342. H.-J. Ahn, I.-H. Kim, J.-C. Yoon, S.-I. Kim and J.-H. Jang, *Chem. Commun.*, 2014, **50**, 2412-2415.
343. S.-M. Jung, I. T. Choi, K. Lim, J. Ko, J. C. Kim, J.-J. Lee, M. J. Ju, H. K. Kim and J.-B. Baek, *Chem. Mater.*, 2014, **26**, 3586-3591.
344. H. Fang, C. Yu, T. Ma and J. Qiu, *Chem. Commun.*, 2014, **50**, 3328-3330.
345. Q. Luo, F. Hao, S. Wang, H. Shen, L. Zhao, J. Li, M. Grätzel and H. Lin, *J. Phys. Chem. C*, 2014, **118**, 17010-17018.
346. S. Das, P. Sudhagar, V. Verma, D. Song, E. Ito, S. Y. Lee, Y. S. Kang and W. Choi, *Adv. Funct. Mater.*, 2011, **21**, 3729-3736.
347. Y. Xue, J. Liu, H. Chen, R. Wang, D. Li, J. Qu and L. Dai, *Angew. Chem. Int. Ed. Engl.*, 2012, **51**, 12124-12127.
348. P. Zhai, T.-C. Wei, Y.-H. Chang, Y.-T. Huang, W.-T. Yeh, H. Su and S.-P. Feng, *Small*, 2014, **10**, 3347-3353.
349. A. G. Kannan, J. Zhao, S. G. Jo, Y. S. Kang and D.-W. Kim, *J. Mater. Chem. A*, 2014, **2**, 12232-12239.
350. X. Xu, D. Huang, K. Cao, M. Wang, S. M. Zakeeruddin and M. Gratzel, *Sci. Rep.*, 2013, **3**, 1489.
351. W. Kubo, S. Kambe, S. Nakade, T. Kitamura, K. Hanabusa, Y. Wada and S. Yanagida, *J. Phys. Chem. B*, 2003, **107**, 4374-4381.
352. G. Boschloo and A. Hagfeldt, *Acc. Chem. Res.*, 2009, **42**, 1819-1826.
353. T. W. Hamann, R. A. Jensen, A. B. F. Martinson, H. Van Ryswyk and J. T. Hupp, *Energ. Environ. Sci.*, 2008, **1**, 66-78.
354. A. Yella, H. W. Lee, H. N. Tsao, C. Yi, A. K. Chandiran, M. K. Nazeeruddin, E. W. Diau, C. Y. Yeh, S. M. Zakeeruddin and M. Gratzel, *Science*, 2011, **334**, 629-634.
355. H. Wu, Z. Lv, Z. Chu, D. Wang, S. Hou and D. Zou, *J. Mater. Chem.*, 2011, **21**, 14815-14820.
356. M. Stefik, J.-H. Yum, Y. Hu and M. Gratzel, *J. Mater. Chem. A*, 2013, **1**, 4982-4987.
357. L. Kavan, J.-H. Yum and M. Grätzel, *Nano Lett.*, 2011, **11**, 5501-5506.
358. J. D. Roy-Mayhew, G. Boschloo, A. Hagfeldt and I. A. Aksay, *ACS Appl. Mater. Interfaces*, 2012, **4**, 2794-2800.
359. M. J. Ju, J. C. Kim, H.-J. Choi, I. T. Choi, S. G. Kim, K. Lim, J. Ko, J.-J. Lee, I.-Y. Jeon, J.-B. Baek and H. K. Kim, *ACS Nano*, 2013, **7**, 5243-5250.
360. M. J. Ju, I.-Y. Jeon, J. C. Kim, K. Lim, H.-J. Choi, S.-M. Jung, I. T. Choi, Y. K. Eom, Y. J. Kwon, J. Ko, J.-J. Lee, H. K. Kim and J.-B. Baek, *Adv. Mater.*, 2014, **26**, 3055-3062.
361. M. J. Ju, I.-Y. Jeon, K. Lim, J. C. Kim, H.-J. Choi, I. T. Choi, Y. K. Eom, Y. J. Kwon, J. Ko, J.-J. Lee, J.-B. Baek and H. K. Kim, *Energ. Environ. Sci.*, 2014, **7**, 1044-1052.
362. V.-D. Dao, L. V. Nang, E.-T. Kim, J.-K. Lee and H.-S. Choi, *ChemSusChem*, 2013, **6**, 1316-1319.
363. P.-T. Shih, R.-X. Dong, S.-Y. Shen, R. Vittal, J.-J. Lin and K.-C. Ho, *J. Mater. Chem. A*, 2014, **2**, 8742-8748.
364. K. S. Lee, Y. Lee, J. Y. Lee, J. H. Ahn and J. H. Park, *ChemSusChem*, 2012, **5**, 379-382.
365. S. Li, Y. Luo, W. Lv, W. Yu, S. Wu, P. Hou, Q. Yang, Q. Meng, C. Liu and H.-M. Cheng, *Adv. Energy Mater.*, 2011, **1**, 486-490.
366. Z. Yang, H. Sun, T. Chen, L. Qiu, Y. Luo and H. Peng, *Angew. Chem. Int. Ed. Engl.*, 2013, **52**, 7545-7548.
367. J. Sun, Y. Li, Q. Peng, S. Hou, D. Zou, Y. Shang, Y. Li, P. Li, Q. Du, Z. Wang, Y. Xia, L. Xia, X. Li and A. Cao, *ACS Nano*, 2013, **7**, 10225-10232.
368. M. Al-Mamun, H. Zhang, P. Liu, Y. Wang, J. Cao and H. Zhao, *RSC Adv.*, 2014, **4**, 21277-21283.

369. J. Zhang, S. Najmaei, H. Lin and J. Lou, *Nanoscale*, 2014, **6**, 5279-5283.
370. L. T. L. Lee, J. He, B. Wang, Y. Ma, K. Y. Wong, Q. Li, X. Xiao and T. Chen, *Sci. Rep.*, 2014, **4**, 4063.
371. Y. Hu, Z. Zheng, H. Jia, Y. Tang and L. Zhang, *J. Phys. Chem. C*, 2008, **112**, 13037-13042.
372. F. Gong, H. Wang, X. Xu, G. Zhou and Z.-S. Wang, *J. Am. Chem. Soc.*, 2012, **134**, 10953-10958.
373. J.-Y. Lin, C.-Y. Chan and S.-W. Chou, *Chem. Commun.*, 2013, **49**, 1440-1442.
374. C.-J. Liu, S.-Y. Tai, S.-W. Chou, Y.-C. Yu, K.-D. Chang, S. Wang, F. S.-S. Chien, J.-Y. Lin and T.-W. Lin, *J. Mater. Chem.*, 2012, **22**, 21057-21064.
375. S.-Y. Tai, C.-J. Liu, S.-W. Chou, F. S.-S. Chien, J.-Y. Lin and T.-W. Lin, *J. Mater. Chem.*, 2012, **22**, 24753-24759.
376. G. Yue, J. Wu, Y. Xiao, M. Huang, J. Lin and J.-Y. Lin, *J. Mater. Chem. A*, 2013, **1**, 1495-1501.
377. C. X. Guo, H. B. Yang, Z. M. Sheng, Z. S. Lu, Q. L. Song and C. M. Li, *Angew. Chem. Int. Ed. Engl.*, 2010, **49**, 3014-3017.
378. J. He, D. Wu, Z. Gao, F. Xu, S. Jiang, S. Zhang, K. Cao, Y. Guo and K. Jiang, *RSC Adv.*, 2014, **4**, 2068-2072.
379. G. Zhu, L. Pan, H. Sun, X. Liu, T. Lv, T. Lu, J. Yang and Z. Sun, *ChemPhysChem*, 2012, **13**, 769-773.
380. Y. Zhu, X. Meng, H. Cui, S. Jia, J. Dong, J. Zheng, J. Zhao, Z. Wang, L. Li, L. Zhang and Z. Zhu, *ACS Appl. Mater. Interfaces*, 2014, **6**, 13833-13840.
381. M. Ye, C. Chen, N. Zhang, X. Wen, W. Guo and C. Lin, *Adv. Energy Mater.*, 2014, **4**, 1301564.
382. C.-C. Lin, D.-Y. Wang, K.-H. Tu, Y.-T. Jiang, M.-H. Hsieh, C.-C. Chen and C.-W. Chen, *Appl. Phys. Lett.*, 2011, **98**, 263509.
383. H. Bi, F. Huang, J. Liang, X. Xie and M. Jiang, *Adv. Mater.*, 2011, **23**, 3202-3206.
384. T. Lin, F. Huang, J. Liang and Y. Wang, *Energ. Environ. Sci.*, 2011, **4**, 862-865.
385. H. Bi, F. Huang, J. Liang, Y. Tang, X. Lu, X. Xie and M. Jiang, *J. Mater. Chem.*, 2011, **21**, 17366-17370.
386. J. Liang, H. Bi, D. Wan and F. Huang, *Adv. Funct. Mater.*, 2012, **22**, 1267-1271.
387. L. Yin, K. Zhang, H. Luo, G. Cheng, X. Ma, Z. Xiong and X. Xiao, *Nanoscale*, 2014, **6**, 10879-10886.
388. H. S. Kim, C. R. Lee, J. H. Im, K. B. Lee, T. Moehl, A. Marchioro, S. J. Moon, R. Humphry-Baker, J. H. Yum, J. E. Moser, M. Gratzel and N. G. Park, *Sci. Rep.*, 2012, **2**, 591.
389. C. Wehrenfennig, G. E. Eperon, M. B. Johnston, H. J. Snaith and L. M. Herz, *Adv. Mater.*, 2014, **26**, 1584-1589.
390. S. D. Stranks, G. E. Eperon, G. Grancini, C. Menelaou, M. J. P. Alcocer, T. Leijtens, L. M. Herz, A. Petrozza and H. J. Snaith, *Science*, 2013, **342**, 341-344.
391. R. F. Service, *Science*, 2014, **344**, 458.
392. H. Zhou, Q. Chen, G. Li, S. Luo, T.-b. Song, H.-S. Duan, Z. Hong, J. You, Y. Liu and Y. Yang, *Science*, 2014, **345**, 542-546.
393. Y. H. Jang, X. Xin, M. Byun, Y. J. Jang, Z. Lin and D. H. Kim, *Nano Lett.*, 2011, **12**, 479-485.
394. J. T.-W. Wang, J. M. Ball, E. M. Barea, A. Abate, J. A. Alexander-Webber, J. Huang, M. Saliba, I. Mora-Sero, J. Bisquert, H. J. Snaith and R. J. Nicholas, *Nano Lett.*, 2013, **14**, 724-730.
395. Z. Zhu, J. Ma, Z. Wang, C. Mu, Z. Fan, L. Du, Y. Bai, L. Fan, H. Yan, D. L. Phillips and S. Yang, *J. Am. Chem. Soc.*, 2014, **136**, 3760-3763.

396. Z. Wu, S. Bai, J. Xiang, Z. Yuan, Y. Yang, W. Cui, X. Gao, Z. Liu, Y. Jin and B. Sun, *Nanoscale*, 2014.

Graphic Abstract

2D materials have been successfully used in various types of solar cells as transparent electrodes, interfacial and active materials.

Biography and photograph

Dr. Zhike Liu is currently working as a postdoctoral fellow in group of Prof. Feng Yan at the Department of Applied Physics of the Hong Kong Polytechnic University. He received his PhD degree in applied physics from the Hong Kong Polytechnic University in 2014. His research interests focus on the synthesis, modification and application of graphene for photovoltaic devices.

Prof. Feng Yan has research interests on thin film transistors, solar cells, 2D materials, organic electronics, biosensors and smart materials. He received his PhD degree in physics from Nanjing University in China. Then he joined the Engineering Department of Cambridge University in Feb 2001 as a Research Associate and joined National Physical Laboratory in UK in April 2006 as a Higher Research Scientist. He became an Assistant Professor at the Department of Applied Physics of the Hong Kong Polytechnic University in September 2006 and was promoted to Associate Professor in July 2012.